UNIVERSITÀ DI PARMA

UNIVERSITA' DEGLI STUDI DI PARMA

DOTTORATO DI RICERCA IN
MEDICINA MOLECOLARE – ODONTOIATRIA DIGITALE

CICLO XXXVI

Impact of Digital Dentistry on Clinical Practice, Research and Education

Coordinatore:
Chiar.mo Prof. Prisco Mirandola

Tutore:
Chiar.mo Prof. Simone Lumetti

Dottorando: Dott. Matteo Meglioli

Anni Accademici 2020/2021 – 2022/2023

INDEX

Introduction

This PhD thesis focus on Digital Dentistry, encompassing various dental fields.

Digital dentistry refers to the use of digital technologies and computer-based systems in various aspects of dental practice, including diagnosis, treatment planning, student education and patient care. A wide range of technologies and techniques that have revolutionized the field of dentistry, making it more efficient, accurate, and patient-friendly.

Some of the key components and applications of digital dentistry include digital imaging, intraoral scanners, computer-aided design (CAD) software, computer-aided manufacturing (CAM) technologies, digitalized treatment planning, guided therapies and advanced training.

Digital radiography, such as intraoral and extraoral X-rays and 3D cone-beam computed tomography (CBCT), provides high-quality images with minimal radiation exposure. These digital images are easier to store, share, and manipulate compared to traditional film-based X-rays.

Intraoral Scanners are devices that capture 3D images of a patient's teeth and oral structures, in contrast with the traditional impression materials. Intraoral scanners are commonly used in everyday clinic for creating digital models of teeth, enabling CAD/CAM workflows.

CAD software allows dentists to design dental restorations (e.g., crowns, bridges, dentures) on a computer. Thanks to CAM technologies, such as milling machines or 3D printers, is possible to fabricate the digital file designed through CAD software.

Imaging and specialized software facilitate the planning of various procedures: surgical, prosthetic, endodontic, and orthodontic ones. Moreover, the use of 3D printed guides can provide valuable support in these dental disciplines.

These digital tools and processes enhance communication with patients and ensures the accurate implementation of treatment plans. They are also used in dental education to train future professionals. 3D printed training models, virtual reality and simulation software provide a safe and realistic way for students to gain hands-on experience and improve their skills before working on actual patients.

Digital dentistry offers numerous advantages, including increased accuracy, reduced treatment times, improved patient comfort, and enhanced communication among clinicians and patients. It has significantly advanced the field of dentistry and continues to evolve with ongoing technological developments.

At first, I focused my researches on 3D printing, keeping an eye on 3D printed patient-specific models that could be used for training students and clinicians.

Technological advancements have been instrumental in driving the evolution of oral and cranio-maxillofacial surgery, with additive manufacturing (AM) processes playing

a pivotal role [1]. Among these AM processes, three-dimensional printing (3DP), often used interchangeably with additive manufacturing, has emerged as a game-changer. This innovative technology involves the layer-by-layer fabrication of objects through computer-aided design/computer-aided manufacturing (CAD/CAM) workflows [2].

Originally developed in the 1980s to expedite the production of customized objects, 3D printing swiftly revolutionized prototyping concepts and found applications across various manufacturing industries. In the medical field, it began to be integrated into procedures and techniques, contributing significantly to fields such as dentistry, maxillofacial surgery, orthopedics, and neurosurgery [3,4]. In the field of oral and craniofacial surgery, 3D printing has become a routine practice, with applications ranging from the creation of surgical templates for enhanced surgical precision to the fabrication of custom implants based on patient radiological data [5,6].

To understand the differences between 3D printing techniques on creating patient-specific models, a systematic review was conducted analyzing the model fabrication step by step.

To harness the potential of 3D printing, clinicians first transform patients' radiological data, typically obtained from computed tomography (CT) or magnetic resonance imaging (MRI) scans, into digital 3D object files, such as standard tessellation language (STL) format. Various 3D printing techniques, including vat photopolymerization (VP), material extrusion (ME), and binder jetting (BJ), are employed for surgical model

fabrication, each with its unique advantages and limitations. These models serve three primary purposes: training, planning, and simulating [7,8].

Training models offer a cost-effective solution for enhancing the quality of dental education by providing students and clinicians with opportunities for high-quality surgical training. They replicate the tactile feedback of actual patients' bone structures, offering a realistic learning experience and alleviating the challenges associated with obtaining cadaveric specimens [10].

Planning models, on the other hand, empower surgeons to visualize and comprehend complex anatomical structures, facilitating meticulous surgical planning and more predictable outcomes in procedures such as orthognathic and reconstructive surgeries [11,12]. The hallmark of planning models lies in their accuracy.

Simulating models represent another facet of 3D printing's impact, enabling clinicians to practice surgical interventions before executing them in clinical settings. These models, characterized by patient-like haptic feedback and mechanical properties, are invaluable for refining surgical techniques and decision-making [13, 14]. The mechanical properties of simulating models are crucial for replicating real surgical conditions.

Choosing the right 3D printing technology and material for each application can be daunting, given the plethora of options available. Our systematic review seeks to correlate specific 3D printing technologies with applications in oral and craniofacial surgery, offering practical insights into material and technique selection.

All considered, we decide to fabricate endodontic simulation models thanks to the usage of 3D printing, to enhance the pre-clinical training of dental students. While traditional methods often involve extracted human teeth, their limitations, including ethical concerns and reduced availability, have driven the development of sophisticated artificial root canals and 3D-printed teeth [15,16]. These replicas provide students with realistic training opportunities and eliminate variability, offering cost-effective alternatives [17]

Thanks to intraoral scanner students' performances and their learning curve were evaluated in an equal manner, obtaining their feedback through a questionnaire.

This research confirmed that beyond clinical applications, IOSs enable objective evaluation of students' performance, enhancing the assessment of their skills in areas like crown preparation and access cavity exercises [18, 19].

Secondly, I mainly focus on intraoral scanners (IOS), a cutting-edge technology in digital dentistry, that is widely used in very dental field [20]. Intraoral scanning, a foundational element of digital workflows, has become indispensable in modern dentistry, emphasizing the importance of practicality, user-friendliness, cost-effectiveness, speed, and accuracy in IOS development [21].

I investigated IOS accuracy in implant-prosthetic treatments and fixed prosthesis. Accuracy, a key parameter, is defined by the ISO as a combination of trueness and precision, where trueness reflects the closeness of scan results to the true reference

value, while precision measures consistency in repeated test results (ISO 5725). A reliable scanner achieves both high trueness and precision, ensuring the faithful reproduction of scanned objects.

The accuracy of digital scanning is particularly relevant in implant-supported prostheses, with its potential to replace traditional impressions for edentulous patients [22, 23]. In this context, scan bodies (SBs) play a critical role, capturing implant position, angle, and height information [24].

While most of the existing literature examines accuracy through absolute variability between scan bodies and implant analog interdistances, there is a notable gap in the understanding of how errors relate to interdistance and angle values, thus addressing the predictability of IOS errors [25, 26]. Thus, our research hypothesis was "Is it possible to find out predictable errors assessing intraoral scanner accuracy in full arch-scan for implant supported rehabilitations?", seeking to address this gap.

Working always on IOSs, a novel digital technique called “Reverse Subgingival Scan” (RSS) was defined, to overcome the limits of existing techniques for performing accurate assessment of the abutments in fixed prosthodontics. [27, 28] This technique allows to perfectly depict abutment subgingival finish lines, and of the transmucosal zone, as conditioned by the provisional restoration.

I also worked on surgical guides, collaborating with Professor Sylvain Catros and his team at the Université de Bordeaux.

Accurate dental implant placement is essential for successful long-term results, and computer-aided techniques have been developed for this purpose. Surgical guides for implant placements must be accurate because deviations between planned and actual implant positions are not allowed. [29] It can occur due to various factors, including clinical conditions, implant systems, and surgical guide design and manufacturing [30-32].

The process of manufacturing surgical guides for guided implant surgery involves patient data acquisition, data processing, and guide design. This includes capturing bone geometry through imaging, creating digital models, and using specialized software to plan and design the surgical guide. Several 3D printing technologies are used for fabricating surgical guides, including stereolithography (SLA), selective laser sintering (SLS) digital light processing (DLP), fused deposition modeling (FDM), inkjet and PolyJet®. The popularity of 3D-printed surgical guides is growing due to their accuracy, cost-effectiveness, and customization. This study aims to evaluate the accuracy of surgical guides fabricated using five different commercial 3D printing technologies (SLA, DLP, FDM, SLS, and Inkjet) and two guide sizes (single implant and full arch), with a focus on trueness and precision. The null hypotheses are related to the impact of technology and guide size on guide accuracy.

In the end, I worked on creating 3D printed scaffolds that can be useful in treating bone defects or tissue engineering in oral surgery [33, 34]. Bone defects, resulting

from various factors, often require intervention due to the body's limited self-healing capacity [35]. Periodontitis, a significant dental challenge, can lead to alveolar bone loss.

Bone replacement is essential for addressing these oral and maxillofacial issues, but challenges persist. Traditional methods involving autografts or allografts have drawbacks, leading to a shift towards synthetic biomaterials and scaffolds [36,37]. These synthetic scaffolds offer advantages such as customizable internal structures and surface characteristics, with 3D printing playing a crucial role in their design and production [38].

To be effective, these scaffolds must mimic native tissue in surface patterns, wettability, growth factors, and biocompatible biomaterials are also essential for regenerative medicine [39].

Thus, scaffolds were fabricated with a FDM printer that was able to print a customized material made by polycaprolactone (PCL) and beta-tricalcium phosphate (β-TCP). PCL is a biocompatible material with a slow degradation rate, enhances scaffold properties [40,41]. The presence of β-TCP alters scaffold surface topography, potentially enhancing bioactivity and graft integration [42], overcoming PCL's limitations: lower strength and hydrophobicity affecting cellular adhesion [43].

This work aims to determine the optimal β-TCP concentration for customizing PCL/β-TCP scaffolds for bone regeneration. It also investigates how PCL 3D-printed scaffolds influence osteoblastic behavior in terms of proliferation and differentiation.

BIBLIOGRAPHY

[1] Naveau A, Bou C, Sharma A. Evolution of Topics in Maxillofacial Prosthetics. Publications. *Int J Prosthodont.* **2018** 31(6):565–568.

[2] ASTM International. Standard Terminology for Additive ManufacturingTechnologies 1,2. **2013** 24.

[3] Crafts TD, Ellsperman SE, Wannemuehler TJ, Bellicchi TD, Shipchandler TZ, Mantravadi AV. Three-Dimensional Printing and Its Applications in Otorhinolaryngology. *Head Neck Surg.* **2017** 156(6):999–1010.

[4] Pacione D, Tanweer O, Berman P, Harter DH. The utility of a multimaterial 3D printed model for surgical planning of complex deformity of the skull base and craniovertebral junction. *J Neurosurg*. **2016** 125(11):1194-1197.

[5] Sánchez-Sánchez Á, Girón-Vallejo Ó, Ruiz-Pruneda R, et al. Three-Dimensional Printed Model and Virtual Reconstruction: An Extra Tool for Pediatric Solid Tumors Surgery. *Eur J Pediatr Surg reports*. **2018** 6(1):e70-e76.

[6] Han Q, Zhao X, Wang C, et al. Individualized reconstruction for severe periprosthetic fractures around the tumor prosthesis of knee under assistance of 3D printing technology: A case report. *Medicine (Baltimore)*. **2018** 97(42):e12726-e12726.

[7] Probst R, Stump R, Mokosch M, Röösli C. Evaluation of an infant temporal-Bone model as training tool. *Otol Neurotol.* **2018** 39(6):e448–e452.

[8] Wiedermann JP, Conchenour C, Joshi AS, Preciado D, Jamshidi A. Utilization of a submental island flap and 3D printed model for skull base reconstruction: Infantile giant cranio-cervicofacial teratoma. *Int J Pediatr Otorhinolaryngol* **2017** Jan;92:143-145.

[9] Somji SH, Valladares A, Ho Kim S, Cheng Paul Yu Y, Froum SJ. The use of 3D models to improve sinus augmentation outcomes - A case report. *Singapore Dent J*. **2017** 38:63-70

[10] Hochman JB, Rhodes C, Wong D, Kraut J, Pisa J, Unger B. Comparison of cadaveric and isomorphic three-dimensional printed models in temporal bone education. *Laryngoscope*. **2015** ;125(10):2353-2357. doi: 10.1002/lary.24919

[11] Mavili ME, Canter HI, Saglam-Aydinatay B, et al. Use of three-dimensional medical modeling methods for the precise planning of orthognathic surgery. J Craniofacial Surg. **2007** 18(4):740–7. 10.4103/JCD.JCD_133_18.

[12] Arce K, Waris S, Alexander AE, Ettinger KS. Novel patient-specific 3D printed fixation tray for mandibular reconstruction with fibular free flaps. 2018. *J Oral Maxillofac Surg* **2018** Oct;76(10):2211-2219.

[13] Yusa K, Yamanochi H, Takagi A, Iino M. Three-dimensional printing model as a tool to assist in surgery for large mandibular tumour: a case report. *J Oral Maxillofac Res* **2017** 8(2):1–7.

[14] Gargiulo P, Arnadottir I, Gislason M, Edmunds K, Olafsson I. New directions in 3D medical modeling: 3D-printing anatomy and functions in neurosurgical planning. *J Healthc Eng*. **2017**.10.1155/2017/1439643/.

[15] Nawrocka, A.; Łukomska-Szymańska, M. Extracted human teeth and their utility in dental research. Recommendations on proper preservation: A literature review. *Dental and medical problems* **2019**, 56, 185-190

[16] Gancedo-Caravia, L.; Bascones, J.; García-Barbero, E.; Arias, A. Suitability of different tooth replicas for endodontic training: perceptions and detection of common errors in the performance of postgraduate students. *International endodontic journal* **2020**, 53, 562-572

[17] Reymus, M.; Fotiadou, C.; Kessler, A.; Heck, K.; Hickel, R.; Diegritz, C. 3D printed replicas for endodontic education. *International endodontic journal* **2019**, 52, 123-130

[18] Seet, R.H.; Soo, P.R.; Leong, K.J.M.; Pang, J.J.H.; Lee, F.K.F.; Tan, M.Y. Crown preparations by undergraduate dental students: A comparison of conventional versus digital assessment via an intraoral scanner. *Journal of dental education* **2020**, 84, 1303-1313

[19] Choi, S.; Choi, J.; Peters, O.A.; Peters, C.I. Design of an interactive system for access cavity assessment: A novel feedback tool for preclinical endodontics. *European journal of dental education : official journal of the Association for Dental Education in Europe* **2023**

[20] Lim JH, Park JM, Kim M, Heo SJ, Myung JY. Comparison of digital intraoral scanner reproducibility and image trueness considering repetitive experience. *J Prosthet Dent* **2018** 119:225–232.

[21] Joda T, Brägger U. Patient-centered outcomes comparing digital and conventional implant impression procedures: a randomized crossover trial. *Clin Oral Implants Res* **2016** 27:e185–e189.

[22] Ender A, Mehl A. Accuracy of complete-Arch dental impressions: A new method of measuring trueness and precision. *J Prosthet Dent* **2013** 109:121–128.

[23] Amin S, Weber HP, Finkelman M, El Rafie K, Kudara Y, Papaspyridakos P. Digital vs. conventional full-arch implant impressions: a comparative study. *Clin Oral Implants Res* **2017** 28:1360–1367.

[24] Mizumoto RM, Yilmaz B, McGlumphy EA, Seidt J, Johnston WM. Accuracy of different digital scanning techniques and scan bodies for complete-arch implant-supported prostheses. *J Prosthet Dent* **2020** 123:96–104.

[25] Mangano F, Gandolfi A, Luongo G, Logozzo S. Intraoral scanners in dentistry: A review of the current literature. *BMC Oral Health* **2017** 17:1–11.

[26] Mangano FG, Admakin O, Bonacina M, Lerner H, Rutkunas V, Mangano C. Trueness of 12 intraoral scanners in the full-arch implant impression: A comparative in vitro study. *BMC Oral Health* **2020** 20:1–21.

[27] Mandelli F, Ferrini F, Gastaldi G, Gherlone E, Ferrari M. Improvement of a Digital Impression with Conventional Materials: Overcoming Intraoral Scanner Limitations. *Int J Prosthodont* **2017** *4:*373–376.

[28] Agustín-Panadero R, Loi I, Fernández-Estevan L, Chust C, Rech-Ortega C, Pérez-Barquero JA. Digital protocol for creating a virtual gingiva adjacent to teeth with subgingival dental preparations, *J Prosthodont Res* **2020** *64,*506–514.

[29] M. Vercruyssen, I. Laleman, R. Jacobs, M. Quirynen, Computer-supported implant planning and guided surgery: a narrative review, Clin Oral Implants Res **2015** 26:69–76

[30] Zhou W, Liu Z, Song L, Kuo C, Shafer DM. Clinical Factors Affecting the Accuracy of Guided Implant Surgery—A Systematic Review and Meta-analysis, *Journal of Evidence Based Dental Practice* **2018** 18:28–40

[31] Matsumura A, Nakano T, Ono S, Kaminaka A, Yatani H, Kabata D. Multivariate analysis of causal factors influencing accuracy of guided implant surgery for partial edentulism: a retrospective clinical study, *Int J Implant Dent.* **2021** 7:28

[32] Rubayo DD, Phasuk K, Vickery JK, Morton D, Lin W-S. Influences of build angle on the accuracy, printing time, and material consumption of additively manufactured surgical templates, *J. Prosthet. Dent.* **2020**

[33] MacKinnon RB, Oomen J, Pedersen Zari M. Promises and Presuppositions of Biomimicry. *Biomimetics* **2020**

[34] Anderson M, Dubey N, Bogie K, Cao C, Li J, Lerchbacker J, Mendonça G, Kauffmann F, Bottino MC, Kaigler D. Three-dimensional printing of clinical scale and personalized calcium phosphate scaffolds for alveolar bone reconstruction. *Dent Mater* **2022** *38*:529-539

[35] Szulc P. Bone turnover: Biology and assessment tools. *Best Practice & Research Clinical Endocrinology & Metabolism* **2018** *32*:725-738

[36] Pilipchuk SP, Plonka AB, Monje A, Taut AD, Lanis A, Kang B. Giannobile, W.V. Tissue engineering for bone regeneration and osseointegration in the oral cavity. *Dent Mater* **2015** *31*:317-338

[37] Bracey DN, Seyler TM, Jinnah AH, Smith TL, Ornelles DA, Deora R, Parks GD, Van Dyke ME, Whitlock PW. A porcine xenograft-derived bone scaffold is a biocompatible bone graft substitute: An assessment of cytocompatibility and the alpha-Gal epitope. *Xenotransplantation* **2019** *26*:e12534

[38] Ahn SH, Lee J, Park SA, Kim WD. Three-dimensional bio-printing equipment technologies for tissue engineering and regenerative medicine. *Tissue Eng Regen Med* **2016** *13*:663-676

[39] Turnbull G, Clarke J, Picard F, Riches P, Jia L, Han F, Li B, Shu W. 3D bioactive composite scaffolds for bone tissue engineering. *Bioactive materials* **2018** *3*:278-314

[40] Wang Y, Wang J, Gao R, Liu X, Feng Z, Zhang C, Huang P, Dong A, Kong D, Wang W. Biomimetic glycopeptide hydrogel coated PCL/nHA scaffold for enhanced cranial bone regeneration via macrophage M2 polarization-induced osteo-immunomodulation. *Biomaterials* **2022** *285*:121538

[41] Siddiqui N, Asawa S, Birru B, Baadhe R, Rao S. PCL-Based Composite Scaffold Matrices for Tissue Engineering Applications. *Molecular Biotechnology* **2018** *60*:506-532

[42] Bruinink A, Bitar M, Pleskova M, Wick P, Krug HF, Maniura-Weber K. Addition of nanoscaled bioinspired surface features: A revolution for bone related implants and scaffolds? *J Biomed Mater Res A* **2014**, *102*:275-294

[43] Siddiqui N, Asawa S, Birru B, Baadhe R, Rao S. PCL-Based Composite Scaffold Matrices for Tissue Engineering Applications. *Molecular Biotechnology* **2018** *60*:506-532

Chapter I

From 3D radiological data to a printable file: an open-source software workflow

INTRODUCTION

In recent years, Additive Manufacturing (AM) is playing a growing role in the medical field. Among all the AM processes, three-dimensional (3D) printing is one of the most interesting. Thanks to this technology it's possible to fabricate objects layer-by-layer through computer-aided design/computer-aided (CAD/CAM) manufacturing workflows. [1]

To simulate and plan complex surgeries, several authors utilized this technology to faithfully reproduce patient's bone structures from radiological data [2-4].

The visual and tactile inspection of 3D printed models allowed an enhanced anatomical understanding, improving the quality of diagnosis and clinical results through simulation of surgical treatments. In oral and maxillofacial surgery, they have been used for mastoidectomies, bone reconstructions, tumor removals, sinus lifts and in implant dentistry [5-11].

Finally, 3D printed models are fundamental tools to improve the quality of teaching, allowing realistic hands-on training and case discussion [12].

Imaging 3D data can be acquired through many exams, such as Computerized Tomography (CT), Cone Beam Computerized Tomography (CBCT), Magnetic Resonance Imaging (MRI), Positron-Emission Tomography (PET), etc. Digital Imaging and COmmunications in Medicine (DICOM) format is the standard file type to archive, process and exchange data. A DICOM 3D imaging file is then processed to a 3D printable object file, also called mesh, which is the digital representation of a geometric model by using a collection of polygons to form the object surface. A mesh is most commonly in the Standard Triangulation Language (STL) file format, which is the reference file type in AM.

The majority of articles in the literature typically presents the radiological images processing briefly, or omit it at all. Thus, it is often difficult for clinicians to replicate a workflow to obtain from their DICOM files

Regarding all the previous considerations, the authors present the image processing workflow currently employed at their institution to obtain correct ready-to-print files through open-source or free software.

TECHNIQUE

This workflow consists of three different steps: the segmentation of the radiological images, the post-processing of the STL mesh and the analysis of the resulting closed file. Three open-source or free software are sequentially used: Horos® (The Horos Project, Switzerland), MeshLab® (CNR, Italy) [13] and MeshMixer® (Autodesk, USA). A

comparative table of the software is presented (Table 1).

		Horos v3.3.5	**Meshlab** v2016.12	**Autodesk Meshmixer** v3.4.35
Supported formats				
	DICOM	YES	NO	NO
	STL	NO	YES	YES
	OBJ	NO	YES	YES
Radiological Images Processing				
	ROI selection	YES	NO	NO
	Segmentation	YES	NO	NO
	Rederization	YES	NO	NO
Measurement				
	Linear	YES	YES	YES
	Volume	NO	YES	YES
Editing				
	Subdivision surfaces on mid-point	NO	YES	NO
	Freehand CAD drawing	NO	NO	YES
	Mesh manipulation	NO	YES	YES
Analysis				
	Wall Thickness	NO	NO	YES
	Holes	NO	YES	YES
	Bad Faces	NO	YES	YES

Table 1: Comparative table of software features.

1. Segmentation

Horos®, a free open source medical viewer, is the software involved for the segmentation of the radiological images. After importing the radiological exam file on Horos, the user must select from the toolbar *3D Viewer* and so *3D Surface Rendering*. Opened this tool, it is important to set the right thresholds, which are user-dependent, using the Horos Toolbar. This step it's probably the most important to obtain an accurate mesh. More it is clear the rendering of DICOM data and less refining interventions of the STL file are required. The right threshold should permit us to visualize all the important biological structures, trying to minimize errors like scattering. (Figure 1) It is suggested to choose a high level of "Resolution" and an intermediate value of "Interactions". The optimal "Pixel Value", last important parameter, is the one that permits to visualize all the interesting structure. Once Horos's semi-automatic segmentation is completed, it is possible to export the STL file.

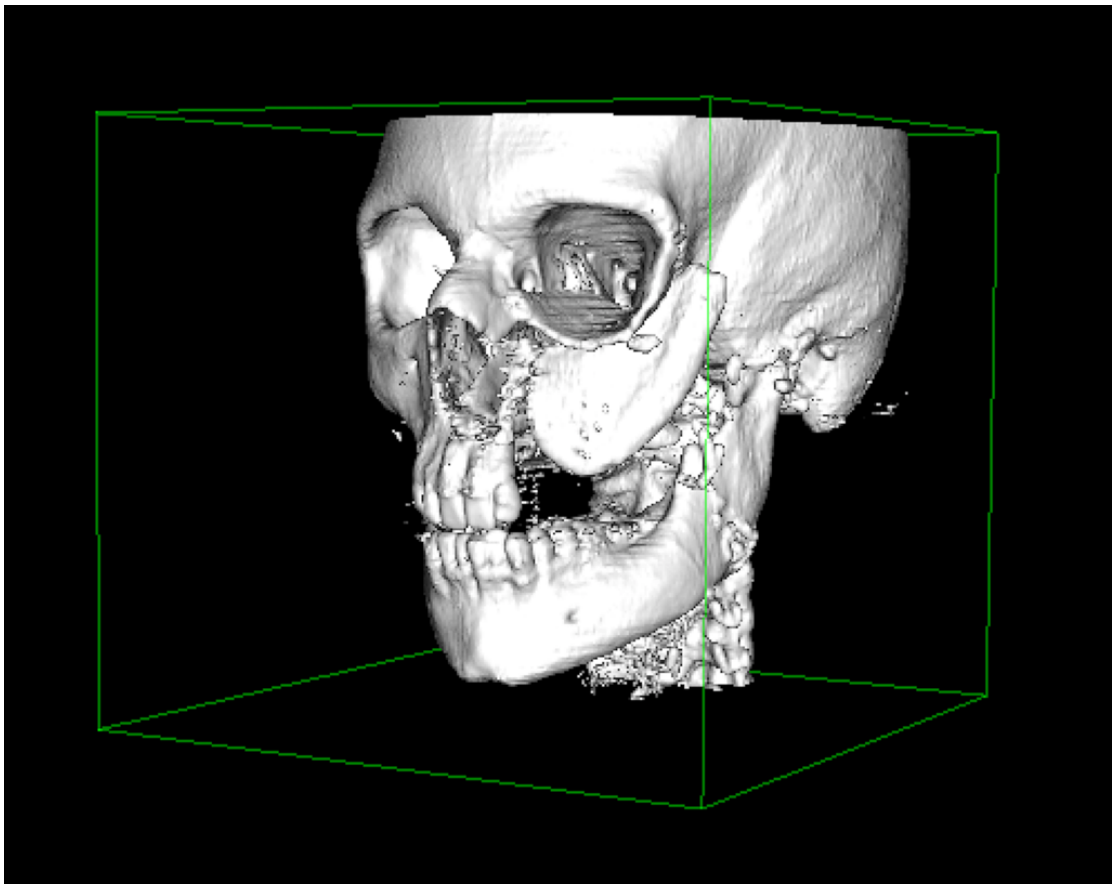

Figure 1. 3D Superficial Rendering via Horos®. Settings: high accuracy, resolution: 0.10, repetitions: 50, pixel value 150.

2. Post-processing

The resulting STL mesh is not ready to be printed for two main reasons: it does not have a closed printable geometry and it presents errors, such as the result of scattering. This phenomenon occurs when X-rays are deflected by the particles of the medium that they traverse.

Thanks to the imaging processing software MeshLab®, it is possible to refine the STL mesh trough several tools and plugins. The first useful one is *Remove Isolated Pieces*, which allows deleting isolated pieces composed by a limited number of triangles. Normally, the mesh contains isolated groups of triangles

that are the result of the X-rays scattering. It is important to remove them because these little pieces do not actually exist, and they generate unprintable STL files.

Having regard for the geometrical coordinates of all the mesh cloud points, it is possible to obtain smoother mesh's surfaces using another plugin: *Subdivision Surfaces: Midpoint*. It uniforms meshes applying a subdivision scheme of triangles' edge, substituting each triangle with four smaller triangles.

Finally, thanks to the tool *Close Holes, it is* possible to close holes smaller than a given threshold. Once accomplished these operations, the refined mesh can be recoded as an STL file. (Figure 2).

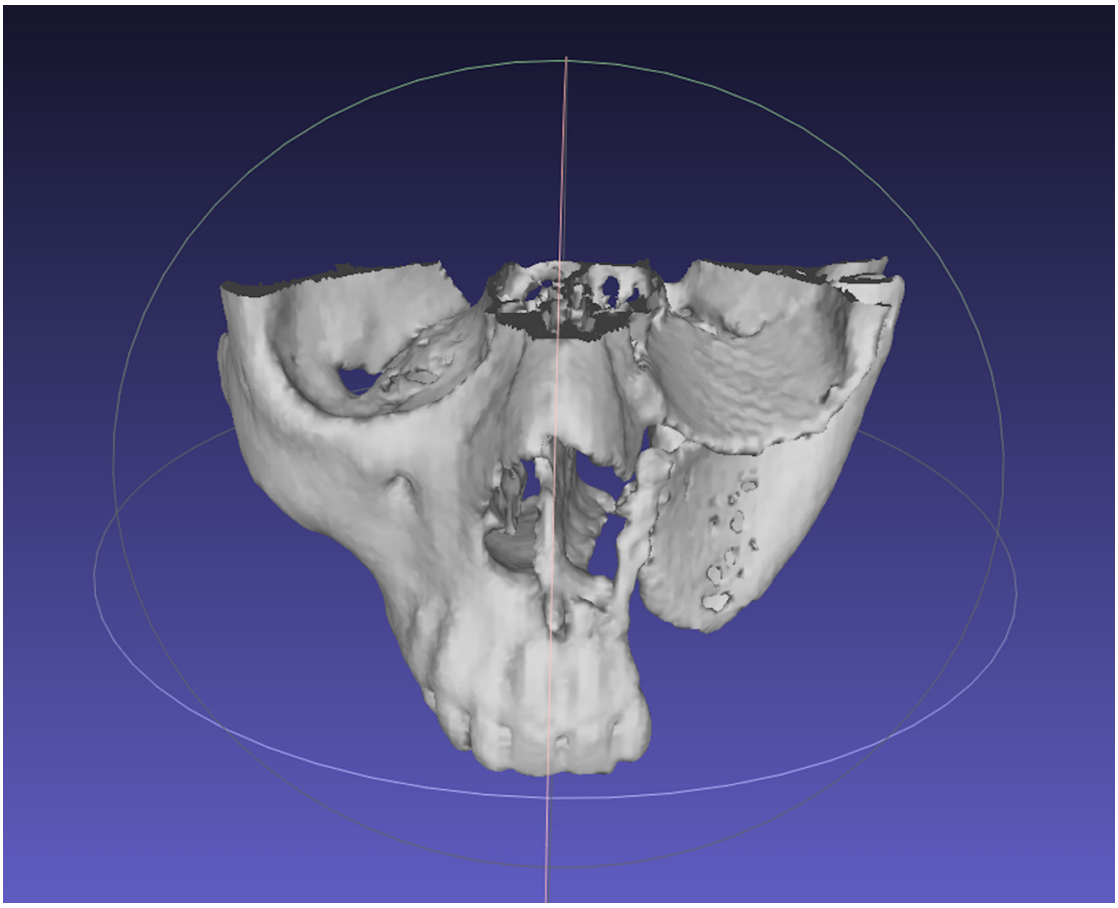

Figure 2. STL image file after discarding the unnecessary regions, removing isolated pieces and smoothing the surface via MeshLab®.

To finish the STL mesh it is possible to utilize MeshMixer®, an optimal 3D modeling software to create, analyse and optimize 3D models. Thanks to the toll *Make Solid*, that the user can figure out after selecting the button *Edit* in the MeshMixer®'s toolbar, it is possible to obtain a closed printable STL geometry. (Figure 3)

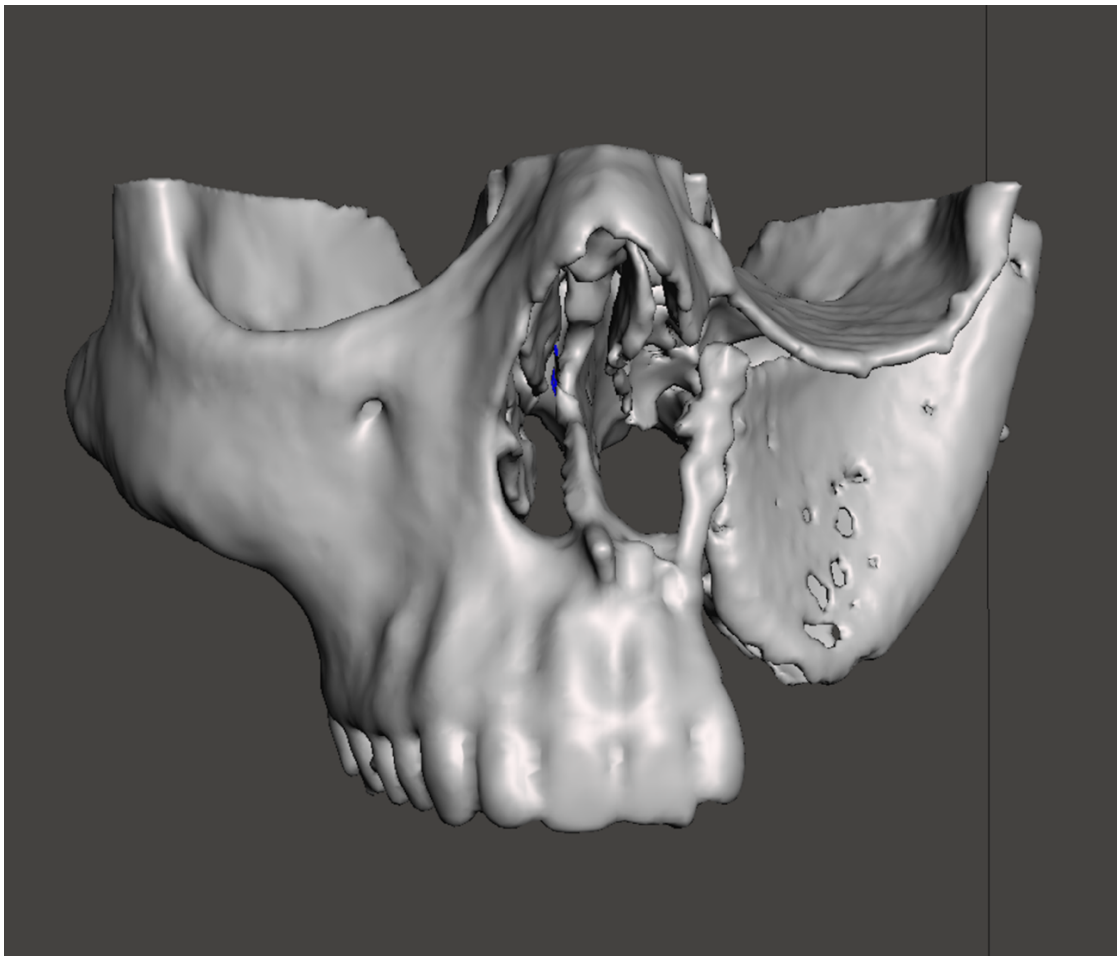

Figure 3. Ready to print STL file obtained via MeshMixer®.

3. Analysis

Authors recommend analyzing the mesh using a practical MeshMixer®'s plug-in called *Inspector,* which can be found in the *Analyse*'s toolbar. It allows seeing if there are floating pieces and holes in the mesh, permitting also to auto-repair them.

After employing these three software, a patient-specific bone model can be made using a 3D printer and every possible material. Depending on the printing technique

involved and the chosen printing material, it may occur to orient the mesh and to create adequate support with dedicated software. Stereolithographic printers require to create a support for the printed object. Using a fused deposition modeling printing technique is important to create a support only when a feature is printed with an overhang beyond 45°. Powder bad fusion doesn't require to create it. In the example shown in figures 1-5 a Form 2 (Formlabs, Somerville, MA) stereolithographic printer, working with the "Dental Model" resin (Formlabs, Somerville, MA), was used to obtain a surgical planning model. The post-curing process, associate with stereolithographic printing technique, was made by Form Wash and Form Cure (Formlabs, Somerville, MA). (Figure 4 and 5)

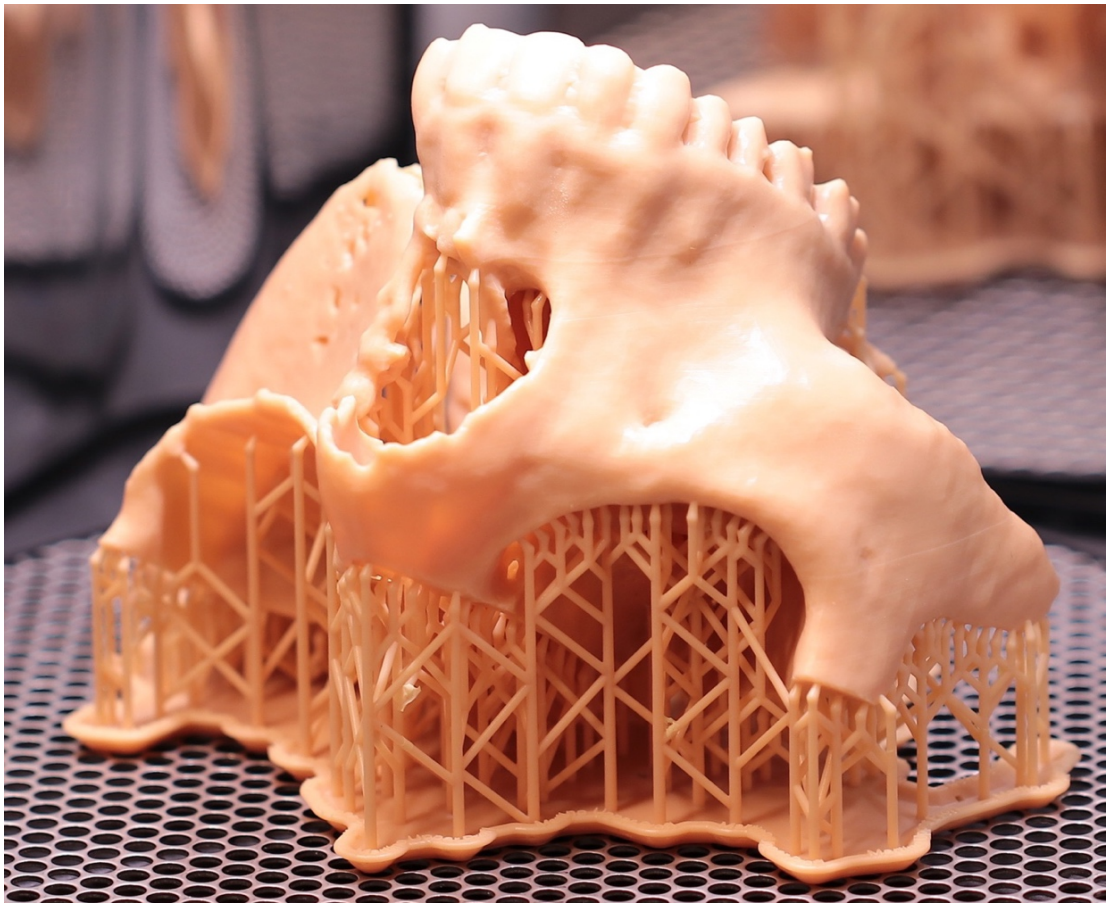

Figure 4. 3D printed model obtained using a stereolithographic printer.

Figure 5. Surgical planning on the 3D printed model.

CONCLUSION

The presented imaging processing workflow represents a proven and cost-effective solution for obtaining 3D printable files.

BIBLIOGRAPHY

[1] ASTM International. Standard Terminology for Additive Manufacturing Technologies 1,2. **2013** 2-4

[2] Yusa K, Yamanochi H, Takagi A, Iino M. Three-Dimensional Printing Model as a Tool to Assist in Surgery for Large Mandibular Tumour: a Case Report. *J Oral Maxillofac Res* **2017** 8(2):1-7.

[3] Sánchez-Sánchez Á, Girón-Vallejo Ó, Ruiz-Pruneda R, et al. Three-Dimensional Printed Model and Virtual Reconstruction: An Extra Tool for Pediatric Solid Tumors Surgery. *Eur J Pediatr Surg reports* **2018** 6(1):e70-e76

[4] Han Q, Zhao X, Wang C, et al. Individualized reconstruction for severe periprosthetic fractures around the tumor prosthesis of knee under assistance of 3D printing technology: A case report. *Medicine (Baltimore)* **2018** 97(42):e12726-e12726

[5] Hochman JB, Rhodes C, Wong D, Kraut J, Pisa J, Unger B. Comparison of cadaveric and isomorphic three-dimensional printed models in temporal bone education. *Laryngoscope.***2015** 125(10):2353-2357.

[6] Wiedermann JP, Conchenour C, Joshi AS, Preciado D, Jamshidi A. Utilization of a submental island flap and 3D printed model for skull base reconstruction: Infantile giant cranio-cervicofacial teratoma. *Int J Pediatr Otorhinolaryngol* **2017** 92(01):143-145.

[7] Jacek B, Radosław W, Wiesław K, et al. 3D printed models in mandibular reconstruction with bony free flaps. *J Mater Sci Mater Med* **2018** 29(2):10-15.

[8] Pacione D, Tanweer O, Berman P, Harter DH. The utility of a multimaterial 3D printed model for surgical planning of complex deformity of the skull base and craniovertebral junction. *J Neurosurg*. **2016** 125(11):1194-1197

[9] Arce K, Waris S, Alexander AE, Ettinger KS. Novel patient-specific 3D printed fixation tray for mandibular reconstruction with fibular free flaps. *J Oral*

Maxillofac Surg **2018** 76(10):2211-2219

[10] Somji SH, Valladares A, Ho Kim S, Cheng Paul Yu Y, Froum SJ. The use of 3D models to improve sinus augmentation outcomes - A case report. *Singapore Dent J*. **2017** 38:63-70.

[11] Nikzad S, Azari A, Ghassemzadeh A. Modified flapless dental implant surgery for planning treatment in a maxilla including sinus lift augmentation through use of virtual surgical planning and a 3-dimensional model. *J Oral Maxillofac Surg*. **2010** 68(9):2291-2298.

[12] Chou PY, Hallac RR, Shih E, et al. 3D-printed models of cleft lip and palate for surgical training and patient education. *Cleft Palate-Craniofacial J*. **2018** 55(3):323-327

[13] Cignoni P, Callieri M, Corsini M, Dellepiane M, Ganovelli F, Ranzuglia G. MeshLab: an Open-Source Mesh Processing Tool. *Eurographics Ital Chapter Conf 2008 Salerno, Italy*. **2008** 129-136.

Chapter II

3D printed bone models in oral and cranio-maxillofacial surgery: a systematic review

INTRODUCTION

Technological development strongly drives the evolution of oral and cranio-maxillofacial surgery [1]. Among all the additive manufacturing (AM) processes, “three-dimensional printing” (3DP), often used synonymously with additive manufacturing, is playing an ever-growing role. This technology involves the fabrication of objects through the deposition of material using a print head, nozzle, or other printing technology [2]. It allows creating objects layer-by-layer through computer-aided design/computer-aided manufacturing (CAD/CAM). It was originally developed in the 1980s to accelerate the production of small and custom-designed objects, but it revolutionized the prototyping concepts and embraced many applications in manufacturing industries. Later on, AM’s applications started to be integrated in several medical techniques and procedures, giving some important inputs to various domains, such as dentistry, maxillofacial surgery, orthopedics and neurosurgery. Frequent clinical applications of 3D printing in everyday practice

include the fabrication of surgical templates employed to improve the accuracy of the surgery and reduce the duration and morbidity of surgical interventions. It is now applied in routine in oral and craniofacial surgery [3, 4]. More recently, the progress made in the 3D-printing of implantable biomaterials were applied to the fabrication of custom implants, based on patients' radiological data: even if a large amount of these commercial custom implants are milled, 3D-printing technologies can be employed for large bone defects reconstruction like cranioplasty [5] or Temporo-mandibular joint replacement [6].

Three-dimensional printing techniques involve creation of accurate physical 3D models from the patient's radiological data. The first step consists in obtaining the Digital Imaging and COmmunications in Medicine (DICOM) files from patient's imaging exams, such as computed tomography (CT) or magnetic resonance imaging (MRI) scans. Then software is used to transform them into a digital 3D object file, such as standard tessellation language (STL), among other formats. For surgical model fabrication, this new file can be printed with different techniques, such as vat photopolymerization (VP), material extrusion (ME) or binder jetting (BJ). 3D printing encompasses different techniques, each of them having its own benefits and drawbacks (Figure 1). Several printing materials can be used, each with specific mechanical and accuracy properties. Sometimes, a post-curing step is required to obtain the finished product [7]. The obtained surgical models can fulfill three different

purposes: training, planning and simulating. An example of three different models is shown in Figure 2.

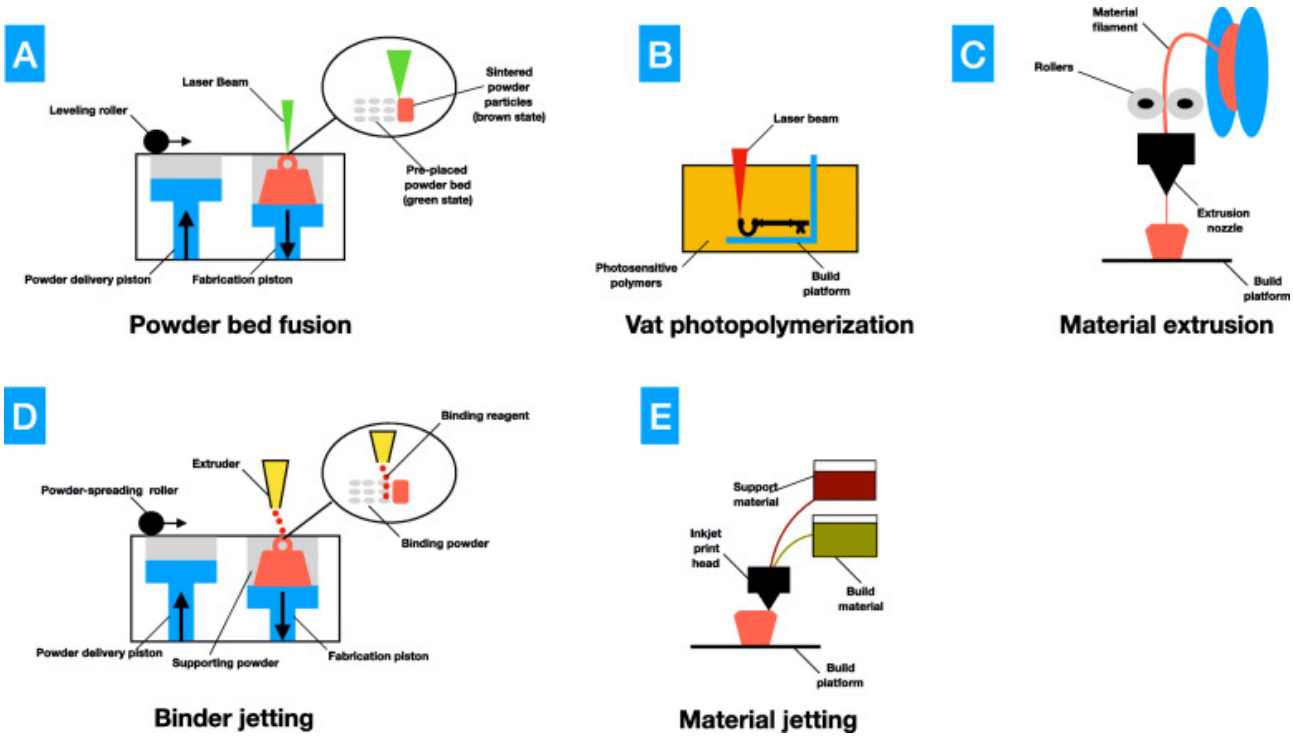

Figure 1. Schematic representation of rapid prototyping techniques for surgery applications: (a) Powder bed fusion (b) Vat photopolymeration (c) Material extrusion (d) Binder jetting (e) Material jetting.

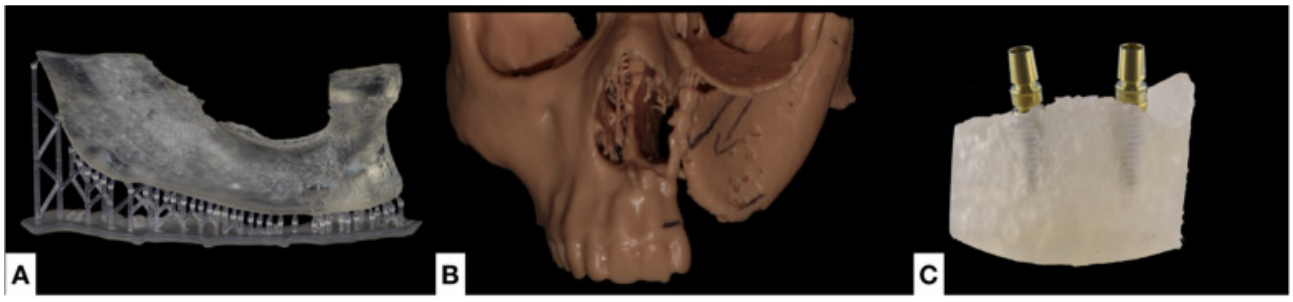

Figure 2. Examples of anatomical models fabricated by Additive manufacturing. A: A mandible model fabricated using SLA to serve as a template for bone allograft preparation during surgery. B: A model fabricated using SLA to visualize the extent of a bone defect.

A training model is produced to enhance the quality of the teaching, by allowing students and clinicians to perform high-quality surgical training. Adequate haptic feedback and moderate cost are the most important characteristic of training models. Instead of training on cadaver or animal models, students can enhance their skills on accurate 3DP models that reproduce the haptic feedback of the patient's bone [8]. Although cadaveric specimens have high anatomical and physical validity, they are often challenging to obtain, lack patient-specific pathologic features, and are associated with costs that may be prohibitive to repetitive training [9]. Several authors described temporal bone surgeries [10, 11], implant treatment or maxillary sinus floor augmentation [12] training in realistic in vitro conditions using these 3D-printed models. Thus, one of the most important characteristics of a training model is the low cost.

Secondly, a 3DP model could be made for planning complex surgeries and to fully understand the patient's conditions. The manipulation of the patient anatomical structures helps to get a better understanding of his specific condition and to plan the required surgical interventions [13]. These models are often used in orthognathic and reconstructive surgeries, giving the possibility of a better comprehension and more predictable results [14–17]. Measurements and surgical pre-operative evaluations can be performed on these models. Thus, the most important characteristic of a planning model is accuracy.

Finally, a simulating model is produced to perform a surgery before it is done in clinics. This type of models must be accurate with a patient-like haptic feedback. Users can act on these models like they are working on patients. Simulating models are used by clinicians before preforming important surgical interventions, such as tumor excisions [18] and pediatric mastoidectomy [19]. The right mechanical properties, such as the elastic modulus, the stiffness or the drilling force, are fundamental parameters that allow the operator to experience haptic feedback similar to that encountered during actual surgery. Thus, one of the most important characteristics of a simulating model is related to its mechanical properties.

A surgeon wanting to invest in a printer can be overwhelmed in his choice by the numerous options available, between printing materials and technologies. Moreover, the cost-benefit ratio must be taken into consideration, as cheap technologies can be sufficient for some applications. Our hypothesis was that each application of the surgical model could be correlated with a specific 3D printing technology. This systematic review investigated the state of the art of printing materials and techniques proposed to create models for training, simulating and planning interventions in oral and craniofacial surgery. The research focused on the regions of head and neck, scanning articles that belong to different fields: dentistry and oral surgery, maxillofacial surgery, ear-nose-throat surgery and cranial surgery. These results also provided practical suggestions for choosing the optimal 3D printing technique and material for each application objective.

MATERIALS AND METHODS

Study protocol

The protocol of this systematic review was registered in 'PROSPERO: International prospective register of systematic reviews' (CRD42019117468) and followed the PRISMA guidelines. The main question, that was not PICO compliant, was: 'What are the existing printed bone models currently used for training, planning and simulating interventions in oral and cranio-maxillofacial surgery?' The impossibility of using a PICO question and performing a meta-analysis are two missing points of PRISMA checklist.

Search strategy

Medline (PubMed) database and Scopus database were searched up to March 10, 2019 with the following equation:

(additive manufacturing OR rapid prototyping OR bone model OR bone models OR anatomical models OR anatomical model OR phantom OR phantoms OR simulation model OR simulation models OR 3D−printed models OR 3D printed models OR 3D−printed model OR 3D printed model) AND (planning OR hands−on OR train OR training OR simulation) AND (surgery OR surgical OR dentistry OR dental OR teaching OR pre−operative) AND (maxillofacial OR oral OR skull base OR jaw bones OR jaw OR sinus OR mandible OR temporal bone OR teeth OR maxilla OR human bone OR implant) NOT biology NOT cartilage NOT mathematical

This process only selected articles that had search terms in the title or in the abstract without any restriction on language.

The search was also launched with the following MeSH (PubMed) terms: *("Surgical Procedures, Operative" OR "Teaching") AND "Printing, Three-Dimensional" AND "Models, Anatomic" AND "Head".*

Other interesting original research articles were added through manual search.

Science mapping

A science mapping analysis of subject domains was performed by using keyword co-occurrence networking on VOSviewer (free software, version 1.6.15, Centre for Science and Technology Studies, Leiden University, The Netherlands, 2017). A network analysis of the Pubmed MeSH keywords was generated from the matrix of retrieved papers (threshold value at 90). The MeSH terms-document matrix allowed to measure document similarities between clusters of topics.

Study selection

All original full papers written in English/French/Italian and dealing with the fabrication of 3D printed models of head bone structures obtained from 3D imaging data were considered as potentially eligible. Case report, case series, pilot studies and comparative studies were included in this research.

Literature reviews, conference abstracts, articles employing animal tissues or cadaver models or models not aimed to the head region were excluded.

Study analysis

All the retrieved references, after launching the search algorithm, were managed using Endnote® Abstracts of studies retrieved using the search strategy and those from additional sources were screened independently by three authors (M.M, A.N. and S.C) to identify studies that potentially met the inclusion criteria. Papers fulfilling the inclusion criteria, and those presenting insufficient data in the title and the abstract to make a decision, were selected for full analysis. After reading the full texts, the proper articles were included in an evidence table. Any disagreement over the eligibility of studies was resolved through discussion and consensus among the authors.

Quality assessment

The quality of the included studies was assessed using a modified version of the Critical Appraisal Skills Programme (CASP) tool [20]. For each of the 10 questions of this tool, there were three possible answers: 'Yes', 'Can't tell' or 'No'. Every 'Yes' scored 1 point, while 'No' or 'Can't tell' scored 0 points. Total scores were converted to percentages and studies were allocated to one of three categories; 'Good quality' for a score of 67–100%, 'Average quality' for 34–66% and 'Poor quality' for 0–33%.

Data extraction

The data were extracted and critically appraised by two independent authors.

Using a standardized data extraction form, the authors extracted the following data: year of publication, data acquisition system, type of printing technique involved,

material, accuracy, production time, haptic feedback, treatment time, clinical outcomes, cost and purpose of the publication: training, planning, simulation (multiple possibilities for each paper).

Data analysis

A narrative synthesis of the data was conducted due to the heterogeneity of study designs and methods. For the same reason it was not possible to perform a meta-analysis. In order to address the general question of defining the state of the art of 3D printing to address the surgical planning, simulation and training needs, the authors identified as crucial these characteristics: accuracy, haptic feedback and cost.

RESULTS

Search general results

After database screening and removal of duplicates using Endnote® [21], 1157 articles were identified. After abstract screening, 119 studies were selected. After full text reading, 64 articles were selected, plus 5 other articles found among the related ones found by additional manual search (Figure 3). The main reason for excluding articles was a content not addressing AM models issues. Many excluded articles dealt with analogic models, virtual models or perfusion-based models, or related to the orthopedic and veterinary fields. Six articles were not written in English/French/Italian.

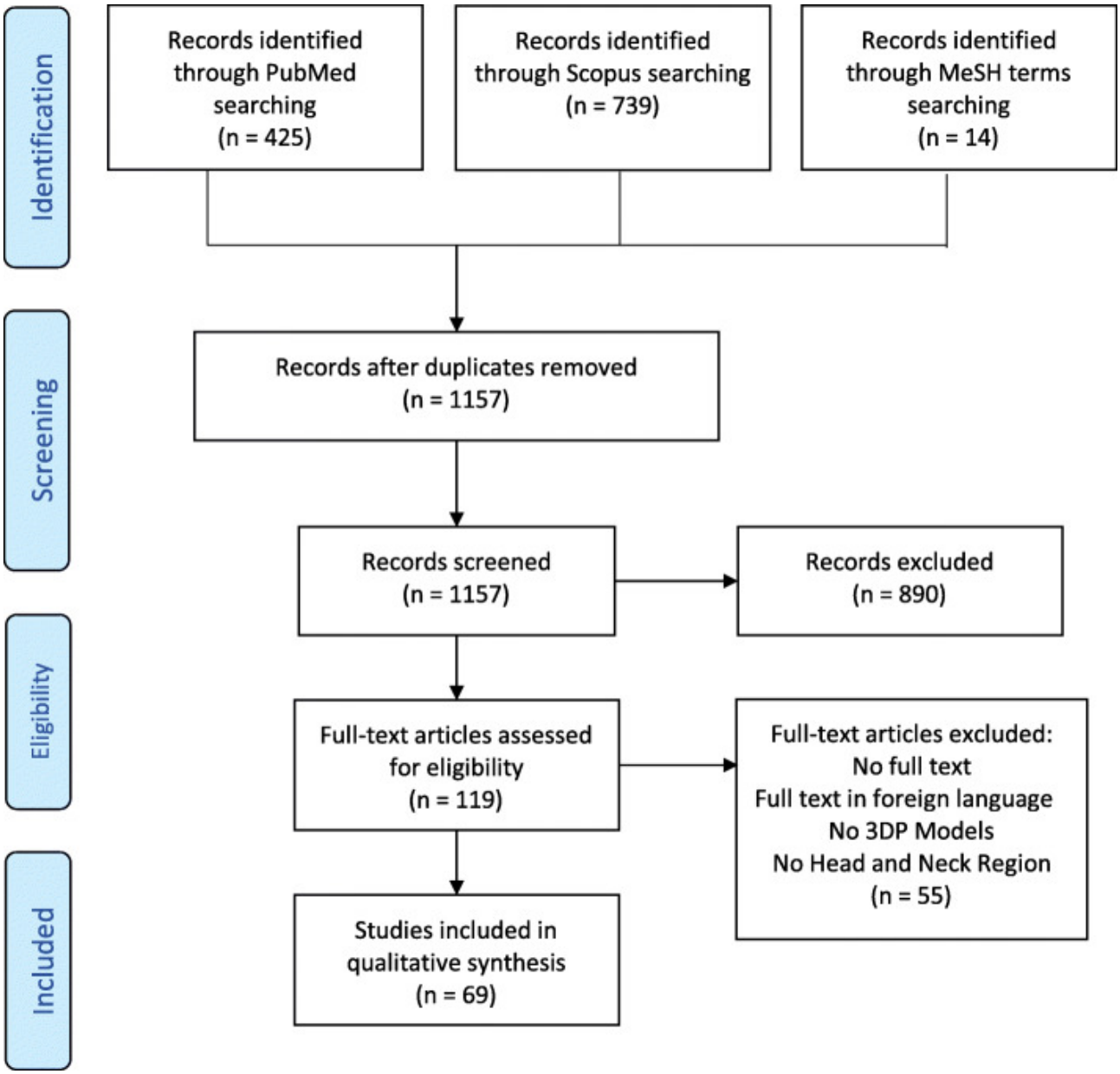

Figure 3. PRISMA flow chart

Eight articles were excluded after reviewers' discussion: three authors involved commercial models [22–24], one article dealt with papercraft models [25], one article dealt with a silicon model molded on a 3D printed mold [26] and 3 articles dealt with other surgical fields (orthopedics [27, 28] and veterinary sciences [29]).

The spatial representation of the relationships between the Mesh keywords was displayed through a science map (Figure 4). The networks noticeably highlighted the interest for modelling human patients from imaging data through a computer assisted procedure. Bone surgery, prosthetic rehabilitation and radiotherapy were among the most represented families of clinical applications. “Mandible” was the most co-occurring bone keywords. “Material testing”, “treatment outcome” and “clinical competence” were often studied. These graphic references did not show any Mesh keywords regarding the 3D printing technologies themselves (under the threshold).

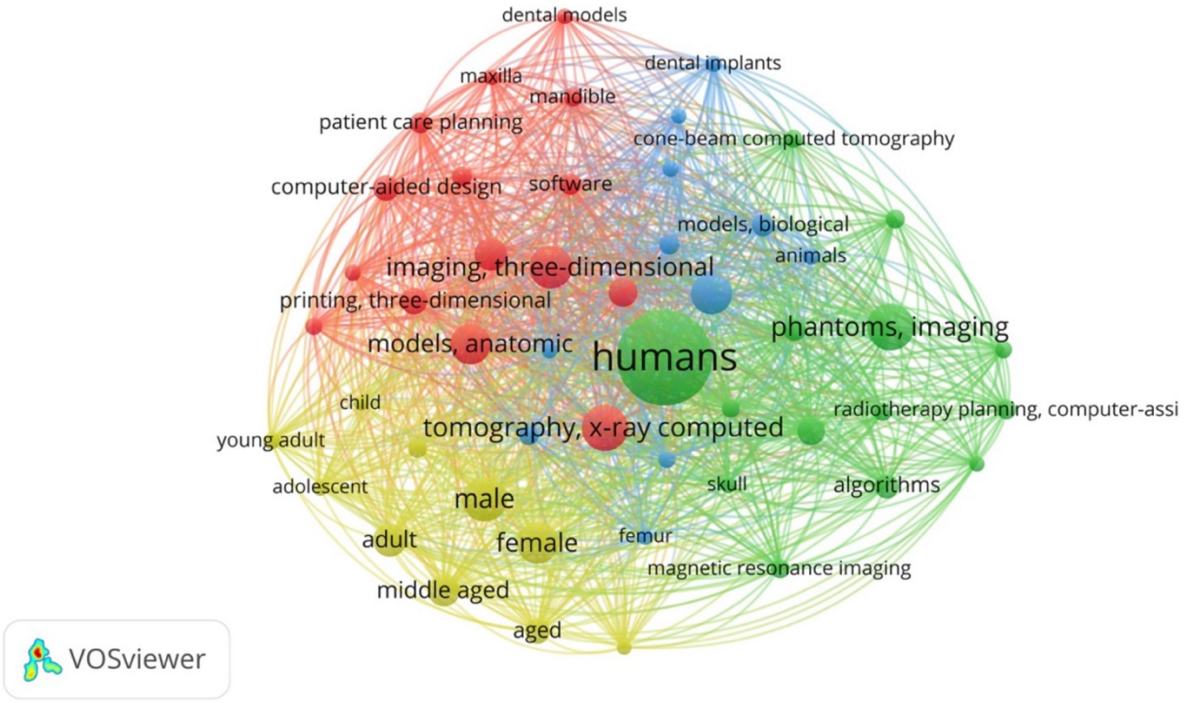

Figure 4. Mesh keyword co-occurrence networks among the retrieved articles. The size of each node is proportionate to its degree and the thickness of the links represents the tie strength.

With the modified Critical Appraisals Skills Programme (CASP) tool [20] the reviewers have identified as “high-quality studies” only 8 original researches. The authors classified as “average quality studies” and “poor quality studies” 46 and 15 articles respectively. The lack of quantitative or rigorous tests and appropriate study designs were found in most of the selected studies. (Table 1)

CASP Questions	**Results**
Was there a clear statement of the aims of this research?	High Quality
Is a qualitative methodology appropriate?	8 Articles
The research was designed appropriate to address the aims of this research?	
Was the recruitment strategy appropriate tothe aims of the research?	Average Quality
Was the data collected in a way that adressed the research issue?	46 Articles
Has the relationship between researcher and participants been adequately considered?	
Have ethical issues been taken into consideration?	Low Quality

CASP Questions	Results
Was the data analysis sufficiently rigorous?	15 Articles
Is there a clear statement of findings?	
How valuable is the research?	

Table 1. CASP questions and results of the quality assessment

Only 5 articles (6%) were published before 2008. Ten articles (18%) were published between 2009 and 2014. Forty-two articles (78%) were published between 2015 and March 10, 2019.

Among all articles, 3 were pilot studies, 12 were case reports, 4 were case series, 29 were validation studies and only 6 were comparative studies. The authors classified as “validation studies” all original researches that had described and eventually evaluated a process to fabricate a printed bone model. The reviewers classified as “comparative studies” all the researches that compared models printed by different techniques or models printed by different printers using the same technique. Lastly, a paper comparing a bone model to a cadaver’s bone was also considered as a comparative study [59]. (Table 2)

Year	Author	Study Design	Country	Domain	Treatment	Target
2019	Lanis A et al. [30]	Case Report	Chile	Dentistry	Implant treatment	Planning
2019	Freiser ME et al. [31]	Validation Study	USA	ENT Surgery	Temporal bone access	Planning, Simulation, Training
2019	Zhuo C et al. [32]	Validation Study	China	ENT Surgery	Endoscopic sinus surgery	Training, Simulation
2018	Bhadra D et al. [33]	Case Report	India	Dentistry	Endodontic retreatment	Planning
2018	Lin B et al. [34]	Validation Study	China	Cranial Surgery	Tumor removal surgery	Planning, Simulation, Training
2018	Probst R et al. [10]	Validation Study	Switzerland - Germany	Cranial Surgery	Temporal pediatric surgery, coclear implantation	Training
2018	Hsieh TY et al. [9]	Validation Study	USA	ENT Surgery	Endoscopic skull base surgery	Planning, Simulation, Training
2018	Reymus M et al. [35]	Validation Study	Germany	Dentistry	Dental traumatology	Training,
2018	Sugahara K et al. [36]	Pilot Study	Japan	Maxillofacial Surgery	Reconstruction and orthognathic surgery	Planning
2018	Werz SM et al. [37]	Validation Study	Germany	Dentistry	General dentistry	Training

Year	Author	Study Design	Country	Domain	Treatment	Target
2018	Chou PY et al. [16]	Validation Study	USA	Maxillofacial Surgery	Cleft lip and palate surgery	Simulation
2018	Arce K et al. [15]	Case Report	USA	Maxillofacial Surgery	Mandibular reconstruction	Planning
2018	Lin WJ et al. [38]	Validation Study	China	ENT Surgery	Sinus and skull base anatomical study	Training
2018	Haffner M et al. [39]	Comparative Study	USA	ENT Surgery	Mastoidectomy	Training
2018	Jacek B et al. [40]	Comparative Study	Poland	Maxillofacial Surgery	Mandibular reconstruction with bony free flap	Planning
2018	Alodadi A et al. [41]	Case Report	Saudi	Dentistry	Implantology	Planning
2018	Reddy GV et al. [42]	Validation Study	India	Maxillofacial Surgery	Orthognathic surgery	Training
2017	Favier V et al. [43]	Comparative Study	France	Cranial Surgery	Skull base endoscopic surgery	Planning, Simulation, Training
2017	Somji SH et al. [12]	Case Report	USA	Dentistry	Sinus augmentation	Planning, Simulation, Training
2017	Gargiulo P et al. [19]	Case Report	Iceland	Cranial Surgery	Tumor removal surgery	Planning, Simulation

Year	Author	Study Design	Country	Domain	Treatment	Target
2017	Alrasheed AS et al. [44]	Validation Study	Canada	Maxillofacial Surgery	Endoscopic sinus surgery	Training
2017	Wang L et al. [45]	Comparative Study	China	Maxillofacial Surgery	Aneurysm surgery	Planning, Simulation, Training
2017	Javan R et al. [46]	Pilot Study	USA	Maxillofacial Surgery	Cranial nerve anatomy	Training
2017	Legocki AT et al. [47]	Case Series	USA	Maxillofacial Surgery	Craniofacial reconstruction	Planning, Simulation, Training
2017	Takahashi K et al. [11]	Validation Study	Japan	ENT Surgery	Temporal bone dissection	Training
2017	Yusa K et al. [18]	Case Report	Japan	Maxillofacial Surgery	Tumor removal	Planning, Simulation
2017	Ghizoni E et al. [48]	Validation Study	Brazil	Maxillofacial Surgery	Craniostenosis	Training
2017	Wiedermann JP et al. [49]	Case Report	USA	Maxillofacial Surgery	Cranio-cervicofacial teratoma	Planning
2017	Oscar Mario Jacobo et Al. [50]	Validation Study	Uruguay	Maxillofacial Surgery	Mandible and orbita recostruction	Planning, Training
2016	Wanibuchi M et al. [51]	Validation Study	Japan	Maxillofacial Surgery	Mastoidectomy	Training

Year	Author	Study Design	Country	Domain	Treatment	Target
2016	Bone TM et al. [52]	Validation Study	USA	ENT Surgery	Temporal bone surgery	Training
2016	Florentino VGB et Al. [53]	Case Report	Brazil	Maxillofacial Surger	Reconstruction of temporal bone	Planning
2016	Kondo K et Al. [54]	Validation Study	Japan	Cranial Surgery	Craniotomy	Training, Simulation
2016	Lim SH et Al. [55]	Validation Study	Korea	Macillo-Facial Surgery	Mandible reconstruction	Planning
2015	Pacione D et al. [56]	Pilot Study	USA	Maxillofacial Surgery	Deformity of the skull base and craniovertebral junction	Planning
2015	Chan HHL et al. [57]	Case Series	Canada	Maxillofacial Surgery	Head and neck surgery	Training, Simulation
2015	Dickinson KJ et al. [58]	Case Report	USA	Maxillofacial Surgery	Endoscopic resection in esophagus	Planning
2015	Hochman JB et al. [59]	Comparative Study	Canada	Maxillofacial Surgery	Mastoidectomy and skull base surgery	Training
2015	Cohen J et al. [60]	Validation Study	USA	Maxillofacial Surgery	Mastoidectomy	Training
2015	Lim C et al. [17]	Case Series	Australia - New Zealand	Maxillofacial Surgery	Orbital reconstruction	Planning
2015	Rose AS et al. [61]	Case Report	USA	ENT Surgery	Mastoidectomy	Planning, Simulation

Year	Author	Study Design	Country	Domain	Treatment	Target
2015	Ernoult C. et Al. [62]	Case Series	France	Maxillofacial Surgery	Reconstructive surgery	Simulation
2015	Mowry SE. et al. [63]	Validation Study	USA	ENT Surgery	Temporal bone access	Training
2015	Hochman JB et al. [64]	Validation Study	Canada	ENT Surgery	Temporal bone surgery	Training
2015	Longfield EA et al. [65]	Validation Study	USA	ENT Surgery	Temporal pediatric surgery	Training
2015	Rose AS et al. [66]	Validation Study	USA	ENT Surgery	Temporal bone surgery	Training
2014	Hochman JB et al. [67]	Case Report	Canada	ENT Surgery	Temporal bone surgery	Training
2014	Chenebaux M et al. [68]	Validation Study	France	ENT Surgery	Temporal bone surgery	Training
2014	Narayanan V et al. [69]	Validation Study	Malaysia	ENT Surgery	Skull base surgery	Training
2014	Cui J et al. [70]	Validation Study	China	Maxillofacial Surgery	Cranial trauma	Planning
2014	Gil RS et al. [71]	Validation Study	Spain	Maxillofacial Surgery	Mandible reconstruction	Planning
2014	Jardini AL et al. [72]	Case Report	Brasil	Cranial Surgery	Cranial reconstruction	Planning
2013	Jabbour P et al. [73]	Validation Study	USA	Cranial Surgery	Presigmoid access	Training

Year	Author	Study Design	Country	Domain	Treatment	Target
2013	Li J et al. [74]	Case Series	China	Maxillofacial Surgery	Orbital reconstruction	Planning
2012	Ciocca L et al. [75]	Case Report	Italy	Maxillofacial Surgery	Mandible reconstruction	Planning
2011	Mori K et al. [76]	Validation Study	Japan	Cranial Surgery	Cerebral revascularization via skull approaches	Training, Simulation
2011	Morrison D et al. [77]	Case Report	Australia	Cranial Surgery	Cranial reconstruction	Planning
2010	Nikzad S et al. [78]	Case Report	Iran	Dentistry	Sinus lift and implant treatment	Planning
2010	Katatny IE et al. [79]	Validation Study	Australia	Maxillofacial Surgery	Mandibular surgery	Planning
2010	Lambrecht JTH et al. [80]	Case Series	Switzerland	Dentistry	Oral surgery	Training
2009	Sohmura T et al. [81]	Case Series	Japan	Dentistry	Implant treatment	Planning, Training
2009	Mori K et al. [82]	Validation Study	Japan	ENT Surgery	Skull base surgery	Training
2009	Radley GJ et al. [83]	Comparative	UK	ENT Surgery	Endoscopic sinus surgery	Training
2009	Cohen A et al. [84]	Case Series	Syria	Maxillofacial Surgery	Mandible reconstruction	Planning

Year	Author	Study Design	Country	Domain	Treatment	Target
2007	Suzuki M et al. [85]	Validation Study	Japan	ENT Surgery	Temporal bone surgery	Training
2007	Mavili ME et al. [86]	Case Series	Turkey	Dentistry	Orthognatic surgery	Planning, Simulation
2004	Suzuki M et al. [87]	Validation Study	Japan	ENT Surgery	Temporal bone access	Training
2003	Muller A et al. [88]	Case Series	Germany	Cranial Surgery	Cranioplasty, tumor removal	Planning, Simulation
1997	Löpponen H et al. [89]	Case Report	Finland	ENT Surgery	Cochlear implant	Simulation, Training

Table 2. General Information of the included studies

Purposes of the articles

The models mentioned in the selected articles were used for different purposes (Table 2). In 31 articles the models were used to plan a surgery, in 19 they were used to simulate the surgery, and in 32 they were used for training of students or clinicians. This total (82) exceeded the total number of papers, as some models were used for multiple purposes.

Surgical field

The reports on 3DP models concerned multiple surgical domains (Table 2). Oral and maxillofacial surgery had the largest share with 43% of articles describing the use of

AM models, followed by ENT surgery (29%), dentistry (14%), and cranial surgery (14%).

Therapy

In dentistry, bone models were more frequently used for simulating dental implant placement [30, 41, 81]. In oral and maxillofacial surgery, the models were more frequently used for planning a bone reconstruction [15–17, 36, 40, 47, 50, 53, 72] or a tumor removal [18, 49, 56]. The models prepared for ENT surgery were mostly used for training surgical temporal access [10, 31, 52, 63–68, 85, 87] and mastoidectomy [39, 51, 59–61]. Finally, in the field of cranial surgery, the models were most frequently used for the training of the pre-sigmoid approach [73] or craniotomy [54]. (Table 2)

Image acquisition and processing

Image acquisition and processing are the first steps to create a 3DP model (Table 3). The most frequently used radiological exam was the CT, followed by cone beam computed tomography (CBCT) and MRI. Software was used to process the radiological data. The most frequently used were Mimics® (Materialise, Leuven, Belgium), followed by OsiriX® (Pixmeo, Geneva, Switzerland) and 3D Slicer® (Surgical Planning Laboratory, Isomics Incorporated, Cambridge, USA). Most of the authors did not specify entirely their digital work-flow to create the STL printable file, making it difficult to reproduce the procedure properly.

Year	Author	Data Acquisition	Images Processing Software	Printing Technique	Material
2019	Lanis A et al. [30]	CBCT	CoDiagnostiX	Vat photopolymerization	Photosentitive Resin
2019	Freiser ME et al. [31]	CT	3D Slicer	Vat photopolymerization	Photosentitive Resin
2019	Zhuo C et al. [32]	CT	Mimics	Material Extrusion	PLA
2018	Bhadra D et al. [33]	CBCT	–	Material Extrusion	–
2018	Lin B et al. [34]	CT	Mimics	Material Jetting	Photosensitive Resin
2018	Probst R et al. [10]	μCT	–	Binder Jetting	Cast Powder and Bonding Agent
2018	Hsieh TY et al. [9]	CT	–	Material Jetting	Photosensitive Resin
2018	Reymus M et al. [35]	CBCT	InVesalius	Vat photopolymerization	Photosensitive Resin
2018	Sugahara K et al. [36]	CT	Mimics	Material Jetting	Photosensitive Resin
2018	Werz SM et al. [37]	CT	3D Slicer	Material Extrusion	PLA, ABS
2018	Chou PY et al. [16]	CT	Mimics	Material Extrusion	ABS

Year	Author	Data Acquisition	Images Processing Software	Printing Technique	Material
2018	Arce K et al. [15]	CT	Mimics	Vat photopolymerization	Photosentive Resin
2018	Lin WJ et al. [38]	CT	Mimics	Material Extrusion	PLA
2018	Haffner M et al. [39]	CT	Slicer	Material Extrusion	PLA, ABS, Nylon, PETG, PC
2018	Jacek B et al. [40]	CT	Slicer	Material Extrusion	ABS
2018	Alodadi A et al. [41]	CBCT	–	–	–
2018	Reddy GV et al. [42]	–	–	–	–
2017	Favier V et al. [43]	CT	Medical Image Segmentation Tool	Binder Jetting, Material Jetting, Powder Bed Fusion, Material Extrusion	Calcium Sulfate Hemihydrate, Opaque Resin, Polyamide, Polycarbonate
2017	Somji SH et al. [12]	CBCT	OsiriX	Vat photopolymerization	Photosensitive Resin
2017	Gargiulo P et al. [19]	CT and MRI	Mimics	Material Extrusion	ABS
2017	Alrasheed AS et al. [44]	CT	Mimics	Material Jetting	Photosensitive Resin

Year	Author	Data Acquisition	Images Processing Software	Printing Technique	Material
2017	Wang L et al. [45]	CTA	Mimics	Material Jetting	Photosensitive Resin
2017	Javan R et al. [46]	MRI	OsiriX	Powder Bed Fusion	Polyamide
2017	Legocki AT et al. [47]	–	OsiriX	Material Extrusion	PLA
2017	Takahashi K et al. [11]	CT	ZedView	Binder Jetting	Plastic Powder and Colored Binders
2017	Yusa K et al. [18]	CT and MRI	ZedView	Binder Jetting	Composite Powder
2017	Ghizoni E et al. [48]	CT	Mimics	Powder Bed Fusion	Polyamide
2017	Wiedermann JP et al. [49]	CT and MRI	–	–	–
2017	Oscar Mario Jacobo et Al. [50]	CT	–	Material Extrusion	PLA
2016	Wanibuchi M et al. [51]	–	–	Powder Bed Fusion	Polyamide and Glass Fiber
2016	Bone TM et al. [52]	CT	OsiriX	Material Extrusion	ABS

Year	Author	Data Acquisition	Images Processing Software	Printing Technique	Material
2016	Florentino VGB et Al. [53]	CT	InVesalius	–	
2016	Kondo K et Al. [54]	CT and MRI	–	Binder Jetting	Calcium sulfate hydrate
2016	Lim SH et Al. [55]	CT	Mimics	Material Jetting	–
2015	Pacione D et al. [56]	CT	Philips Intellispace Portal	Material Jetting	Photosensitive Resin
2015	Chan HHL et al. [57]	CT	Mimics	Material Extrusion	ABS, ABS and Powder, Polycarbonate
2015	Dickinson KJ et al. [58]	CT and MRI	Mimics	Material Jetting	Photosensitive Resin
2015	Hochman JB et al. [59]	CT	Mimics	Binder Jetting	Composite Powder
2015	Cohen J et al. [60]	CT	ITK-Snap	Material Extrusion	ABS
2015	Lim C et al. [17]	CT	–	Material Extrusion	–
2015	Rose AS et al. [61]	CT	Mimics	Material Jetting	Photosensitive Resin
2015	Ernoult C. et al. [62]	–	OsiriX	Material Extrusion	ABS

Year	Author	Data Acquisition	Images Processing Software	Printing Technique	Material
2015	Mowry SE. et al. [63]	CT	OsiriX	Material Extrusion	ABS
2015	Hochman JB et al. [64]	µCT	Mimics	–	–
2015	Longfield EA et al. [65]	CT	–	Binder Jetting	–
2015	Rose AS et al. [66]	CT	Mimics	Material Jetting	Photosensitive Resin
2014	Hochman JB et al. [67]	CT	Mimics	Binder Jetting	Composite Powder and Colored Binders
2014	Chenebaux M et al. [68]	CT	Magics	Vat photopolymerization	Photosensitive Resin
2014	Narayanan V et al. [69]	CT and MRI	Biomodroid	Material Jetting	Photosentive Resin
2014	Cui J et al. [70]	CT	Materialise	Powder Bed Fusion	Polystirene
2014	Gil RS et al. [71]	CT	Materialise	Vat photopolymerization, Powder Bed Fusion	–
2014	Jardini AL et al. [72]	CT	InVesalius	Binder Jetting	–
2013	Jabbour P et al. [73]	–	–	–	–
2013	Li J et al. [74]	CT	3DMSR	Powder Bed Fusion	Polystirene

Year	Author	Data Acquisition	Images Processing Software	Printing Technique	Material
2012	Ciocca L et al. [75]	CT	CFT	Material Extrusion	ABS
2011	Mori K et al. [76]	–	–	Powder Bed Fusion	Polyamide
2011	Morrison D et al. [77]	CT	Mimics	Material Extrusion	ABS
2010	Nikzad S et al. [78]	CT	Simplant	Binder Jetting	Polyamide
2010	Katatny IE et al. [79]	CT	InVesalius	Material Extrusion	ABS
2010	Lambrecht JTH et al. [80]	CBCT	Magics	Material Jetting	–
2009	Sohmura T et al. [81]	CT	VGStudio Max	Material Extrusion	ABS
2009	Mori K et al. [82]	CT	–	Powder Bed Fusion	Polyamide
2009	Radley GJ et al. [83]	µCT	Mimics	Powder Bed Fusion	Polyamide
2009	Cohen A et al. [84]	CT	Magics	Material Jetting	–
2007	Suzuki M et al. [85]	CT	–	Vat photopolymerization	–

Year	Author	Data Acquisition	Images Processing Software	Printing Technique	Material
2007	Mavili ME et al. [86]	CT	Mimics	Material Jetting	–
2004	Suzuki M et al. [87]	CT	–	Powder Bed Fusion	Polyamide
2003	Muller A et al. [88]	CT	–	Vat photopolymerization	Photosensitive resin
1997	Löpponen H et al. [89]	CT	–	Vat photopolymerization	Photosensitive resin

Table 3. Workflow's analysis of the included studies

Printing systems and materials

Material extrusion (ME) printing was the preferred technique to create models, followed by material jetting (MJ), respectively 32% and 22% of the articles (Table 3). Binder jetting and vat photopolymerization (VP) technique were both involved in 10% of papers. Powder bed fusion printers were used in 16% of articles while 9% did not mentioned the type of 3D printer involved. Among all the references selected, the most frequently used material was acrylonitrile butadiene styrene (ABS), currently only used with material extrusion printers.

Quantitative evaluation

Accuracy and mechanical characteristics are strongly dependent on the 3D printer's characteristics, on the involved printer material and the size of the model. Only three authors analyzed the mechanical properties of their models through quantitative tests [43, 67, 83]. Due to the differences in the printing materials and measuring methods, it was not possible to compare their results (Table 4). For the same reason, it is impossible to compare the model accuracy, despite the fact that several authors measured the geometric discrepancy (Table 5) [9, 43, 51, 61, 79]

Year	Author	Objective	Methods	Results
2017	Favier V et al. [43]	Evaluation of several consumer-grade materials for creating patient-specific 3D-printed skull base model for anatomical learning and surgical training.	Four different materials were compared to fabricate the models Force sensors were used to evaluate: - Average force needed to break thin walls with the surgical suction tip - Energy spent and reported instantaneous forces during a 6 mm depth drill	All materials displayed higher mechanical properties than human cadaver bone Resin and PA were not adapted because forces exceeded to break thin walls were too high (200 N). Using "Multicolor" and PC, the forces applied were 1.6 to 2.5 / 3.5 times higher than bone. Energy spent during drilling was respectively 1.6 and 2.6 times higher on bone than on PC and Multicolor. Finally, PC and Multicolor were the more adapted materials for this application.

Year	Author	Objective	Methods	Results
2014	Hochman JB et al. [67]	To generate a rapid-prototyped temporal bone model from computed tomography (CT) data with a specific focus on internal anatomic fidelity.	Three point bending tests, using a Texture Analyzer® were performed to determine the elastic modulus and yield point. Thanks to a 3-axis accelerometer the drill vibration during the drilling was evaluated on different materials.	The printed bone models were highly realistic. Void space representation was excellent with 88% concordance between cadaveric bone and the resultant rapid-prototyped temporal bone model. Ultimately, cyanoacrylate with hydroquinone was determined to be the most appropriate infiltrant for both cortical and trabecular simulation. The mechanical properties of all tested infiltrants were similar to real bone
2009	Radley GJ et al. [83]	To fabricate and characterize human sinus phantoms by 3D printing for surgery simulation	A modified surgical instrument was used to evaluate the necessary force to break thin walls made by test materials compared to cadaver bone.	The materials that could be successfully combined into a suitable fluid were polyurethanes, polishes, and suspended cellulose/polyesters (hardeners).

Table 3. Quantitative evaluations of 3DP models' mechanical properties

Year	Author	Objective	Methods	Results / Conclusion
2018	Hsieh TY et al. [9]	Fabrication of sinus and skull base 3D-printed models for endoscopic skull base surgery	Numerical measurements and image navigation were used to localize several landmarks on the CT images of the patients compared to the CT of the 3DP model. Evaluation of the surgeons perceptions (Likert scale) after dissecting printed models (Haptic Feedback and anatomical accuracy)	Comparisons demonstrated less than 5% difference between the images. Lickert scores were positive for haptic feedback (4,67/5) and anatomical accuracy (4/5)
2017	Favier V et al. [43]	Evaluation of several consumer-grade materials for creating patient-specific 3D-printed skull base model for anatomical learning and surgical training.	4 different printing materials were compared for accuracy, surgical forces needed to break and drill thin walls	PC and PA displayed the highest printing accuracy. The use of printed models in PC is a good substitute to human cadaver bone for skull base surgery simulation
2017	Legocki AT et al. [47]	Evaluation of the feasibility of using low-cost 3D printers for the fabrication of anatomical	Comparison of in-house printing process of surgical models vs commercial printed models.	Similar results for the accuracy of both techniques Nerve canal visibility, tooth root visibility, and sterilizability were inferior for in house models

Year	Author	Objective	Methods	Results / Conclusion
		models for craniofacial reconstruction	3 different mandible models Analogical measurements with digital caliper + other criteria (cost, production speed, sterilization …)	Overall, the in-house technique is adapted for education and surgical planning, including preoperative plates bending.
2016	Wanibuchi M et al. [51]	Fabrication of a 3D temporal bone model and validation of accuracy	Accuracy was investigated by fusion of the original CT of patient's temporal bone and the 3DP model's CT	The differences between both CT images were below 1 mm The printed models are adapted for surgical training.
2015	Rose AS et al. [61]	Producing a patient-specific model for pre-operative simulation in pediatric otologic surgery	Case report of cholesteatoma Measurement and comparison of distances between several anatomic landmarks (CT scan / Printed model / During surgery)	The variability was minimal, in terms of absolute distance (mm) and relative distance (%), in measurements between anatomic landmarks obtained from the patient intra-operatively, the pre-operative CT scan and the 3D-printed models.
2010	Katatny IE et al. [79]	Simulation of shape and CT values of pulmonary parenchyma and lesions of various sizes using 3DP	Comparison of patient original CT and printed model CT	High accuracy was observed Patient-specific CT imaging phantoms can be obtained by FDM printer It can be used for the calibration of CT intensity and validation of image quantification software.

Table 4. Studies including a quantitative evaluation of 3DP models' accuracy

Qualitative evaluation

Most of the authors analyzed the accuracy and haptic feedback of their models using self-made questionnaires and they usually concluded that 3DP models were accurate. Two authors declared respectively less than 100 and 125 µm of geometrical discrepancy between the real bone and the model [33, 81]. Some other authors stated that discrepancies could reach 680 µm, depending on the size of the model [47]. The haptic feedback was declared adequate in 75% of articles that investigated it through qualitative tests. A model made of calcium sulfate hemihydrate was considered “too hard” [43] and another 3DP model was “too soft” [65]. Few authors showed that it was difficult to print small bones [10, 52, 63] and it was reported that some materials melted during drilling [37, 43]. Few authors reported benefiting of a reduction in treatment time up to 20% in the operating room thanks to the models [18, 50, 75]. A third (35%) of the articles affirmed that the clinical outcomes could potentially be improved by using these techniques, thanks to the better planning and the enhanced comprehension of the patient pathological status. Considering costs and production time, ME printed models were the cheapest [38, 39, 42, 60] and the fastest printers [65, 67]. Cost-effectiveness depended on each clinical case and was more striking when several models needed [82]. Only 7% of the authors suggested that their method was not cost-effective [43, 61, 63, 78].

DISCUSSION

Our original impression was validated by the results, suggesting that, before investing in a printer, the major application of the models needs to be considered. Oral and maxillofacial models for bone surgery applications are mostly used for planning and simulating surgical interventions. Printed products exhibit a wide range of different properties, varying with the machine and the printing material. The main results showed that surgical treatment times can be reduced up to 20%, and that the failure rate tends to decrease [40, 50, 71]. Many authors suggested that clinical outcomes can be improved, but their findings were not supported by any control group [12, 18, 19, 33–36, 41, 42, 50, 56, 58, 76, 78, 86]. Only Banaszewski et al. involved a control group to compare the use of the 3D printed model for planning the surgical reconstruction of the mandible to the traditional technique. They found that the functional and aesthetic results were greater in the group where a 3DP models were applied [41]. A planning model needs to be accurate, but cheap also, as one patient cannot cover extensively all expenses. A training model requires essentially to reproduce relevant haptic feedback and to be an inexpensive investment. These two qualities are also expected to simulate a surgical intervention, but also with a high level of accuracy.

Accuracy

The MJ printers are currently the most accurate printers, with printed models exhibiting a geometrical discrepancy of 90 µm when compared to the patient's bone [76]. The second most accurate printing technique, according to the analyzed articles, is powder bed fusion (PBF). Wanibuchi et al. showed an accuracy ranging from 100 µm to 300 µm on a temporal bone model measured with a digital caliper [51]. This result was confirmed by another study where a geometrical discrepancy of 150 µm was observed between the model and the bone [43]. BJ and ME were reported to be less accurate methods. A geometrical discrepancy of 400 µm was observed when using a BJ printer to print a skull base [43]. Most of the researches involving ME printers did not measure quantitatively the models' accuracy, except in one case where they reported a discrepancy reaching 680µm [47]. Our study did not retrieve any paper measuring the accuracy of VP printers, but was previously reported as being high [8]. The lack of quantitative evaluation of the printing accuracy was one of the major limitations of the studies included in this review. The accuracy is related to the printer, the radiological image segmentation process, the size of the printed object and the printing material. For example, a ME printer cannot reach the same precision as an VP or MJ printer due for first to the dimension of the nozzle, but its accuracy could be sufficient to reach the operator's purposes. Depending on the radiological images processing technique a 3D-printed model will always exhibit some discrepancies, the operator has to keep it in mind processing the radiological data.

Haptic feedback

Good haptic feedback is the most important characteristic of training models and it is strongly dependent on the mechanical characteristics of the printing material. The two fundamental parameters for a model that aims to reproduce the bone haptic feedback are adequate elastic modulus and tensile strength. No quantitative test is currently available to describe the surgeon's haptic feedback during a surgical intervention. Most of the authors created their own questionnaires and asked students and surgeons with different experience about their sensations. Thus, the results were difficult to compare as evaluation protocols were different and because of the conclusions subjective. However, most of them were satisfied with their printed models.

The principal materials for ME printers were polylactic acid (PLA), ABS, polycarbonate (PC), polyethylene terephthalate glycol-modified (PETG) and nylon. In the articles included in this review, there was no consensus regarding the best material to reproduce the bone characteristics. One of the PLA's advantages was its biological properties, as it is known to be biodegradable and non-toxic. Moreover, its haptic feedback was similar to bone at low temperature while drilling [37]. Haffner et al., compared five different materials, and stated that PETG was the most realistic material, followed by PC, PLA and ABS. Nylon properties were considered as not realistic enough [39]. PC was blamed to melt too easily during drilling while ABS could easily reproduce the bone haptic feedback during a cortical mastoidectomy [43].

Favier et al. compared the mechanical characteristics of their models. With Young's Modulus respectively of 2000–3000 N/mm2 and 1700 N/mm2, the MJ and PBF printed models were considered as realistic. Regarding PBF printing, Mori et al. reported that their model was realistic but the feeling of drilling the cancellous part of the bone model lacked the 'crispy touch' of real bone [82]. This subjective declaration underlines the need for objective criteria to evaluate the haptic feedback of the models. Among all the materials used in the BJ printing technique, cyanoacrylate powder with hydroquinone resembled the most to sheep cortical bone, which was often used as a surgical training model [85].

Unfortunately, no author did quantitative or comparative tests using models printed by VP. However, most authors suggested that this technique was efficient for creating adequate models, enhancing the quality of the training [12, 35] and suitable for planning complex surgeries [15] or dental implant treatments [30].

The segmentation technique is also an important parameter that it has to be considered for obtaining realistic 3D printed models. Segmenting the trabecular bone structures results in more realistic haptic feedback when compared to fully solid prints.

Cost

Cost remains an important parameter that cannot be ignored. There are multiple additional costs in terms of software, printers, printing materials, operators and training hours to produce an in-house 3DP model.

To print a model, the first step is to process the DICOM file into an STL file. Among all the commercial software available, the commercial software package Mimics®, was the most widely used software, despite a relatively high cost when compared to others. Many free or open-source software are available, like ITK-Snap®, Slicer® or InVesalius® [31, 35, 39, 40, 60, 79]. OsiriX® possesses a free version (demo) that allows to export STL renderings [12, 46, 47, 52, 63].

ME printers were the cheapest printers, with reported prices ranging between 2500$ and 3000$ [47, 82]. However, as previously mentioned, these showed limitations in terms of accuracy. PLA and ABS were the cheapest reported materials [32, 37, 39, 47, 52, 82]. PC cost was reported to range from 105$ to 155$ for the production of a mandible [43, 57]. The cost for a temporal bone model using BJ was around 400$ [67]. MJ models costs ranged from 270$ to 1000$. One team affirmed that these models were too expensive [66], but two others suggested that they were satisfied by their investment in these models [15, 56]. LS printers are not cheap, but no authors talked mentioned any price. Printing a skull base using polyamide with an LS printer was reported to cost 250–280$ [85]. Two teams used VP printers and they declared being satisfied by the results [12, 35]. A forgotten cost is related to the post-curing machine for object printed trough VP technologies.

The production time can also be considered as a decisive cost. ME printers were the fastest, producing a pediatric temporal bone model in 4.5 h and a mandible with a maxilla in 6 h [37, 39]. The production time of an MJ model was less than a day [9, 56].

The time needed to design the STL file is also important to consider. Only one author discussed about the total production time of a LS printer and reported a need for 4 to 5 days [43]. The learning curve of a few months to master and to properly use the software for STL processing is obvious. In every case, the conversion from the DICOM to an adequate STL file could take several hours. One author reported that “the 3DP technique is really cost-effective, only if the operator plans to produce several models to amortize the cost of the 3D printer” [82].

It’s important to know these costs because the cost-benefit ratio has to be considered before investing in this technique that can get several advantages, but it presents some drawbacks in comparison to traditional techniques [63, 78].

Suggestions

As pre-surgical tools, 3D models can make the surgical outcomes more predictable and safer, reducing the surgeon’s stress and the intervention time [40, 50]. Furthermore, they can strongly improve the quality of clinical education, allowing students to simulate various surgical interventions and to discuss easily about their clinical cases with their mentors [34, 35, 42].

Evaluating the best image processing workflow remains difficult as no author described neither the entire workflow not the human cost involved. The most used training models are made with ME printers. This technology is the cheapest and allows producing suitable training models, despite their limited accuracy. The most appropriate ME printing materials are ABS, PLA and PETG [43]. Temporal bone models

printed with PETG were reported to ensure adequate haptic feedback while perform drilling, and they were very helpful during training sessions [39].

To obtain an adequate simulation model, BJ and VP printers seem more indicated. They showed adequate performances in reproducing training models of the maxilla and their accuracy is really satisfying for creating planning models [12, 18]. It is also possible to create models for simulating surgeries, thanks to their good haptic feedback [12, 14, 18]. Also MJ printers allow to produce models that provide good haptic feedback and that can be used to simulate complex surgeries before entering the operating room [14]. Generally, they cost more than the VP ones, as well as the BJ ones [35, 61]. PBF printers allow to produce accurate bone models in polyamide and glass fiber, but without satisfying haptic feedback [82].

Printing time and cost are very variable, depending directly on the type of 3D printer, the printing material, the accuracy and the mechanical characteristics required. Figure 5 demonstrates the main differences among the analyzed 3D printing technologies, depending on the applications.

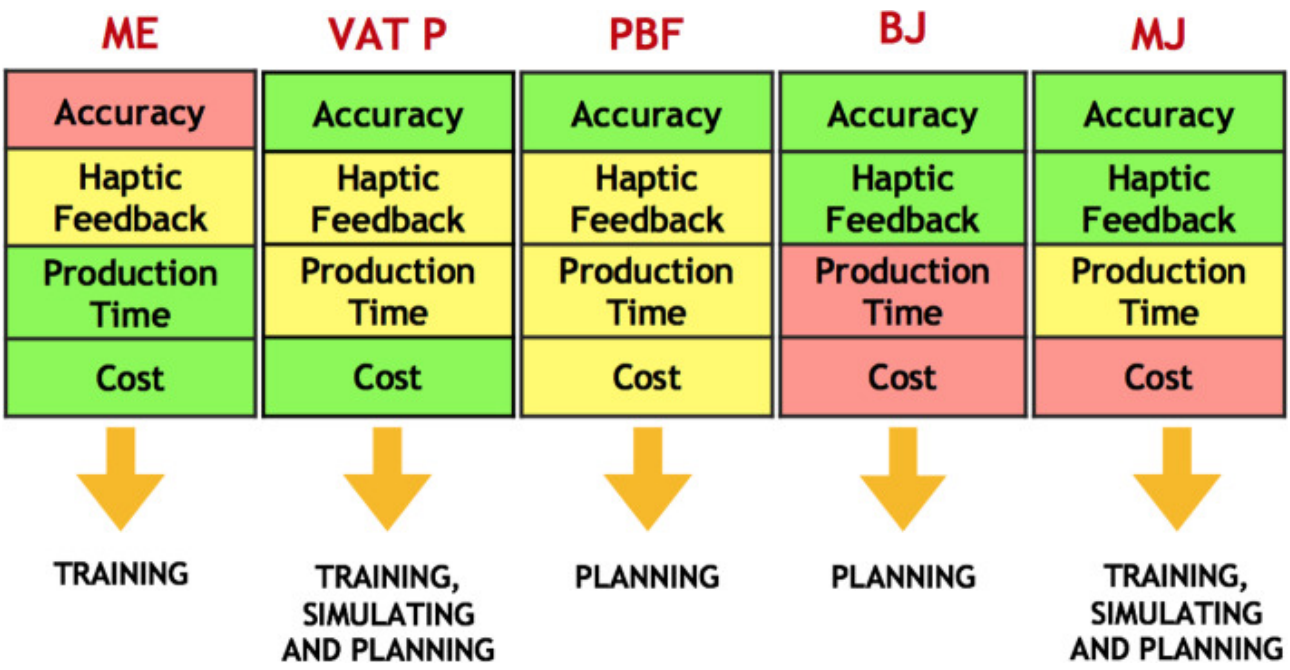

Figure 5. Advantages (green) and limitations (red) of different 3D printing technology to create 3D anatomical models. These characteristics lead the choice for the best 3D printer technique for every clinical or academical purpose

CONCLUSION

The present literature review showed that nowadays, AM models are useful tools in the surgical field. Several parameters must be considered before choosing a 3D printing model workflow, such as the processing software, the type of 3D printer, the expected mechanical characteristics, accuracy and haptic feedback of the printing material, the production time and the human and material costs.

Due to the large amount of different parameters that must be considered by the operator, the financial investment in a 3D printer should be made with the precise idea of the final application.

Limitations

This analysis was at first limited by the diversity of workflows and applications, involving different materials, printers and testing methods. Despite difficulties for comparing results from a study to another, some common protocols were found for the 3 main purposes of 3D-printed bone models (planning, simulation and training). The lack of common reliable qualitative tests to evaluate the models was an evident limitation, thus future studies should focus on standardized methods to evaluate 3D-printed models of bone macro- and micro-structures.

BIBLIOGRAPHY

[1] Naveau A, Bou C, Sharma A. Evolution of Topics in Maxillofacial Prosthetics Publications. *Int J Prosthodont* **2018** 31(6):565–568.

[2] ASTM International. Standard Terminology for Additive Manufacturing Technologies 1,2. **2013** 2–4.

[3] D'Haese J, Ackhurst J, Wismejier D, et al. Current state of the art of computer-guided implant surgery. *Periodontology 2000* **2017** 73(25):121–133.

[4] Lin HH, Lonic D, Lo LJ, et al. 3D printing in orthognathic surgery − a literature review. *J Formos Med Assoc* **2018** 117(7):547–558.

[5] Gonzalez Perez Somarriba B, Centeno G, Vallellano C et al. Evaluation of total alloplastic temporo-mandibular joint replacement with two different

types of prostheses: A three-year prospective study. *Med Oral Patol Oral Cir Bucal* **2016** 21(6):e766-e775.

[6] Champeaux C, Froelich S and Caudron Y. Titanium Three-Dimensional Printed Cranioplasty for Fronto-Nasal Bone Defect **2019** 30(6):1802–1805.

[7] Park JY, Gao G, Jang J, Cho D. 3D printed structures for delivery of biomolecules and cells: tissue repair and regeneration. *J Mater Chem B* **2016** 10.1039/C6TB01662F.

[8] Crafts TD, Ellsperman SE, Wannemuehler TJ, Bellicchi TD, Shipchandler TZ, Mantravadi AV. Three-Dimensional Printing and Its Applications in Otorhinolaryngology. *Head Neck Surg* **2017** 156(6):999–1010.

[9] Hsieh TY, Cervenka B, Dedhia R, Strong EB, Steele T. Assessment of a patient-specific, 3-dimensionally printed endoscopic sinus and skull base surgical model. *JAMA Otolaryngol - Head Neck Surg* **2018** 144(7):574–579.

[10] Probst R, Stump R, Mokosch M, Röösli C. Evaluation of an infant temporal-Bone model as training tool. *Otol Neuroto.* **2018** 39(6):e448–e452.

[11] Takahashi K, Morita Y, Ohshima S, Izumi S, Kubota Y, Yamamoto Y, Takahashi S, Horii A. Creating an optimal 3D printed model for temporal Bone dissection training. *Ann Otol Rhinol Laryngol* **2017** 126(7):530–536.

[12] Somji SH, Valladares A, Ho Kim S, Cheng Paul Yu Y, Froum SJ. The use of 3D models to improve sinus augmentation outcomes - a case report. *Singap Dent J* **2017** 38:63–70.

[13] Marconi S, Pugliese L, Botti M, et al. Value of 3D printing for the comprehension of surgical anatomy. *Surg Endosc* **2017** 10.1007/s00464-017-5457-5.

[14] Xiao Y, Sun X, Wang L, Zhang Y, Chen K, Wu G. The application of 3D printing Technology for Simultaneous Orthognathic Surgery and Mandibular Contour Osteoplasty in the treatment of craniofacial deformities. *Aesthet Plast Surg* **2017** 41(6):1413–1424.

[15] Arce K, Waris S, Alexander AE, Ettinger KS. Novel patient-specific 3D printed fixation tray for mandibular reconstruction with fibular free flaps. *J Oral Maxillofac Surg* **2018**

[16] Chou PY, Hallac RR, Shih E, et al. 3D-printed models of cleft lip and palate for surgical training and patient education. *Cleft Palate-Craniofacial J* **2018** 55(3):323–327

[17] Lim C, Campbell D, Cook N, Erasmus J. A case series of rapid prototyping and intraoperative imaging in orbital reconstruction. *Craniomaxillofacial Trauma Reconstr* **2015** 08(02):105–110

[18] Yusa K, Yamanochi H, Takagi A, Iino M. Three-dimensional printing model as a tool to assist in surgery for large mandibular tumour: a case report. *J Oral Maxillofac Res* **2017** 8(2):1–7.

[19] Gargiulo P, Arnadottir I, Gislason M, Edmunds K, Olafsson I. New directions in 3D medical modeling: 3D-printing anatomy and functions in neurosurgical planning. *J Healthc Eng* **2017**

[20] Critical Appraisal Skills Programme (2018). CASP Qualitative Checklist. [online] Available at: https://casp-uk.net/wp-content/uploads/2018/01/CASP-Qualitative-Checklist-2018.pdf. Accessed: 20/11/2018. 1994;(2018).

[21] EndNote X9, Clarivate Analytics, Web of Science. Philadelphia; Clarivate. 2013(64).

[22] He LH, Purton D, Swain M. A novel polymer infiltrated ceramic for dental simulation. *J Mater Sci Mater Med* **2011** 22(7):1639–1643.

[23] He LH, Foster Page L, Purton D. An evaluation of dental operative simulation materials. *Dent Mater J* **2012** 31(4):645–649.

[24] Güth JF, Ponn A, Mast G, Gernet W, Edelhoff D. Description and evaluation of a new approach on pre-clinical implant dentistry education based on an innovative simulation model. *Eur J Dent Educ* **2010** 14(4):221–226.

[25] Hiraumi H, Sato H, Ito J. Papercraft temporal bone in the first step of anatomy education. *Auris Nasus Larynx* **2017** 44(3):277–281.

[26] Chang DR, Lin RP, Bowe S, et al. Fabrication and validation of a low-cost, medium-fidelity silicone injection molded endoscopic sinus surgery simulation model. *Laryngoscope* **2017** 127(4):781–786

[27] Wang MY, Wang JQ, Shi Y, et al. Printed three-dimensional anatomic templates for virtual preoperative planning before reconstruction of old pelvic injuries. *Chin Med J* **2015** 128(4):477–482

[28] Brouwers L, Teutelink A, van Tilborg FAJB, de Jongh MAC, Lansink KWW, Bemelman M. Validation study of 3D-printed anatomical models using 2 PLA printers for preoperative planning in trauma surgery, a human cadaver study. *Eur J Trauma Emerg Surg* **2018** 0(0):1–8

[29] Athanasiou KA, Verstraete FJM, Winer JN, Cissell DD, Arzi B, Lucero S. The application of 3-dimensional printing for preoperative planning in oral and maxillofacial surgery in dogs and cats. *Vet Surg* **2017** 46(7):942–951.

[30] Lanis A, Alvarez del Canto O, Barriga P, Polido WD, Morton D. Computer-guided implant surgery and full-arch immediate loading with prefabricated-metal framework-provisional prosthesis created from a 3D printed model. *J Esthet Restor Dent* **2019** 31(3):199–208

[31] Freiser ME, Ghodadra A, Hirsch BE, AA MC. Evaluation of 3D Printed Temporal Bone Models in Preparation for Middle Cranial Fossa Surgery. *Otol Neurotol* **2019** 40(2):246–253

[32] Zhuo C, Lei L, Yulin Z, et al. Creation and validation of three-dimensional printed models for basic nasal endoscopic training. *Int Forum Allergy Rhinol* **2019** 00(0):1–7

[33] Bhadra D, Shah NC, Arora A, Meetkumar SD. Deducing a surgical dilemma using a novel three Dimensionaldimensional printing technique Dhaval. *J Conserv Dent* **2018** 21:582–585

[34] Lin B, Zhu Y, Liu Y, et al. Using three-dimensional printing to create individualized cranial nerve models for Skull Base tumor surgery. *World Neurosurg* **2018** 120:e142–e152

[35] Reymus M, Fotiadou C, Hickel R, Diegritz C. 3D-printed model for hands-on training in dental traumatology. *Int Endod J* **2018** 51(11):1313–1319.

[36] Sugahara K, Takano M, Koyama Y, et al. Novel condylar repositioning method for 3D-printed models. Maxillofac Plast Reconstr Surg **2018** 40(1):0–4.

[37] Werz SM, Zeichner SJ, Berg BI, Zeilhofer HF, Thieringer F. 3D printed surgical simulation models as educational tool by maxillofacial surgeons. *Eur J Dent Educ* **2018** 22(3):e500–e505.

[38] Lin WJ, Lin W, Lin JC, et al. A novel three-dimensional-printed paranasal sinus–skull base anatomical model. *Eur Arch Oto-Rhino-Laryngol* **2018** 275(8):2045–2049

[39] Haffner M, Quinn A, Hsieh TY, Strong EB, Steele T. Optimization of 3D print material for the recreation of patient-specific temporal Bone models. *Ann Otol Rhinol Laryngol* **2018** 127(5):338–343

[40] Jacek B, Radosław W, Wiesław K, et al. 3D printed models in mandibular reconstruction with bony free flaps. *J Mater Sci Mater Med* **2018** 29(2):10–15.

[41] Alodadi A. Utilizing three-dimensional printing in treating challenged dental implant cases. *World J Dent* **2018** 9(3):235–241

[42] Reddy GV, Vasamsetty P, Kumar Malyala S, Alwala A. Training young maxillofacial surgeons or trainees using additive manufacturing. *Mater Today Proc.* **2018** 5(2):4046–4049.

[43] Favier V, Zemiti N, Mora OC, Subsol G, Captier G, Lebrun R, Crampette L, Mondaine M, Gilles B. Geometric and mechanical evaluation of 3D-printing materials for skull base anatomical education and endoscopic surgery simulation - A first step to create reliable customized simulators. *PLoS One* **2017** 12(12):e0189486.

[44] Alrasheed AS, Nguyen LHP, Mongeau L, Funnell WRJ, Tewfik MA. Development and validation of a 3D-printed model of the ostiomeatal complex and frontal sinus for endoscopic sinus surgery training. *Int Forum Allergy Rhinol* **2017** 7(8):837–841.

[45] Wang L, Ye X, Hao Q, et al. Comparison of two three-dimensional printed models of complex intracranial aneurysms for surgical simulation. *World Neurosurg* **2017** 103:671–679

[46] Javan R, Davidson D, Javan A. Nerves of steel: a low-cost method for 3D printing the cranial nerves. *J Digit Imaging* **2017** 30(5):576–583.

[47] Legocki AT, Duffy-Peter A, Scott AR. Benefits and limitations of entry-level 3-dimensional printing of maxillofacial skeletal models. *JAMA Otolaryngol - Head Neck Surg* **2017** 143(4):389–394

[48] Ghizoni E, Ph D, Paulo J, et al. 3D-printed Craniosynostosis model: a new simulation surgical tool. *World Neurosurg* **2017**

[49] Wiedermann JP, Joshi AS, Jamshidi A, Conchenour C, Preciado D. Utilization of a submental island flap and 3D printed model for skull base reconstruction: infantile giant cranio-cervicofacial teratoma. *Int J Pediatr Otorhinolaryngol* **2017** 92:143–145

[50] Jacobo OM, Giachero VE, Hartwig DK, Mantrana GA. Three-dimensional printing modeling: application in maxillofacial and hand fractures and resident training. *Eur J Plast Surg* **2018** 41(2):137–146.

[51] Wanibuchi M, Noshiro S, Sugino T, et al. Training for Skull Base surgery with a colored temporal Bone model created by three-dimensional printing technology. *World Neurosurg* **2016** 91:66–72.

[52] Bone TM, Mowry SE. Content validity of temporal Bone models printed via inexpensive methods and materials. *Otol Neurotol* **2016** 37(8):1183–1188.

[53] Florentino VGB, De Mendonça DS, Bezerra AV, et al. Reconstruction of frontal bone with custom-made prosthesis using rapid prototyping. *J Craniofac Surg* **2016** 27(4):e354–e356

[54] Kondo K, Harada N, Masuda H, et al. A neurosurgical simulation of skull base tumors using a 3D printed rapid prototyping model containing mesh structures. *Acta Neurochir* **2016** 158(6):1213–1219

[55] Lim SH, Kim YH, Kim MK, Nam W, Kang SH. Validation of a fibula graft cutting guide for mandibular reconstruction: experiment with rapid prototyping mandible model. *Comput Assist Surg* **2016** 21(1):9–17.

[56] Pacione D, Tanweer O, Berman P, Harter DH. The utility of a multimaterial 3D printed model for surgical planning of complex deformity of the skull base and craniovertebral junction. *J Neurosurg* **2016** 125(11):1194–1197.

[57] Chan HHL, Siewerdsen JH, Vescan A, Daly MJ, Prisman E, Irish JC. 3D rapid prototyping for otolaryngology-head and neck surgery: applications in image-guidance, surgical simulation and patient-specific modeling. *PLoS One* **2015** 10(9):1–18.

[58] Dickinson KJ, Matsumoto J, Cassivi SD, et al. Individualizing Management of Complex Esophageal Pathology Using Three-Dimensional Printed Models. *Ann Thorac Surg* **2015** 100(2):692–697

[59] Hochman JB, Rhodes C, Wong D, Kraut J, Pisa J, Unger B. Comparison of cadaveric and isomorphic three-dimensional printed models in temporal bone education. *Laryngoscope.* **2015** 125(10):2353–2357

[60] Cohen J, Reyes SA. Creation of a 3D printed temporal bone model from clinical CT data. *Am J Otolaryngol - Head Neck Med Surg* **2015** 36(5):619–624

[61] Rose AS, Webster CE, Harrysson OLA, Formeister EJ, Rawal RB, Iseli CE. Pre-operative simulation of pediatric mastoid surgery with 3D-printed temporal bone models. *Int J Pediatr Otorhinolaryngol* **2015** 79(5):740–744

[62] Ernoult C, Bouletreau P, Meyer C, Aubry S, Breton P, Bachelet JT. Reconstruction assistée par l'impression 3D en chirurgie maxillofaciale. *Rev Stomatol Chir Maxillofac Chir Orale.* **2015** 116(2):95–102

[63] Mowry SE, Jammal H, Myer C, Solares CA, Weinberger P. A novel temporal bone simulation model using 3D printing techniques. *Otol Neurotol* **2015** 36(9):1562–1565

[64] Hochman JB, Rhodes C, Kraut J, Pisa J, Unger B. End user comparison of anatomically matched 3-dimensional printed and virtual haptic temporal Bone simulation: a pilot study. *Otolaryngol - Head Neck Surg (United States)* **2015** 153(2):263–268

[65] Longfield EA, Brickman TM, Jeyakumar A. 3D printed pediatric temporal Bone. *Otol Neurotol.* **2015** 36(5):793–795

[66] Rose AS, Kimbell JS, Webster CE, Harrysson OLA, Formeister EJ, Buchman CA. Multi-material 3D models for temporal bone surgical simulation. *Ann Otol Rhinol Laryngol.* **2015** 124(7):528–536

[67] Hochman JB, Kraut J, Kazmerik K, Unger BJ. Generation of a 3D printed temporal bone model with internal fidelity and validation of the mechanical construct. *Otolaryngol - Head Neck Surg (United States).* **2014** 150(3):448–454.

[68] Chenebaux M, Lescanne E, Robier A, Kim S, Bakhos D. Evaluation of a temporal bone prototype by experts in otology. *J Laryngol Otol* **2014** 128(7):586–590

[69] Narayanan V, Narayanan P, Rajagopalan R, et al. Endoscopic skull base training using 3D printed models with pre-existing pathology. *Eur Arch Oto-Rhino-Laryngology* **2015** 272(3):753–757

[70] Cui J, Chen L, Guan X, Ye L, Wang H, Liu L. Surgical planning, three-dimensional model surgery and preshaped implants in treatment of bilateral craniomaxillofacial post-traumatic deformities. *J Oral Maxillofac Surg* **2014** 72(6):1138.e1–1138.e14

[71] Gil RS, Roig AM, Obispo CA, Morla A, Pagès CM, Perez JL. Surgical planning and microvascular reconstruction of the mandible with a fibular flap using computer-aided design, rapid prototype modelling, and precontoured titanium reconstruction plates: a prospective study. *Br J Oral Maxillofac Surg* **2015** 53(1):49–53.

[72] Jardini AL, Larosa MA, Filho RM, et al. Cranial reconstruction: 3D biomodel and custom-built implant created using additive manufacturing. *J Cranio-Maxillofacial Surg* **2014** 42(8):1877–1884.

[73] Jabbour P, Chalouhi N. Simulation-based neurosurgical training for the presigmoid approach with a physical model. *Neurosurgery* **2013** 73(4):2011–2014

[74] Li J, Li P, Lu H, et al. Digital design and individually fabricated titanium implants for the reconstruction of traumatic zygomatico-orbital defects. *J Craniofac Surg* **2013** 24(2):363–368

[75] Ciocca L, Mazzoni S, Fantini M, Persiani F, Marchetti C, Scotti R. CAD/CAM guided secondary mandibular reconstruction of a discontinuity defect after ablative cancer surgery. *J Cranio-Maxillofacial Surg* **2012** 40(8):e511–e515

[76] Mori K, Yamamoto T, Nakao Y, Esaki T. Surgical simulation of cerebral revascularization via skull base approaches in the posterior circulation using three-dimensional skull model with artificial brain and blood vessels. *Neurol Med Chir (Tokyo)* **2011** 51(2):93–96

[77] Morrison DA, Guy DT, Day RE, Lee GYF. Simultaneous repair of two large cranial defects using rapid prototyping and custom computer-designed titanium plates: a case report. *Proc Inst Mech Eng Part H J Eng Med.* **2011** 225(11):1108–1112

[78] Nikzad S, Azari A, Ghassemzadeh A. Modified flapless dental implant surgery for planning treatment in a maxilla including sinus lift augmentation

through use of virtual surgical planning and a 3-dimensional model. *J Oral Maxillofac Surg* **2010** 68(9):2291–2298

[79] Katatny IE, Masood SH, Morsi YS. Evaluation and Validation of the Shape Accuracy of FDM Fabricated Medical Models. *Adv Mater Res* **2009** 83–86:275–280.

[80] Lambrecht JTH, Berndt D, Christensen AM, Zehnder M. Haptic model fabrication for undergraduate and postgraduate teaching. *Int J Oral Maxillofac Surg* **2010** 39(12):1226–1229.

[81] Sohmura T, Kusumoto N, Otani T, Yamada S, Wakabayashi K, Yatani H. CAD/CAM fabrication and clinical application of surgical template and bone model in oral implant surgery. *Clin Oral Implants Res* **2009** 20(1):87–93.

[82] Mori K. Dissectable modified three-dimensional temporal bone and whole skull base models for training in skull base approaches. *Skull Base* **2009** 19(5):333–343.

[83] Radley GJ, Sama A, Watson J, Harris RA. Characterization, quantification, and replication of human sinus bone for surgery simulation phantoms. *Proc Inst Mech Eng Part H J Eng Med* **2009** 223(7):875–887.

[84] Cohen A, Laviv A, Berman P, Nashef R, Abu-Tair J. Mandibular reconstruction using stereolithographic 3-dimensional printing modeling technology. *Oral Surg Oral Med Oral Pathol Oral Radiol Endodontol* **2009** 108(5):661–666.

[85] Suzuki M, Hagiwara A, Ogawa Y, Ono H. Rapid-prototyped temporal bone and inner-ear models replicated by adjusting computed tomography thresholds. *J Laryngol Otol.* **2007** 121(11):1025–1028.

[86] Mavili ME, Canter HI, Saglam-Aydinatay B, et al. Use of three-dimensional medical modeling methods for the precise planning of orthognathic surgery. *J Craniofacial Surg* **2007** 18(4):740–7

[87] Suzuki M, Ogawa Y, Kawano A, Hagiwara A, Yamaguchi H, Ono H. Rapid prototyping of temporal bone for surgical training and medical education. *Acta Otolaryngol* **2004** 124(4):400–402

[88] Müller A, Krishnan KG, Uhl E, Mast G. The application of rapid prototyping techniques in cranial reconstruction and preoperative planning in neurosurgery. *J Craniofac Surg* **2003** 14(6):98

[89] Löppönen H, Holma T, Sorri M, et al. Computed tomography data based rapid prototyping model of the temporal bone before cochlear implant surgery. *Acta Oto-Laryngologica, Suppl* **1997** 6489(529):47–49.

Chapter III

A novel self-assessment method for training access cavity on 3D printed endodontic models

INTRODUCTION

The primary goal of root canal treatment is to heal or prevent apical periodontitis [1], a tooth disorder highly frequent among adults [2]. Since the endodontic specialty it is still not established in Italy, root canal treatments are frequently performed by general dentists, who, in many cases, do not reach optimal standards [3,4]. The average quality of endodontic treatments performed by general dentists was found suboptimal also in other countries [5-7]. A possible cause could be an inadequate training during the undergraduate curriculum [8].

Pre-clinical training is a fundamental learning step for dental students to become familiar with the techniques and procedures that they will then apply in a clinical setting [9]. In consideration of the importance of pre-clinical training in dental education, every improvement is strongly encouraged and new technologies can serve this purpose [10]. In a joined position statement of the European Society of Endodontology (ESE) and Association for Dental Education in Europe (ADEE) it was

recommended the development of intelligent systems to facilitate preclinical skills training and to provide instantaneous feedback on performance [11].

Extracted teeth have long been used in pre-clinical training in endodontics because they are cost-free, allows students to practice with a range of anatomical variations and pathologies and provide valuable haptic feedback, allowing students to develop the tactile sensitivity and manual dexterity necessary for successful endodontic procedures [12,13]. According to recent studies, human extracted teeth are used for endodontic training in 82.1%, 73% and 100% of Italian, English and Spanish dental schools, respectively [14-16]. Nevertheless, the use extracted teeth shown some limitations. For example, with the improvement of oral health in the general population and with the new therapeutic possibilities for teeth that were previously destined for extraction, the availability of extracted teeth suitable for practice has decreased [17]. The use of extracted teeth may carry ethical concerns and require preventive measures to avoid the risk of cross-infections [13,18]. In addition, the lack of uniformity of natural teeth poses difficulties during classroom exercises and when student learning is assessed [19].

For these reasons, increasingly sophisticated artificial root canals have been put on the market, from canals of different shapes and dimension in clear resin blocks to plastic typodonts [20,21]. In particular, some companies are specialized in the production of 3D printed teeth from X-ray tomography or micro-tomography scans of extracted teeth [19].

In various medical fields students can enhance their skills on accurate 3D printed models that reproduce the haptic feedback of the patient's tissues [22]. Several authors described temporal bone surgeries [23,24] implant treatment or maxillary sinus floor augmentation [25] training in realistic in vitro conditions using these 3D-printed models.

In the dental field these models are mostly involved with students for preclinical education in caries excavation, direct capping of the pulp, core build-up, and crown preparation [26].

The cost of these replicas depends on the type of tooth and how accurate the anatomical characteristics are. Given the need to simultaneously and repeatedly train multiple students, a large number of replicas must be utilized, making low cost a crucial characteristic of any effective training model [27]. The gradual reduction of 3D printer costs has made possible to print teeth in-house [28]. The advantages of using 3D printed teeth are the potentially infinite availability of tooth replicas and the elimination of variability of natural teeth [12].

Intraoral scanners (IOSs) are widely diffuse tools that allow dentists to create detailed digital impressions [29]. The functioning of these devices is based on a light source, such as a laser or structured light, which is projected onto the object undergoing scanning. Imaging sensors capture the resulting images, which are subsequently processed by the scanning software. This software analyzes the images and generates point clouds, which are collections of points representing the object's surface. These

point clouds are then transformed into a 3D surface model, also known as a mesh, through a process called triangulation [30]. Besides their valuable use in clinical practise, IOSs showed several possible applications in dental education. Seet et al. assessed the effectiveness of IOSs in student crown preparation evaluation and concluded that they can overcome limitations in conventional assessment of objective parameters and some subjective parameters [31]. Park et al. reported the benefits of a computer-assisted design/computer-assisted manufacturing (CAD/CAM) learning software which allows students to objectively assess their performance in preclinical prosthodontics [32]. Most recently, Choi et al. used IOS as a feedback tool to assess student access cavity on 3D printed teeth [33].

The purpose of this study was to describe a new learning method adopted in the cavity access exercises at Parma dental school.

MATERIALS AND METHODS

The project involved the nineteen fifth-year dental students who attended the Endodontics course at Parma University from September 2022 to January 2023. The undergraduate endodontic program consists of 50 hours of theory lessons and 75 hours of pre-clinical training. Pre-clinical training consists essentially of applying the notions learned during frontal lessons on endodontic treatment from pulp cavity opening to canal shaping, cleaning, and obturation on extracted teeth under the direct supervision of the tutors. Contrary to previous years, in the course 2022-2023,

the students also practiced on 4 to 5 in-house 3D printed teeth, as well as on a similar number of natural teeth.

Replicates of teeth 1.1 and 3.6, reproducing internal and external anatomy, were obtained as follows. STL teeth files were freely available on the web [34]. Using PreForm software (Formlabs, Somerville, US) STL files were loaded and an adequate 3D printing support was designed (Figure 1).

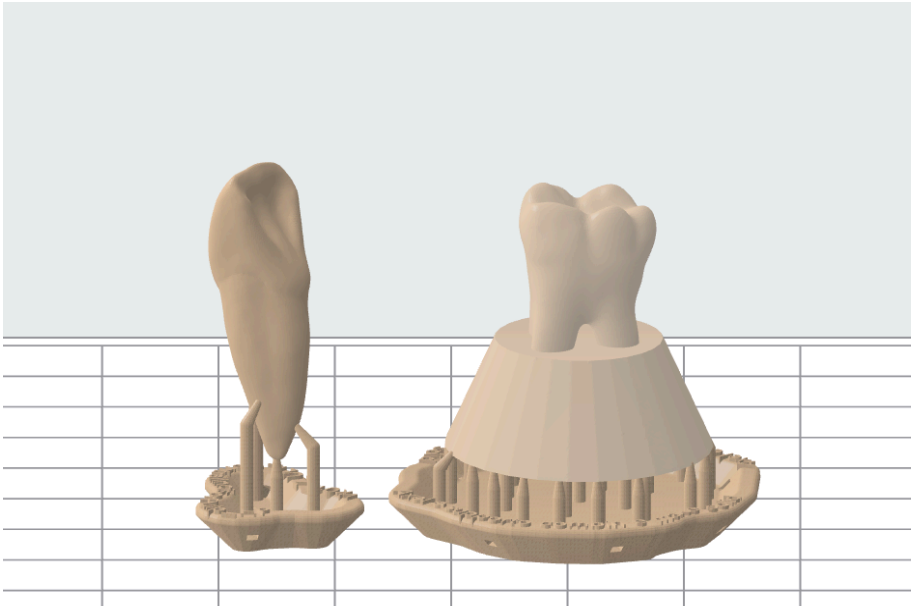

Figure 1. STL files loaded on PreForm software and creation of the 3D printed support.

Layer thickness of 100µm was set. A vat Photopolymerization 3D printer (Form 2, Formlabs, Somerville, US), charged with Model V2 resin (Formlabs, Somerville, US), was used. This resin, which was fabricated to produce dental master models, was chosen for its mechanical characteristics and accuracy.

After 3D printing, the post-curing process was performed using Form Wash and Form Cure (Formlabs, Somerville, US). First, the models were immersed in 97% isopropyl alcohol for 10 minutes using Form Wash and then polymerized 80 minutes at 60°C using Form Cure. After removing the 3D printing support, the resulting teeth were ready-to-use (Figure 2).

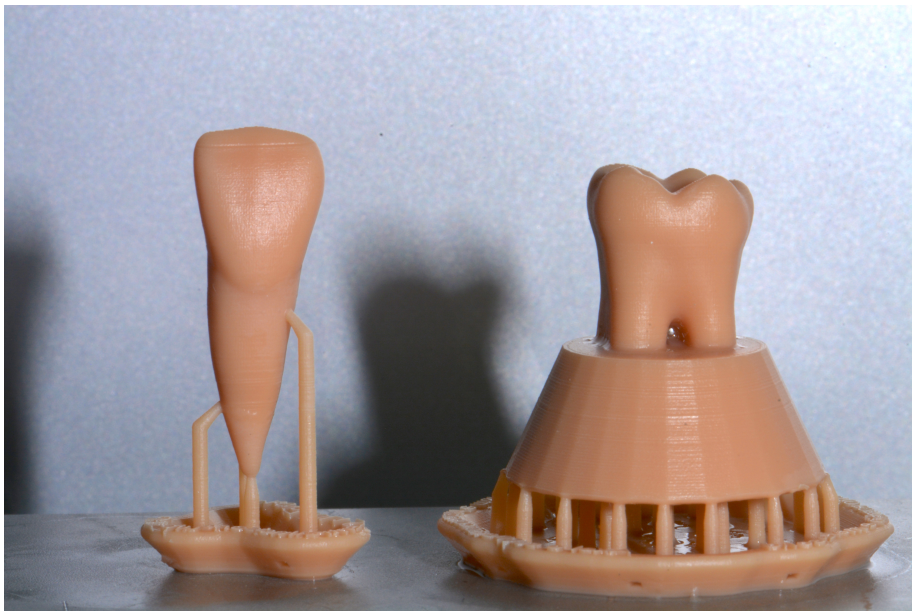

Figure 2. 1.1 and 3.6 tooth replicas after post-curing process

The students performed access cavities using burs mounted on air-driven and motor-driven handpieces, as usual (Figure 3).

Figure 3. Access cavity exercises on 3D printed teeth during student pre-clinical training

Differently from the training on natural teeth, the students, during the training on printed teeth, were not under the direct supervision of the tutors. The assessment of the access cavities was carried out as follows. The prepared teeth were scanned with Omnicam (Dentsply Sirona, Charlotte, US). If any voids or scanning errors were found in the resulting 3D model after each scan, the tooth was rescanned as needed. Scan data were exported from the Omnicam station as STL files and visualised using Meshlab software (Visual Computing Lab, Pisa, Italy). This open-source software allowed the students to view the prepared tooth by rotating it in space and enlarging the image as desired to better evaluate the size, shape, extent, complete deroofing, convenient form, gouging, and the presence of perforations. Additionally, the software allowed the student to align their model with an ideal access cavity obtained

by scanning a model prepared by the teacher, to make a direct comparison and highlight the differences (Figure 4). Thanks to Meshlab it was also possible to mathematically evaluate the geometric difference between the scanned teeth employing a quantitative approach. This was achieved by utilizing a tool known as “Hausdorff distance”. Hausdorff algorithm is commonly used to assess the dissimilarity or similarity between two sets of points within a metric space [35,36]. By applying the Hausdorff distance, we were able to determine the extent to which the sets of points deviated from each other. Specifically, the Hausdorff distance calculates the maximum distance between any point in one set and its nearest counterpart in the other set, thereby providing a measure of how far apart the sets are. Notably, this distance metric takes into account both directions, considering the longest distance from any point in one set to its closest point in the other set. To quantify the discrepancy between the models created by the students and the ideal model, we calculated the Hausdorff distance values. These values represented the dissimilarity between the two sets of points. Subsequently, we derived the root mean square (RMS) from these Hausdorff distance values. The RMS is a statistical measure that entails calculating the square root of the arithmetic mean of the squares of a given set of values. In simpler terms, it offers a way to determine the average value of a set of numbers, considering both positive and negative values. By employing the RMS, we obtained a comprehensive assessment of the overall disparity between the

models. This quantitative analysis provided valuable insights into the extent of variation between the students' prepared tooth and the teacher’s one.

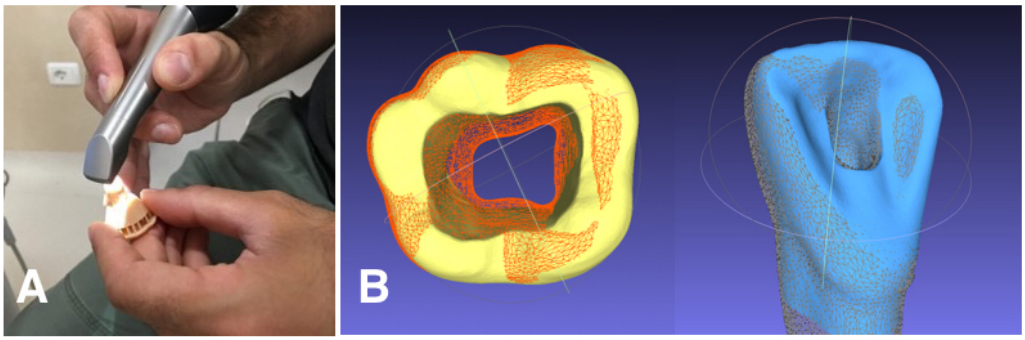

Figure 4. Digital scanning of the prepared tooth (A) and visualization via MeshLab software (B)

At the end of the course and after the approval of the local research ethics board (protocol number 94637/2023), the students' feedback and satisfaction with the access cavity training were investigated using a voluntary questionnaire. Students were invited to participate through e-mail with Google form. They were informed of the purpose of the survey and that the answers would be treated anonymously, and that the questionnaire would not influence the evaluation of learning. The students were asked about difficulties in obtaining extracted teeth, differences between natural teeth and 3D printed teeth, usefulness of 3D printed teeth in preclinical training, and usefulness of self-assessment using digital scanning and alignment software (See Supplementary Materials). For most of the questions, students had to answer using a 5-point Likert scale (1-strongly disagree, 2-disagree, 3-neutral, 4-

agree, 5-strongly agree). In some closed questions, the students could answer "yes/no" or "less/equal/more". Open-ended questions were asked on the benefits of using natural teeth or artificial teeth and their overall experience with the proposed training program.

RESULTS

From the teacher's perspective, this novel learning approach was simple, straightforward and affordable. After preparing the STL files, the printing time was approximately 12 minutes per tooth. The cost of the resin for each tooth was around 0,54 euros. The time needed for scanning each tooth was approximately 1 minute.

The RMS values obtained by comparing the openings made by the students in the molars with the reference openings had an average of 0.269 ± 0.05 mm (n = 44, min = 0,134 mm, max = 0,336 mm). The RMS values obtained by comparing the openings made by the students in the incisors with the reference openings had an average of 0.279 ± 0.07 mm (n = 44, min = 0,07 mm, max = 0,396 mm). The RMS values obtained by comparing the openings made by the students in the total of the teeth with the reference openings had an average of 0.274 ± 0.06 mm (n = 88, min = 0,07 mm, max = 0,396 mm).

The response rate to the questionnaire was 100% and all the students answered all the questions. Overall, student feedback on the use of 3D in-house printed teeth and intraoral scanning for access cavity training was positive (Figure 5).

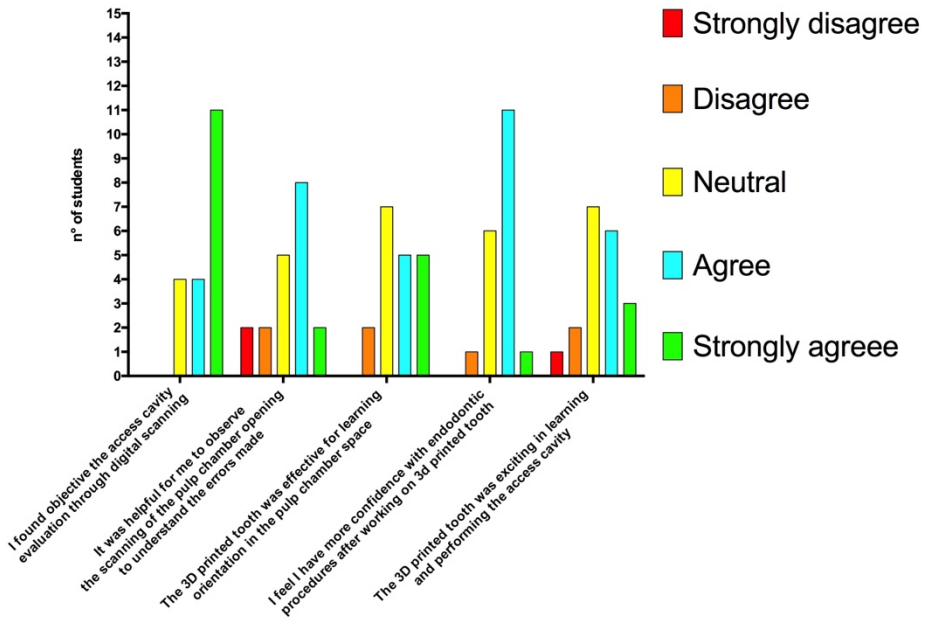

Figure 5. Student feedback after access cavity exercises using in-house 3D printed teeth and digital scanning

15 (79%) and 14 (74%) agreed with the statements "It was helpful for me to observe the scanning of the pulp chamber opening to understand the errors made" and "I believe that analyzing the pulp chamber opening through digital scanning would be more useful compared to direct inspection," respectively. Only four students disagreed with the statement “I found objective the access cavity evaluation through digital scanning" Most of the students (16/19, 84%) found that the 3D printed tooth had pulp morphology that was easy to understand, and only three students (16%) found it difficult to locate anatomical references for a correct opening in the 3D printed tooth. Most students (11/19, 58%) found 3D printed teeth to be more suitable for the practical exam compared to natural teeth.

According to student opinions, the main drawback of printed teeth was the different tactile sensation compared to human dentin (Fig 6).

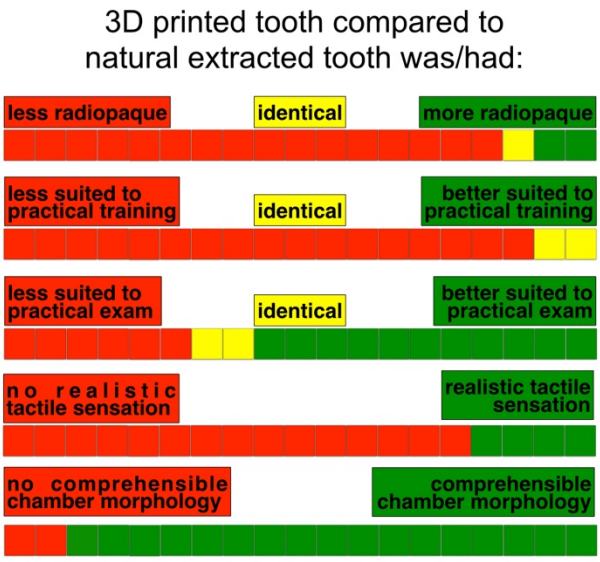

Figure 6. Comparison of the 3D printed teeth and extracted teeth according to the students' answers.

All the students found the resin of 3D printed teeth to be softer than the dentin of natural teeth, and 15/19 (79%) stated that the 3D printed teeth did not provide a realistic tactile sensation during preparation. Only seven students (37%) agreed with the statement "The 3D printed tooth is very useful in acquiring fine sensitivity in the use of rotary instruments for the preparation of the pulp chamber access." A minority of students (6/19, 32%) agreed with the statement "The 3D printed tooth using 3D technology is a valid alternative to the extracted human tooth for training exercises," and nine students (47%) agreed with the statement "The printed tooth was

stimulating in learning and performing the access cavity." Some students found it difficult to collect extracted teeth (4/19, 21%).

In the free text section of the questionnaire, students reported several advantages of implementing access cavity training with 3D printed teeth. Some students appreciated the higher availability, the absence of cross-infection risk, and the lower risk of fracture of 3D printed teeth compared to natural teeth. The possibility of repeating the exercise on the same model was found useful for perfecting the technique in the early stages of learning, as well as the possibility of using an identical model simultaneously for all trainees. Other students reported that training with a model having a standard pulp chamber with no calcification or anatomical variations was advantageous in the initial stages. One student stated that printed teeth allow for a standardized assessment system. Many students suggested, for future courses, to increase the hardness of the resin to have a better tactile sensation and to prevent the bur from getting stuck. In addition, they demanded for other types of 3D printed teeth.

DISCUSSION

Root canal treatment aims to cure or prevent apical periodontitis [1,37]. To achieve this goal, each stage of the treatment must be carried out properly [38]. The access cavity is one of the most critical technical stages and must be performed with the utmost care and precision. If it’s not executed correctly, the subsequent management

of the root canal system can be severely compromised [39]. It was reported that the access cavity creation was a stressful procedure for dental students [40] and that was often associated with iatrogenic procedural errors that could lead to canals being left untreated, scarcely disinfected, insufficiently shaped and filled [41]. An improper access cavity may lead to the failure of the treatment. For these reasons, dental educators should strive to develop pre-clinical learning methods and new technologies can assist them in this task.

In this study, we describe a new learning method adopted at the Dental School of Parma for access cavity exercises using in-house 3D printed teeth and an IOS. The use of 3D printed teeth in endodontic education is not a novelty [27,41-43]. Indeed, in recent years, different factory-manufactured 3D models have been introduced in the market [19]. Compared to previous artificial teeth, 3D printed ones are more realistic, being capable of faithfully reproducing endodontic anatomy. On the other hand, their high cost puts a limit in their usage in high quantities. The constantly declining costs of in-house 3D printing offers the possibilities for dental schools of self-production in high quantities of models that are not yet available on the market or are too expensive to purchase [28,34,44,45]. In most cases, the workflow to obtain 3D printed teeth starts with DICOM files of the natural tooth, derived from a CBCT or microCT scan. The DICOM files are then converted into STL files and thoroughly refined, prepared, and smoothed with dedicated software before being printed [46,47]. This type of processing typically requires many hours of work and represents the main limitation

of the production process. For practical reasons, in this preliminary project, we decided to use STL files freely available on the Web. Our aim was to verify the feasibility of printing and, obtained positive feedback from the students, we planned to produce teeth starting from scans of natural teeth for future Endodontic courses. In addition, in the free text section of the questionnaire, we received a specific request from a student to produce other types of teeth. According to the student's answers, 3D printed teeth resulted having a correct pulp morphology and identifiable anatomical references for a conventional access cavity opening, but similarly to what reported in other studies [27,48-50], the material consistency was not hard enough compared to the dentin of natural teeth. So, our models could not reproduce the tactile perception with rotating instruments. A possible solution was proposed by Robberecht et al., who developed a method for producing ceramic-based models [51,52]. Despite the hardness of these artificial root canals, thanks to the use of hydroxyapatite, has been found to be comparable to that of natural teeth, the difficulty and complexity of the production phases prevent their widespread use. The most practical way, partly already pursued by some manufacturers [19], is to develop new resins and advanced post-printing processes capable of obtaining models with mechanical characteristics that overlap with those of natural teeth.

After access cavity training, we used an IOS, available in the clinical area of our dental school, to acquire digital impressions of the prepared teeth. Using MeshLab, a free STL processing software, the scans were viewed by the students with the possibility

of enlarging the models and rotating them at 360 degrees. This enables students to observe in detail the tooth preparations. Secondly, the software allowed to superimpose the student's model with an ideal cavity access made by the teacher in a previously scanned tooth. In this way, it was possible to instantly highlight the differences, both in excess and in deficiency, in the extension and shape of the cavity. Iatrogenic errors such as incomplete deroofing, gouging or perforations could be easily identified. Using the Hausdorff distance tool included in Meshlab it was possible to instantaneous quantify quantitatively the discrepancy between the student and the reference models. We have planned to analyze in the future the accuracy of this value in assessing the quality of access cavity openings. If the RMS value proves to be a valid surrogate for the traditional evaluation by the instructor, it can be used for both self-assessment and formal examination assessment.

Students' answers reported high levels of satisfaction with the new self-assessment method. This high approval rating might be due not only to the immediacy of the visual feedback, but also to the generally enthusiastic attitude of dental students towards digital dentistry [53]. Commercial digital evaluation systems, such as PrepCheck® (Dentsply Sirona©, Bensheim, Germany) Dental Teacher™ (KaVo©, Biberach, Germany), Compare© (Planmeca©, Helsinki, Finland) that report feedback on students' prosthetic preparations through a comparison with reference preparation scans are already available [54-56]. To the best of our knowledge, only another study used IOS as a learning tool for students in endodontic preclinical

training. Choi and colleagues [33] investigated student's overall experience with a new learning method involving commercial 3D printed teeth, an IOS and a new software, called 3D Dental Aling. Despite some differences between the two protocols (commercial versus in-house 3D printed teeth, Emerald versus Omnicam IOS and 3D Dental Aling versus Meshlab software), both teaching methods received similar positive feedback from students. In our study, we decided to use in-house 3D printed teeth to limit costs and to not have restrictions on the number of teeth available. 3D Dental Align was a custom-developed software based on the 3D Slicer platform. It was designed by the authors to optimize workflows for instructors and students. Aligning the models through Meshlab was more complex, but all the students were able to use it under the instructor's supervision. We involved Omnicam 2.0 because it was already available in our operative clinical department. A recent study found that Emerald IOS (Planmeca, Helsinki, Finland) was statistically weaker in accuracy and precision than Omnicam [57]. The impact of the IOS reliability on access cavity evaluation should be investigated in future studies.

CONCLUSION

The usage of extracted teeth in dental education comes with inherent limitations, including decreased availability and ethical concerns surrounding their procurement. However, emerging technologies such as 3D printing present an appealing alternative. 3D printed teeth offer several advantages, including enhanced accessibility and the

ability to replicate realistic dental structures. By leveraging these technologies, dental educators can overcome the challenges associated with traditional teaching methods. The results of this study proved that the integration of the 3D printing, IOSs and mesh processing software brings further benefits to pre-clinical training and assessment in dental education. This digital approach facilitates the evaluation of student performance in a more efficient and objective manner.

Further research is necessary to fully explore and validate the effectiveness of this innovative learning method when compared to traditional approaches.

BIBLIOGRAPHY

[1] Ørstavik D. Endodontic Treatment of Apical Periodontitis. *In Essential Endodontology* **2019** pp. 313-344.

[2] Jakovljevic A, Nikolic N, Jacimovic J, Pavlovic O, Milicic B, Beljic-Ivanovic K, Miletic,M, Andric M, Milasin, J. Prevalence of Apical Periodontitis and Conventional Nonsurgical Root Canal Treatment in General Adult Population: An Updated Systematic Review and Meta-analysis of Cross-sectional Studies Published between 2012 and 2020. *Journal of endodontics* **2020** 46:1371-1386.e1378,

[3] Dolci M, Migliau G, Besharat ZM, Besharat LK, Gallottini L. Prevalence and distribution of endodontic treatments and apical periodontitis in an Italian population sample. *European Journal of Inflammation* **2016** 14:48-53,

[4] Generali P, Vellani C, Tozzi S, Ciacci L, Nertani P. Prevalence of chronic apical periodontitis and quality of endodontic treatment in an adult Italian population. *G Ital Endod* **2007** 21:35-40.

[5] Gencoglu N, Pekiner FN, Gumru B, Helvacioglu D. Periapical status and quality of root fillings and coronal restorations in an adult Turkish subpopulation. *European journal of dentistry* **2010** 4:17-22.

[6] Peters LB, Lindeboom JA, Elst ME, Wesselink PR. Prevalence of apical periodontitis relative to endodontic treatment in an adult Dutch population: a repeated cross-sectional study. *Oral surgery, oral medicine, oral pathology, oral radiology, and endodontics* **2011** 111, 523-528

[7] Di Filippo G, Sidhu SK, Chong BS. Apical periodontitis and the technical quality of root canal treatment in an adult sub-population in London. *Br Dent J* **2014**

[8] De Moor R, Hülsmann M, Kirkevang LL, Tanalp J, Whitworth J. Undergraduate curriculum guidelines for endodontology. *International endodontic journal* **2013** 46:1105-1114

[9] Seijo MO, Ferreira EF, Ribeiro Sobrinho AP, Paiva SM, Martins RC. Learning experience in endodontics: Brazilian students' perceptions. *Journal of dental education* **2013** 77:648-655.

[10] Iacopino AM. The Influence of “New Science” on Dental Education: Current Concepts, Trends, and Models for the Future. *Journal of dental education* **2007** 71:450-462

[11] European Society of Endodontology. ESE/ADEE Position statement - Assessment of undergraduate dental students. **2018**

[12] Decurcio DA; Lim E, Nagendrababu V, Estrela C, Rossi-Fedele G. Difficulty levels of extracted human teeth used for pre-clinical training in endodontics in an Australian dental school. *Australian endodontic journal: the journal of the Australian Society of Endodontology* Inc **2020** 46:47-51

[13] Holden A, Dracopoulos S. Owning the tooth: exploring the ethical and legal issues relating to the use of extracted human teeth in dental education in Australia. *Australian Dental Journal* **2017** 62:146-151

[14] Mergoni G, Citterio I, Toffoli A, Macaluso GM, Manfredi M. How Is Endodontics Taught in Italy? A Survey of Italian Dental Schools. *Journal of clinical medicine* **2022**

[15] Al Raisi H, Dummer PMH, Vianna ME. How is Endodontics taught? A survey to evaluate undergraduate endodontic teaching in dental schools within the United Kingdom. *International endodontic journal* **2019** 52:1077-1085

[16] Segura-Egea JJ, Zarza-Rebollo A, Jiménez-Sánchez MC, Cabanillas-Balsera D, Areal-Quecuty V, Martín-González J. Evaluation of undergraduate Endodontic teaching in dental schools within Spain. *International endodontic journal* **2021** 54:454-463

[17] Nawrocka A, Łukomska-Szymańska M. Extracted human teeth and their utility in dental research. Recommendations on proper preservation: A literature review. *Dental and medical problems* **2019** 56:185-190

[18] Western JS, Dicksit DD. A systematic review of randomized controlled trials on sterilization methods of extracted human teeth. *Journal of conservative dentistry* **2016** 19, 343-346

[19] Gancedo-Caravia L, Bascones J, García-Barbero E, Arias A. Suitability of different tooth replicas for endodontic training: perceptions and detection of common errors in the performance of postgraduate students. *International endodontic journal* **2020** 53:562-572

[20] Nassri MR, Carlik J, Da Silva CR Okagawa RE, Lin S. Critical analysis of artificial teeth for endodontic teaching. *Journal of applied oral science* **2008** 16:43-49

[21] Spenst A, Kahn H. The use of a plastic block for teaching root canal instrumentation and obturation. *Journal of endodontics* **1979** 5:282-284

[22] Crafts TD, Ellsperman SE, Wannemuehler TJ, Bellicchi TD, Shipchandler TZ, Mantravadi AV. Three-Dimensional Printing and Its Applications in Otorhinolaryngology-Head and Neck Surgery. *Otolaryngology-head and neck surgery : official journal of American Academy of Otolaryngology-Head and Neck Surgery* **2017** 156:999-1010

[23] Probst R, Stump R, Mokosch M, Röösli C. Evaluation of an Infant Temporal-Bone Model as Training Tool. *Otology & neurotology : official publication of the American Otological Society, American Neurotology Society [and] European Academy of Otology and Neurotology* **2018** 39:e448-e452

[24] Takahashi K, Morita Y, Ohshima S, Izumi S, Kubota Y, Yamamoto Y, Takahashi S, Horii A. Creating an Optimal 3D Printed Model for Temporal Bone Dissection Training. *The Annals of otology, rhinology, and laryngology* **2017** 126:530-536

[25] Somji SH, Valladares A, Ho Kim S, Cheng Paul Yu Y, Froum SJ. The use of 3D models to improve sinus augmentation outcomes - A case report. *Singapore dental journal* **2017** 38:63-70

[26] Höhne C, Schmitter M. 3D Printed Teeth for the Preclinical Education of Dental Students. *Journal of dental education* **2019** 83:1100-1106

[27] Dobroś K, Hajto-Bryk J, Zarzecka J. Application of 3D-printed teeth models in teaching dentistry students: A scoping review. *European journal of dental education: official journal of the Association for Dental Education in Europe* **2023** 27:126-134

[28] Reymus M, Fotiadou C, Kessler A, Heck K, Hickel R, Diegritz C. 3D printed replicas for endodontic education. *International endodontic journal* **2019** 52:123-130,

[29] Mangano F, Gandolfi A, Luongo G, Logozzo S. Intraoral scanners in dentistry: a review of the current literature. *BMC Oral Health* **2017** 17:149

[30] Imburgia M, Logozzo S, Hauschild U, Veronesi G, Mangano C, Mangano FG. Accuracy of four intraoral scanners in oral implantology: a comparative in vitro study. *BMC Oral Health* **2017** 17:92

[31] Seet RH, Soo PR, Leong KJM, Pang JJH, Lee FKF, Tan MY. Crown preparations by undergraduate dental students: A comparison of conventional versus digital assessment via an intraoral scanner. *Journal of dental education* **2020** 84:1303-1313,

[32] Park CF, Sheinbaum JM, Tamada Y, Chandiramani R, Lian L, Lee C, Da Silva J, Ishikawa-Nagai S. Dental Students' Perceptions of Digital Assessment Software for Preclinical Tooth Preparation Exercises. *Journal of dental education* **2017** 81:597-603

[33] Choi S, Choi J, Peters OA, Peters CI. Design of an interactive system for access cavity assessment: A novel feedback tool for preclinical endodontics. *European journal of dental education: official journal of the Association for Dental Education in Europe* **2023**

[34] Cresswell-Boyes AJ, Barber AH, Mills D, Tatla A, Davis GR. Approaches to 3D printing teeth from X-ray microtomography. *Journal of microscopy* **2018** 272:207-212

[35] Becker K, Wilmes B, Grandjean C, Drescher D. Impact of manual control point selection accuracy on automated surface matching of digital dental models. *Clinical Oral Investigations* **2018** 22:801-810

[36] Cignoni P, Rocchini C, Scopigno R. METRO: Measuring error on simplified surfaces. *Computer Graphics Forum* **1998** 17:167-174

[37] Iandolo A, Pantaleo G, Malvano M, Simeone M, Amato M. Nonsurgical management of complex endodontic cases with several periapical lesions: a case series. *Giornale Italiano di Endodonzia* **2016** 30:101-110.

[38] Iandolo A. Modern Endodontics. *Dentistry journal* **2022** 11

[39] Adams N, Tomson PL. Access cavity preparation. *British Dental Journal* **2014** 216:333-339

[40] Mocny-Pachońska K, Doniec RJ, Wójcik S, Sieciński S, Piaseczna NJ, Duraj KM, Tkacz EJ. Evaluation of the Most Stressful Dental Treatment Procedures of Conservative Dentistry among Polish Dental Students. *International journal of environmental research and public health* **2021** 18:4448

[41] Haji-Hassani N, Bakhshi M, Shahabi S. Frequency of Iatrogenic Errors through Root Canal Treatment Procedure in 1335 Charts of Dental Patients. *Journal of international oral health* **2015** 7:14-17.

[42] Chan DC, Frazier KB, Tse LA, Rosen DW. Application of rapid prototyping to operative dentistry curriculum. *Journal of dental education* **2004** 68:64-70.

[43] Reis T, Barbosa C, Franco M, Baptista C, Alves N, Castelo-Baz P, Martin-Cruces J, Martin-Biedma B. 3D-Printed Teeth in Endodontics: Why, How, Problems and Future-A Narrative Review. *International journal of environmental research and public health* **2022** 19

[44] Reymus M, Liebermann A, Diegritz C, Keßler A. Development and evaluation of an interdisciplinary teaching model via 3D printing. *Clinical and experimental dental research* **2021** 7:3-10

[45] Kustra P, Dobroś K, Zarzecka J. Making use of three-dimensional models of teeth, manufactured by stereolithographic technology, in practical teaching of endodontics. *European journal of dental education: official journal of the Association for Dental Education in Europe* **2021** 25:299-304

[46] Pouhaër M, Picart G, Baya D, Michelutti P, Dautel A, Pérard M, Le Clerc J. Design of 3D-printed macro-models for undergraduates' preclinical practice of endodontic access

cavities. *European journal of dental education: official journal of the Association for Dental Education in Europe* **2022** 26:347-353

[47] Tonini R, Xhajanka E, Giovarruscio M, Foschi F, Boschi G, Atav-Ates A, Cicconetti A, Seracchiani M, Gambarini G, Testarelli L et al. Print and Try Technique: 3D-Printing of Teeth with Complex Anatomy a Novel Endodontic Approach. *Applied Sciences* **2021** 11:1511.

[48] Al-Sudani DI, Basudan SO. Students' perceptions of pre-clinical endodontic training with artificial teeth compared to extracted human teeth. *European journal of dental education: official journal of the Association for Dental Education in Europe* **2017** 21:e72-e75

[49] Kolling M, Backhaus J, Hofmann N, Keß S, Krastl G, Soliman S, König S. Students' perception of three-dimensionally printed teeth in endodontic training. *European journal of dental education: official journal of the Association for Dental Education in Europe* **2022** 26:653-661

[50] Tsai ST, Ho YC, Tsai CL, Yang SF, Lai YL, Lee SY. Evaluation of students' self-assessment performance in preclinical endodontic training by means of rubrics and a 3D printed model. *Journal of the Formosan Medical Association = Taiwan yi zhi* **2022** 121:2203-2210

[51] Robberecht L, Chai F, Dehurtevent M, Marchandise P, Bécavin T, Hornez JC, Deveaux E. A novel anatomical ceramic root canal simulator for endodontic training. *European journal of dental education : official journal of the Association for Dental Education in Europe* **2017** 21:e1-e6

[52] Robberecht L, Hornez JC, Dehurtevent M, Dufour T, Labreuche J, Deveaux E, Chai F. Optimization and Preclinical Perception of an Artificial Simulator for Endodontic Training: A Preliminary Study. *Journal of dental education* **2017** 81:326-332.

[53] Sharab L, Adel M, Abualsoud R, Hall B, Albaree S, De Leeuw R, Kutkut A. Perception, awareness, and attitude toward digital dentistry among pre-dental students: an observational survey. *Bulletin of the National Research Centre* **2022** 46:246

[54] Sadid-Zadeh R, Sannito NM, DeLuca JT. Comparison of Effectiveness of Two Teaching Methods on Acquisition of Skills in Preclinical Fixed Prosthodontics. *Journal of dental education* **2019** 83:314-321

[55] Corne P, Joseph D, Hirtz P, Durand JC, Fages M, Vincent M, Balthazard R. Study of the use in autonomy of intraoral scanning systems to optimise dental students' performances in fixed prosthodontics practical learning in second year. *European journal of dental education: official journal of the Association for Dental Education in Europe* **2022**

[56] Stoilov M, Trebess L, Klemmer M, Stark H, Enkling N, Kraus D. Comparison of Digital Self-Assessment Systems and Faculty Feedback for Tooth Preparation in a Preclinical Simulation. *International journal of environmental research and public health* **2021** 18

[57] Diker B, Tak Ö. Comparing the accuracy of six intraoral scanners on prepared teeth and effect of scanning sequence. *The journal of advanced prosthodontics* **2020** 12:299-306

Chapter IV

Subgingival zone detection via Reverse Subgingival Scan

INTRODUCTION

Among the limits of intraoral scanning techniques [1,2], poor and/or time consuming sulcular anatomy and subgingival finish lines reading are particularly important [3]. This is because intraoral scanners (IOSs) cannot overcome the tendency of the gum to collapse [4,5]. Clinicians prefer to use a retraction cord to assess the sulcular anatomy, often switching to conventional impression materials. Conventional techniques can alter the sulcus anatomy and do not provide precise information on the transverse dimension of the sulcus, as conditioned by the provisional restoration. Accurate imaging of the prepared tooth's subgingival area and its sulcular anatomy is crucial, particularly in aesthetic areas. However, it is difficult to capture the emergence profile and the soft tissue around the abutments particularly when a vertical preparation is employed [6].

Mandelli et al. suggested a hybrid digital and analogue technique to obtain a deeper reading of the sulcus in challenging clinical situations [7] at the cost of increased procedural complexity, with the use of double retraction cord. Agustín-Panadero et

al. proposed a protocol for taking digital impressions of subgingival finish lines without using double-cord retraction (Figure 1). However, their alignment method, based on external landmarks, is liable to error [8].

We propose a digital technique, the RSS, to overcome the limits of existing techniques for performing accurate assessment of the abutments, of their subgingival finish lines, and of the transmucosal zone, as conditioned by the provisional restoration.

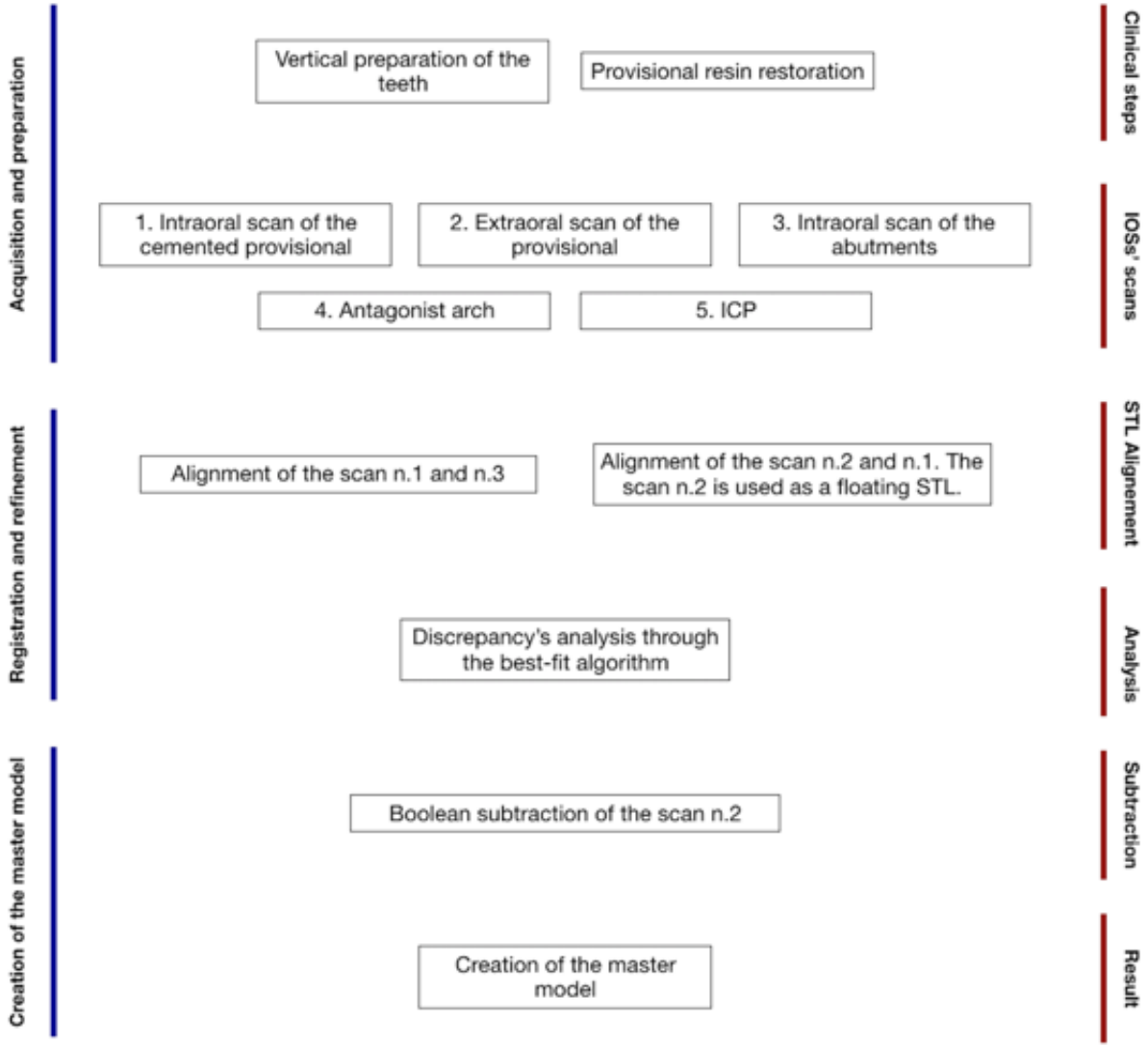

Figure 1. Schematic of the protocol of Agustín-Panadero et al.

TECHNIQUE

Teeth (#43, #44, and #45) were prepared with a vertical finish line at the bottom of the gingival sulcus (Figure 2) A provisional restoration made of composite material (Structur CAD, VOCO) was directly relined (Structur 3, VOCO) to achieve the optimal result in terms of function and aesthetics (Figure 3). Great care should be employed in this step, because the provisional is the source of the image of the abutments and of the sulcular morphology.

Figure 2. Preparation of the abutments (teeth #43, #44, #45).

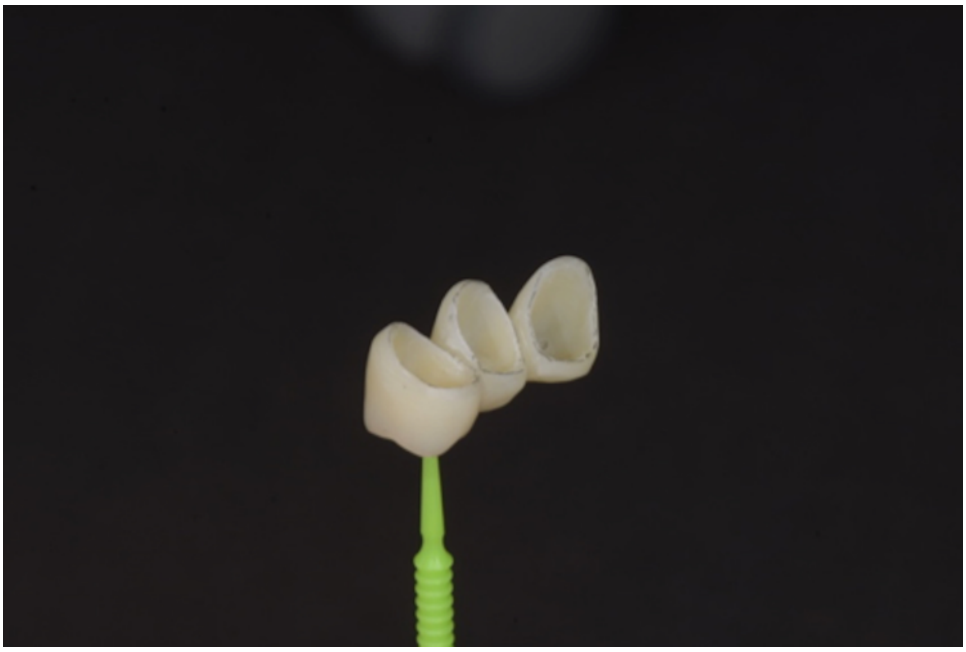

Figure 3. Provisional restorations made in composite.

The master model was obtained by integrating two intraoral digital impressions (Figure 4) plus a scan of the temporary crowns using a Carestream CS3600 (Carestream Dental). The first impression scans the abutments, without retractor cords, following the recommended scanning protocol (both arches plus intercuspidal position). Next, an impression with the provisional restoration in place was taken. Subsequently, temporary crowns were scanned extraorally, acquiring their inner and outer margins (Figure 5). The resulting STL files were processed to produce a digital master model in which the data of the finish line of the abutments and of the surrounding tissues were derived from the temporary crowns. The workflow was performed using MeshMixer (Autodesk) and Exocad (Align Technology) (Figure 6).

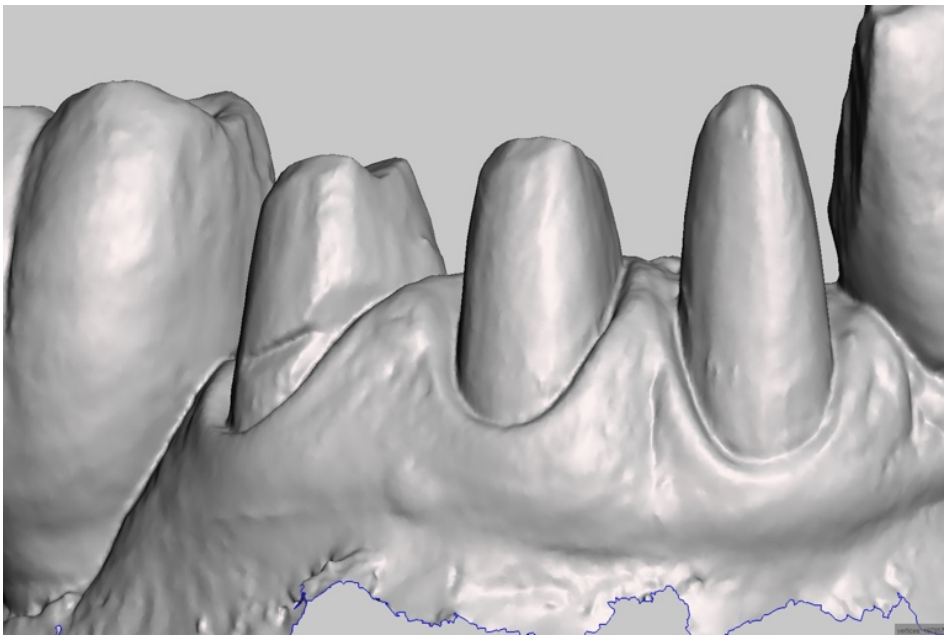

Figure 4. Digital impression of the abutments.

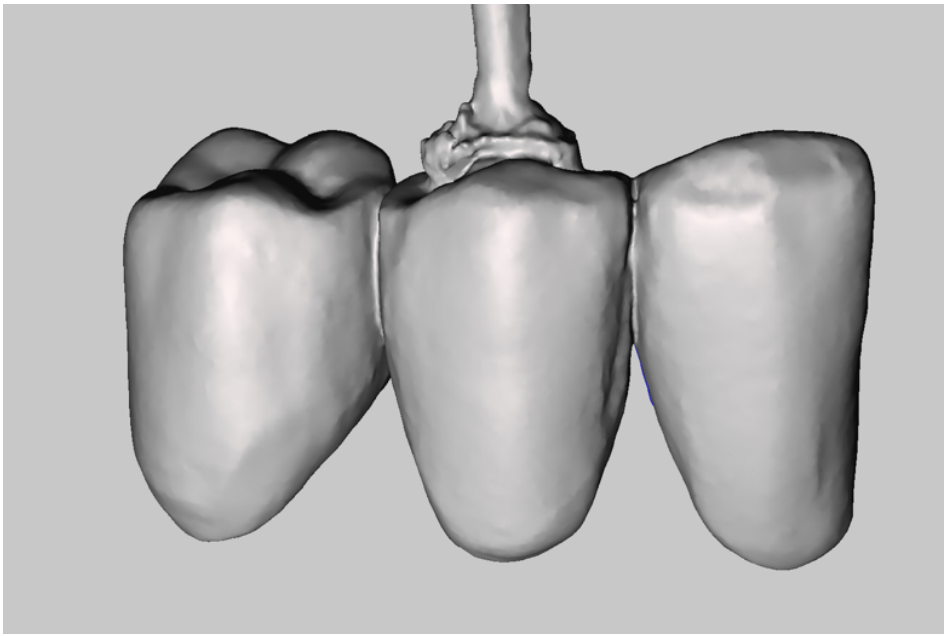

Figure 5. Scan of the provisional restoration.

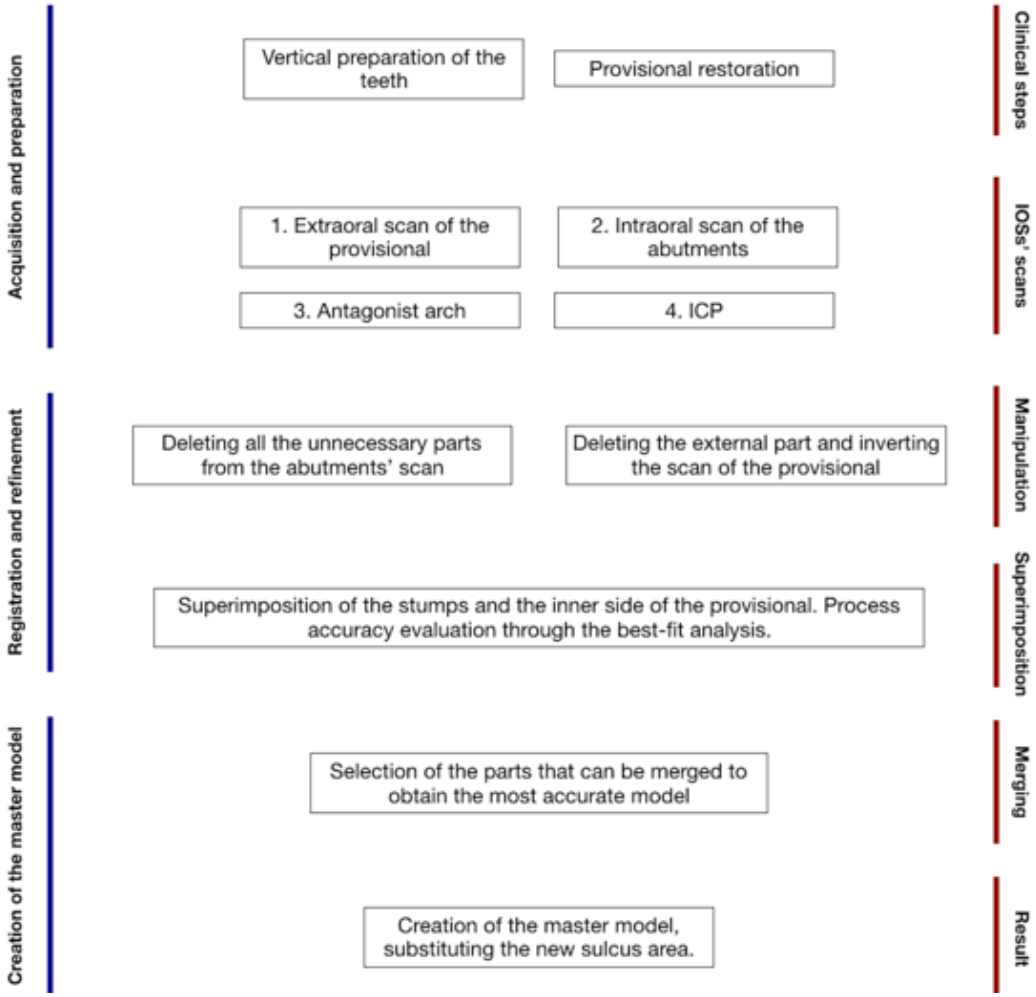

Figure 6. Schematic of the method.

Software Workflow

1. Cleaning STL Files

The first step is to prepare impression files suitable for subsequent steps. After importing the scan of the abutments and the provisional restoration into MeshMixer, we select and delete all of the unnecessary triangles of the mesh using the tool "Delete". In the abutments scan, it is mandatory to maintain information related to tooth preparation. The buccal and lingual sides are minimised and the teeth adjacent to the preparations are removed (Figure 7). The provisional restoration scan provides

information on the emergency profile and finish line of the crown, and therefore the cervical part and the inner side of the crown are carefully maintained (Figure 8). Because the scan represents the negative of the abutment, the next step is re-orienting the triangles of the STL file. This manipulation is performed via the command “Flip Normal,” after selecting the entire mesh surface (Figure 9).

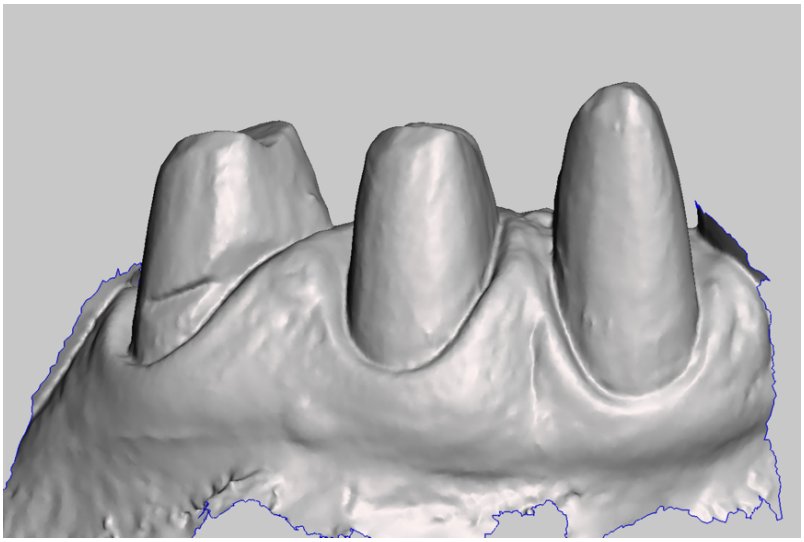

Figure 7. Digital impression of the abutments.

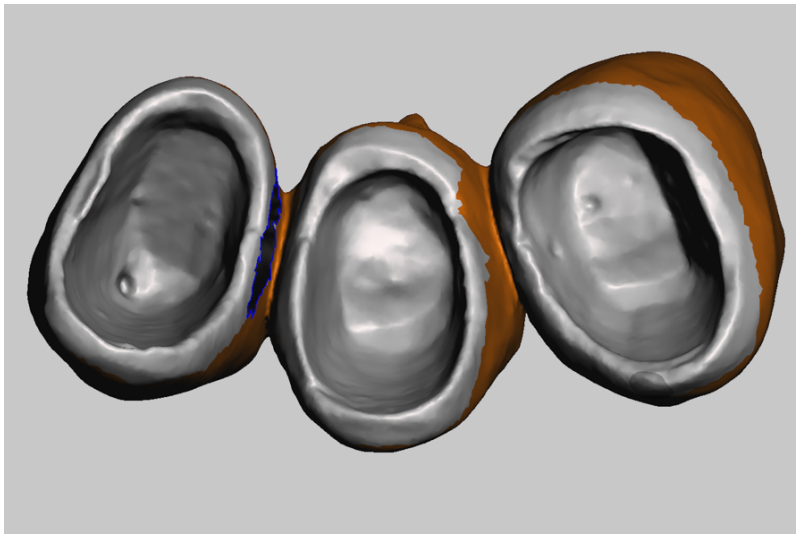

Figure 8. Selection of unnecessary areas.

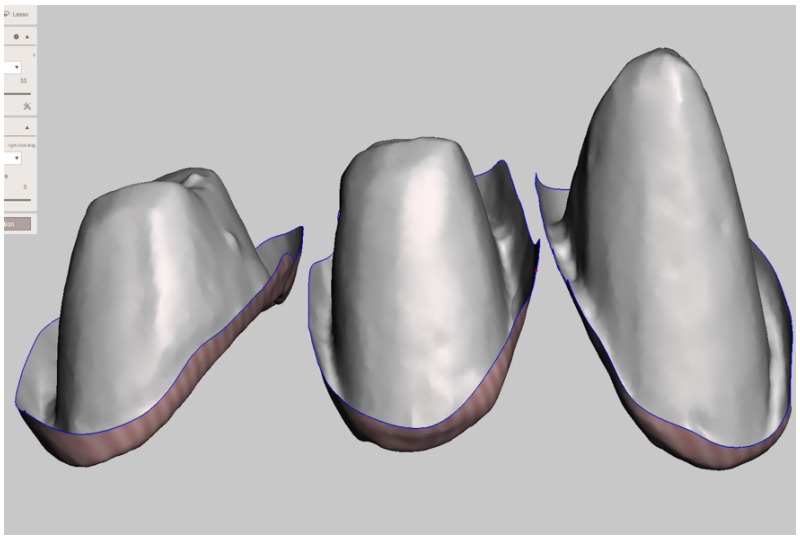

Figure 9. Manipulation of the inside area of the provisional restoration after deleting all unnecessary areas.

2. Registration of the Scans

Using Exocad, we align and match the two STL files. Then we manually select the reference points and perform an automatic alignment using the “Best-fit” algorithm (Figure 10). To maintain the reciprocal position of the files, the tool “Mesh Register” is used. At this stage, the STL meshes show superimposed areas that do not match. Thus, we save the registered files separately and export them to MeshMixer.

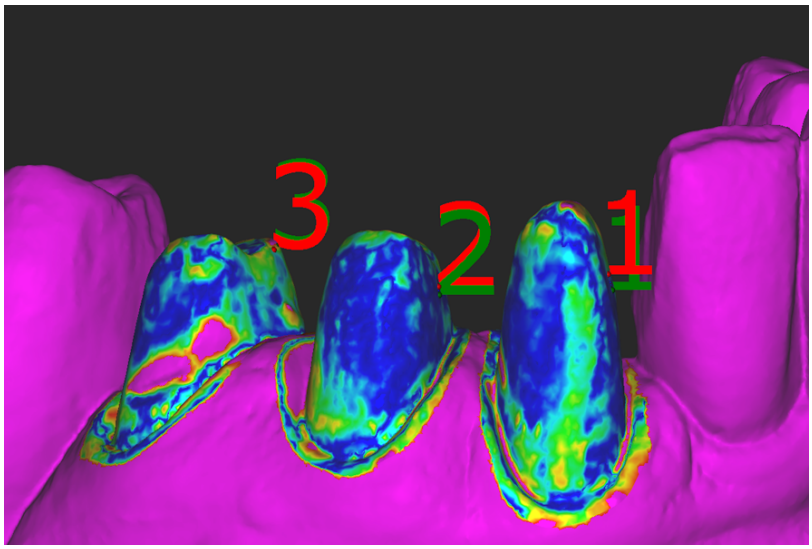

Figure 10. Alignment of the two STL files.

3. Creation of the Master Model

Using MeshMixer it is possible to detect and delete superimposed areas not intended to be part of the master model (Figure 11). From the abutment scan, we retain the coronal and medial third of the prepared teeth, whereas from the scan of the provisional restoration we use the sulcus and finish line data (Figure 12 and 13). Using the MeshMixer “Join” tool, we fuse the data in the two original STL files into a single, merged file (Figure 14), representing the subgingival zone. The final step is to match this file to the direct scan of the abutment. Then we import the file into Exocad and substitute the abutments of the original scan with the new ones that include more precise information on the subgingival zone. This last step is performed using the “Multi-die” tool (Figure 15). This method generates a master model in Exocad (Figure 16). When modelling the definitive restoration, the dental technician should consider that the master scan of the abutments, derived from the provisional restoration, does not provide information on the luting agent’s thickness. The operator should add this space using CAD software.

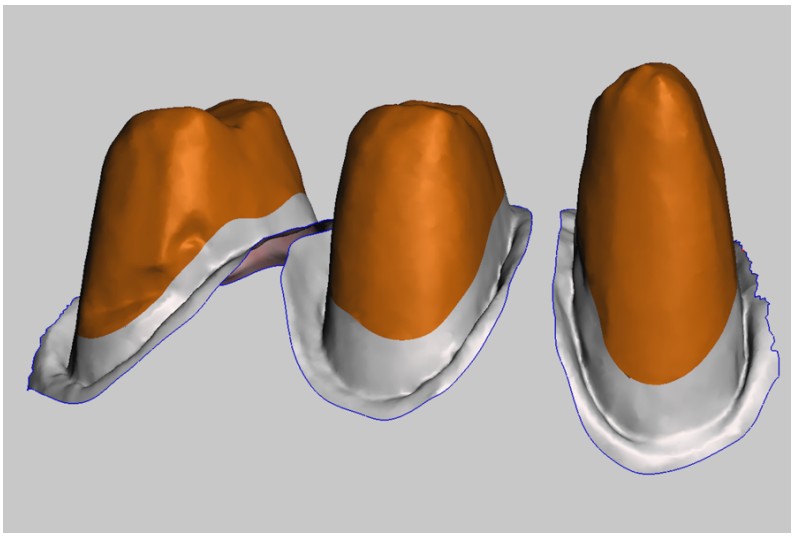

Figure 11. Selection of the zones in the intraoral digital impression that are important to maintain.

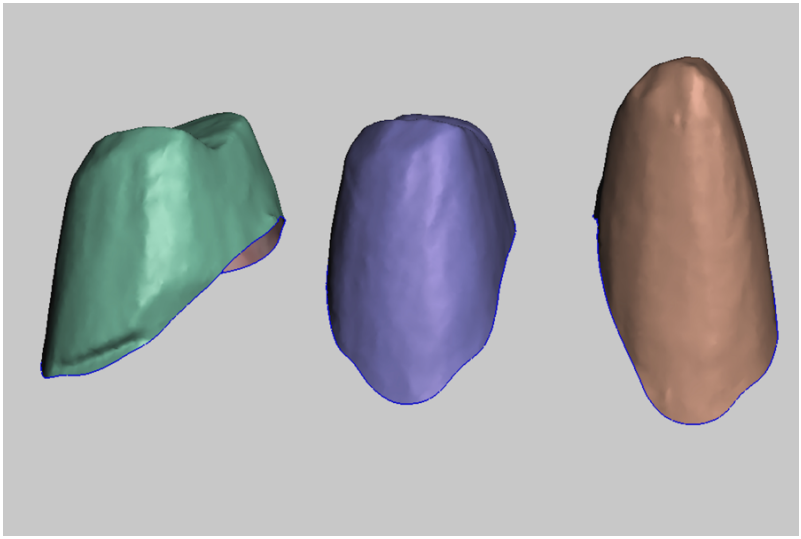

Figure 12. Coronal and median thirds derived from the intraoral digital impression

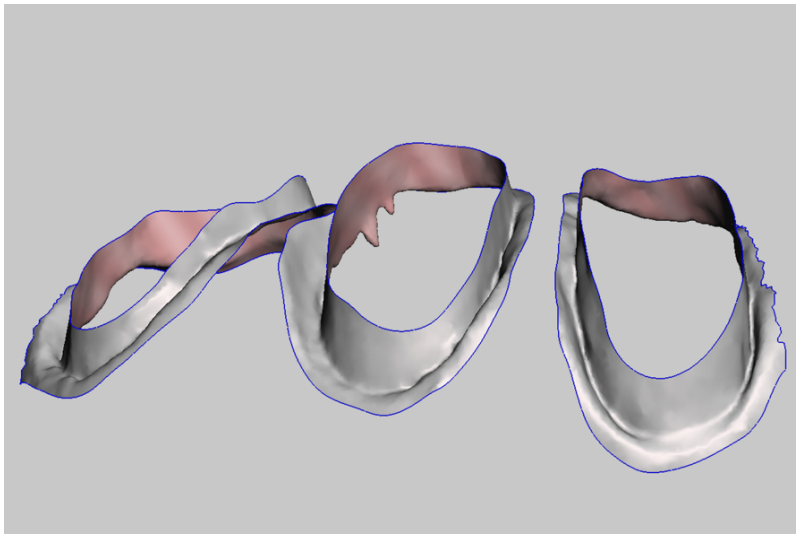

Figure 13. Subgingival zone derived from the scan of the provisional restoration.

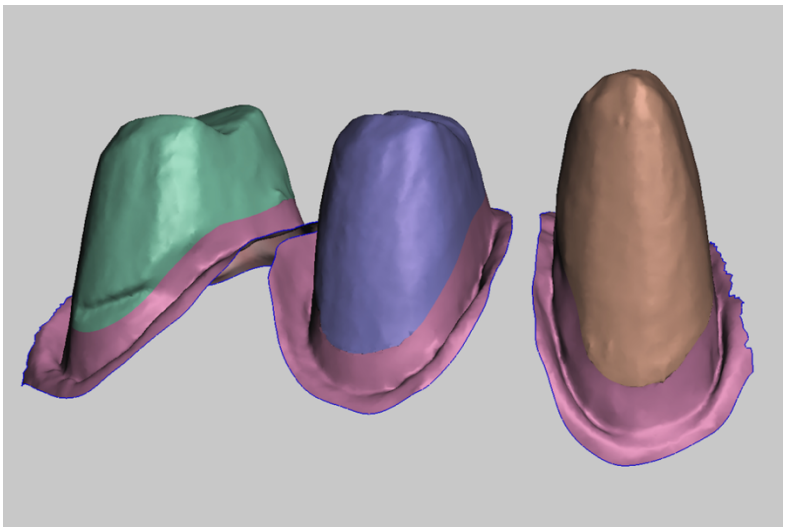

Figure 14. Deriving a unified file from two separate parts.

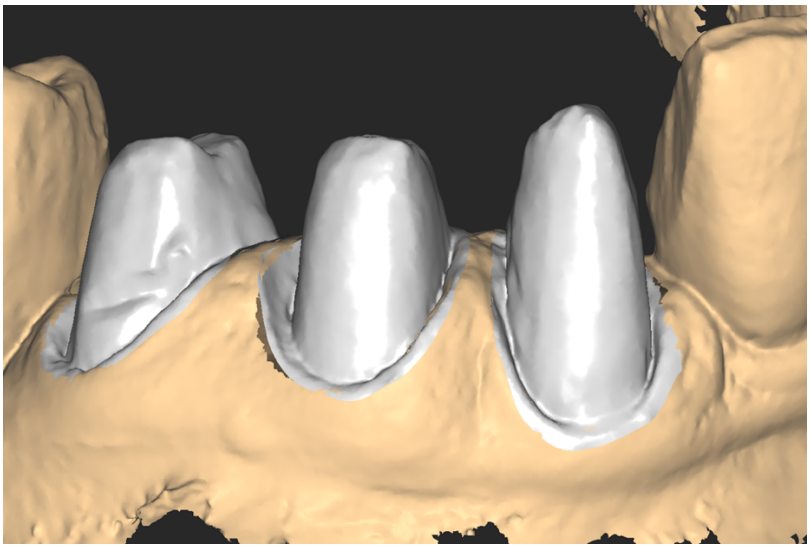

Figure 13. Substitution of the digital abutments on the master model.

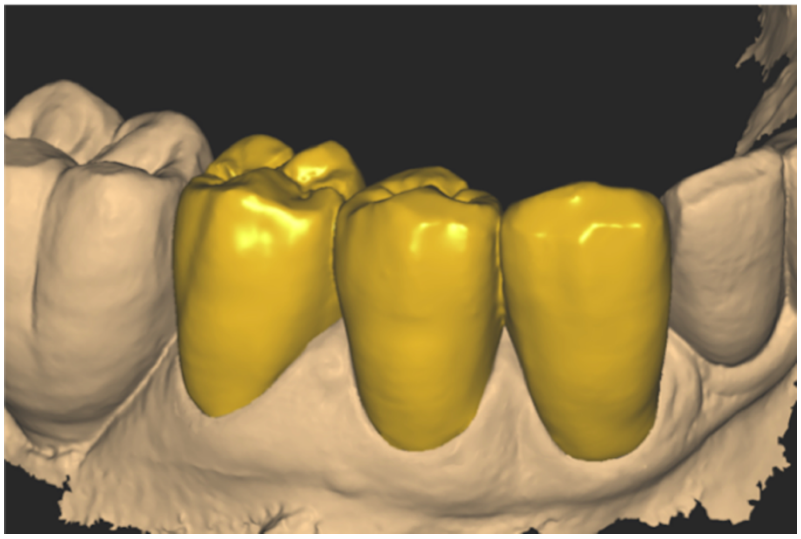

Figure 16. Modelling the zirconia crowns

To further detail the workflow and to serve as a proof-of-concept clinical case, crowns were designed and milled from 1200 MPa zirconia blocks (Dental Direkt). To test *ex vivo* the fitting of the zirconia crowns, a master model was printed using a Form 2 printer (Formlabs), and the resin "Model" with accuracy on the z-axis set to 25 µm. The crowns obtained were judged for clinical fit by a clinician (Figure 17). The rate of compression of sulcular tissues was good. A radiographic control taken after luting showed a proper fit (Figure 18).

Figure 17. Crowns cemented.

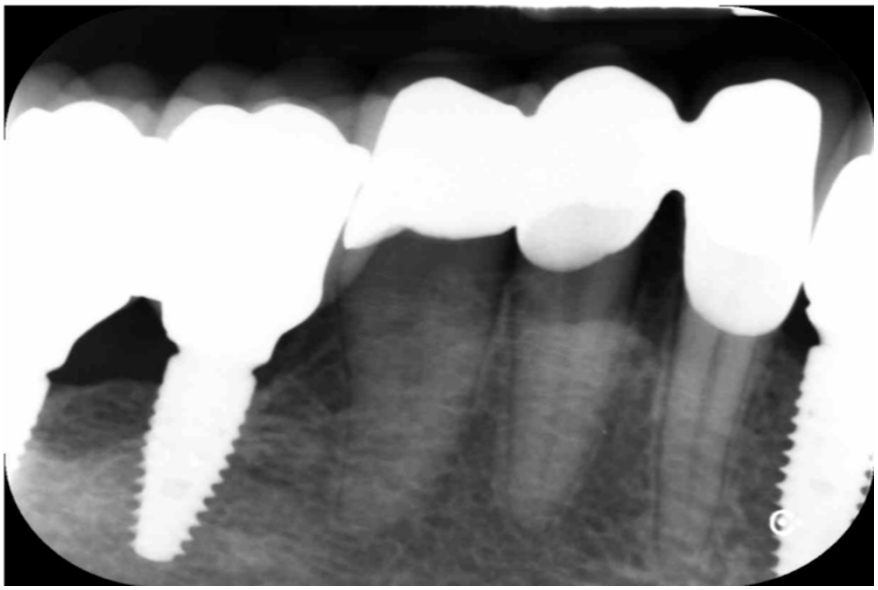

Figure 18. Radiographic control at the time of luting.

DISCUSSION

Direct scanning of the provisional restoration, introduced by Agustín-Panadero *et al.*, is limited to situations in which the clinician chooses to fabricate a crown with the exact finish line of the provisional prosthesis or more coronal. The method is limited by the need for alignment of the STL files based on external landmarks, i.e., using the adjacent teeth as reference points to integrate the full arch, abutment, and provisional scan, so that the abutment is aligned using the outer surface of the provisional [8]. Conversely, the RSS method uses the abutment and the inverted scan of the provisional as matching surfaces.

The main limit of the RSS technique is its dependant on the quality of the provisional restoration, which must be very precise to obtain an adequate master model and a sulcular anatomy without distortion. In addition, this method is limited to cases in

which the finish line of the final crown is at the same level or more coronal than that of the provisional. Further studies are needed to confirm the viability of the procedure in everyday clinical practice.

CONCLUSION

The RSS technique enables accurate imaging of the gingival sulcus anatomy and the prepared tooth finish line without using retraction cords and/or conventional impression materials.

BIBLIOGRAPHY

[1] Braian M, Wennerberg A. Trueness and precision of 5 intraoral scanners for scanning edentulous and dentate complete-arch mandibular casts: A comparative *in vitro* study. *J Prosthet Dent* **2019** *122:*129-136.

[2] Winkler J, Gkantidis N. Trueness and precision of intraoral scanners in the maxillary dental arch: An *in vivo* analysis. *Sci Rep* **2020** *10:*1–11.

[3] Nedelcu R, Olsson P, Nyström I, Thor A. Finish line distinctness and accuracy in 7 intraoral scanners versus conventional impression: an in vitro descriptive comparison. *BMC Oral Health* **2018** *21:*18:27.

[4] Mangano F, Gandolfi A, Luongo G, Logozzo S. Intraoral scanners in dentistry: A review of the current literature. BMC Oral Health. **2017** 17:1–11.

[5] Li J, Chen Z, Wang M, Wang HL, Yu H. Dynamic changes of peri-implant soft tissue after interim restoration removal during a digital intraoral scan. *J Prosthet Dent* **2019** *122:*288–294.

[6] Monaco C, Evangelisti E, Scotti R, Mignani G, Zucchelli G. A fully digital approach to replicate peri-implant soft tissue contours and emergence profile in the esthetic zone. *Clin Oral Implants Res* **2016** *12*:1511–1514.

[7] Mandelli F, Ferrini F, Gastaldi G, Gherlone E, Ferrari M. Improvement of a Digital Impression with Conventional Materials: Overcoming Intraoral Scanner Limitations. *Int J Prosthodont* **2017** *4:*373–376.

[8] Agustín-Panadero R, Loi I, Fernández-Estevan L, Chust C, Rech-Ortega C, Pérez-Barquero JA. Digital protocol for creating a virtual gingiva adjacent to teeth with subgingival dental preparations, *J Prosthodont Res* **2020** *64* 506–514.

Chapter V

Accuracy of commercial 3D printers for the fabrication of surgical guides in dental implantology

INTRODUCTION

The accurate placement of dental implants is crucial to prevent lesions of anatomical structures and to optimize prosthetic rehabilitation, leading to a long-term clinical success. Consequently, various computer- aided implant surgery have been developed in order to optimize the placement of dental implants [1]. Hämmerle et al. [2], differentiates computer-guided surgery from computer-navigated surgery. On one hand, computer-navigated surgery is a dynamic assistance that requires a surgical navigation system to reproduce virtually the drilling planning directly from computerized tomographic data. This system allows "live" intraoperative changes in implant position. On the other hand, computer-guided surgery is a static assistance that requires a physical surgical guide. The guide is 3D-printed and reproduces the virtual drilling planning directly from computerized tomographic and surface data. Guided surgery, compared to traditional techniques, allows to a more accurate implant placement. Indeed, computer-guided surgery was shown to provide more accuracy than freehand surgery [3,4] when compared to either semi-guided, fully

guided [5], or computer-navigated surgery [6]. Among the surgical guides, the “fully-guided” guide offers more guarantees to control the drill angulation, depth and location of the implant. This technique is associated with reduced surgical time, reduced invasiveness and optimal prosthetic results. Currently, fully-guided or “fully constrained” surgery is considered as the most reproducible technique for placing an implant [7]. However, bias in implant placement are still reported.

Several studies have compared the position of the placed implant with respect to planning for both (x,y,z) axis and angulation. The deviation between the planned and effective implant position can be caused by multiple factors. Based on the literature, the error factors can be classified in three categories (i) clinical situation derived factor [8,9], (ii) implant system derived factors [10] and (iii) surgical guide design [11,12] and manufacturing derived factor [13,14]. For example, Putra et al. [15] showed in a literature review that guides produced by a conventional method induce a higher angular deviation than a 3D-printed guide.

The manufacturing of a surgical guide for guided implant surgery requires three steps: (i) acquisition of patient data, (ii) data processing, (iii) guide manufacturing. The data acquisition consists in capturing the patient’s bone geometry via a Cone Beam Computed Tomography (CBCT) or CT-scan exam in the Digital Imaging and Communication in Medicine (DICOM) format. In parallel, the surface geometry is registered via optical scanning (3D intra-oral scanner, IOS) and processed to obtain a digital model in Standard Tessellation Language (STL) format. Then, a dedicated

software allows the matching of DICOM and STL file, to plan the surgery, and to design a surgical guide. The ready-to-print STL file of the guide is then exported.

The most common 3D-printing technologies used to fabricate surgical guides in dental implantology are stereolithography (SLA), Digital Light Processing (DLP), inkjet and its derivative PolyJet®. However, there are other AM technologies available such as Selective Laser Sintering (SLS), 3-Dimensional Printing (3DP) and Fused Deposition Modeling (FDM). Although a variety of materials can be used with these technologies, plastics, resin or plastic-based materials are the most commonly used materials for dental applications [16]. Chen et al. [17] have also used Direct Metal Printing (DMP) technology to manufacture Co-Cr surgical guides but this technology is not widely used for this application probably because its use is more complex, and the overall costs (including printer device and consumables) are higher than resin printers. However, SLA was until recently the most used technology for guide manufacturing, and resin guides were often called “stereolithographic guides” in the surgical literature.

SLA is a process based on the polymerization of monomer resin by a laser beam. After creating a layer, the moving platform is lowered into the reservoir tank and this process continues layer-by-layer until the printed part is completed [18]. DLP is also a vat-photopolymerization technology according to the American Society for Testing Material (ASTM). The main difference between SLA and DLP is the light source. The DLP system takes advantage of a digital micromirror device (DMD) to project a mask

of light that allows a layer to be cured in a few seconds [19]. In one hand, according to Taormina et al. [20], a faster 3D construction process would lead to intrinsic lesser accuracy. On the other hand, SLA provides a smaller minimum feature size thanks to a laser spot size smaller than the minimum pixel size of the DMD.

PolyJet® printing is also based on a layer-by-layer technology. The process consists in the selective deposition of material droplets onto the building platform and their immediate solidification by a light source (usually a UV lamp attached to the print heads), allowing layers to be built up [21,22]. The main advantages of this technology are good print resolution and the possibility to print simultaneously a wide range of material, such as plastics, resins and elastomers, simultaneously, and color parts. Limitations include the high cost of the device and the instability of the resin-based materials overtime, that is a common problem to all resin-based technologies.

SLS technology uses a high-power laser beam that selectively irradiates a powder bed to produce localized thermal sintering. While the material partially absorbs at the laser source wavelength, irradiation induces locally elevated temperatures, allowing sintering to occur, i.e., powder particle sintering without melting [23].

In FDM manufacturing process, a filament of material is put through a heated nozzle head and melt for extrusion. Then the material is printed layer-by-layer on a receiving platform [24].

The popularity of AM surgical guides increases due to their accuracy, associated with reduced cost, reduced surgical time, and customization to patient's geometry for

subsequent patient and surgeon benefits. The accuracy of surgical guides is therefore dependent on the 3D-printing technique and method involved for their fabrication.

The aim of this study was to evaluate trueness and precision of surgical guides fabricated by five different commercial AM technologies (SLA, DLP, FDM, SLS and Inkjet). Moreover, each AM technology was evaluated for trueness and precision using two different surgical guides (small extent = single implant and large extent = full arch). The null hypotheses were that AM technology and surgical guide size did not affect trueness and precision of CAD-CAM surgical guides.

MATERIALS AND METHODS

1. Surgical planning

The CoDiagnostix® (Straumann group, Basel, Switzerland), software was used for planning guided implant surgery in two patients. The first case (large-extent Surgical Guide (SG)) was a full-arch guide to place four implants in the mandible, with two lateral anchor pins. The second case (small-extent SG) aimed to place a single implant (tooth #11) and it was limited to two adjacent teeth (Figs. 1a and 1b). STL files of both guides were obtained for the two planifications.

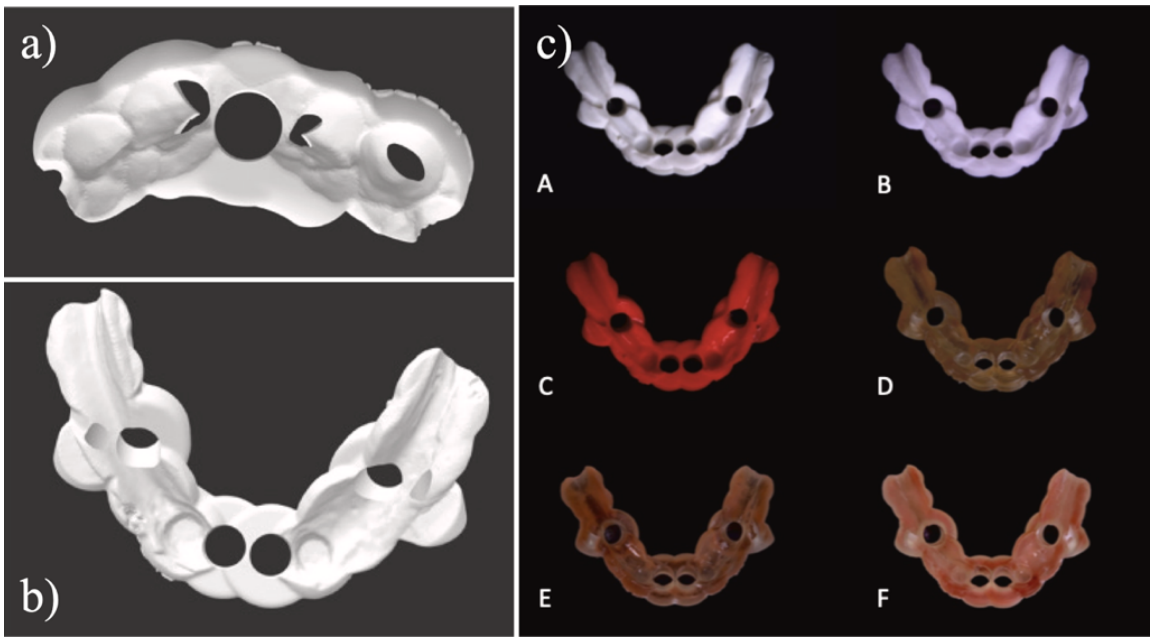

Figure 1. a) STL files of small-extent surgical guides and b) large extent surgical guides. c) Large-extent surgical guides manufactured by A. Stratasys J750; B. Prodways P1000; C. Raise 3D Pro2; D. Form2; E. Rapid Shape D40; F. Cara Print 4.0.

2. Surgical guides fabrication

Each surgical guide was 3D-printed using five different AM tech- nologies SLA, DLP, FDM, SLS and Polyjet®. Each type of guide was printed six times with each technique to evaluate the internal accuracy.

Surgical guides printed by SLA were produced with a Form2 desktop printer (Formlabs Inc, Somerville, MA, USA) and a biocompatible photo- curable resin Dental SG® (Formlabs Inc, Somerville, MA, USA) was used. The guides were printed with a platform inclination of 15◦. A post- printing UV treatment was applied, according to the manufacturer's recommendations.

Surgical guides printed by DLP technologies were produced with two different commercial devices. The first device was a Rapid Shape D40 (Rapid Shape,

Heimsheim, Germany) printer, and the biocompatible resin Sheraprint SG 100 (SHERA Werkstoff-Technologie GmbH & Co. KG, Lemförde, Germany) was used. The second device was a Cara Print 4.0 (Kulzer GmbH, Hanau, Germany) printer, and the biocompatible resin Dima Print Guide (Kulzer GmbH, Hanau, Germany) was used. The guides were printed without platform inclination. A post-printing UV treatment was applied, according to the manufacturers' recommendations.

Surgical guides printed by FDM were produced with a Raise 3D Pro2 printer (Raise 3D Technologies Inc, Irvine, CA, USA), and a Premium PLA filament (Raise 3D Technologies Inc, Irvine, CA, USA) was used. The guides were printed with a platform inclination of 60◦

Surgical guides printed by SLS were produced with a Prodways P1000 (Prodways Group, Paris, France), and a polyamide powder PA12- L 1600 (Prodways Group, Paris, France) was used. The guides were printed without platform inclination.

Surgical guides printed by Polyjet® were produced using Stratasys J750 printer (Stratasys Ltd, Eden Prairie, MN, USA) and a photosensitive polymer liquid VeroWhitePlusTM (Stratasys Ltd, Eden Prairie, MN, USA) was used.

Finally, 72 samples were obtained (2 guides design, 6 printers, 6 replicates). Figure 1c displays the large extent SG produced with different printing techniques.

2.3. Surface scanning, image analysis of the surgical guide and statistical analysis

After the fabrication, the guides were coated by the dental technician with an anti-reflective spray (Helling 3D Scan Spray; Laser design, MN, USA), and they were surface

scanned with a tridimensional dental scanner (CARES 7 Series; Straumann group, Basel, Switzerland). The spray had an average thickness of 2.8 µm. The resulting STL files were compared with the initial design files using a surface matching software (Geomagic Control X®; 3D System Inc, Morrisville, NC, USA). In order to ensure relevant and pertinent calculations, only the underside surface guide sections facing the occlusal areas and surgical fixations pins were included in the analysis.

To describe the accuracy of a measurement method, the International Organization for Standardization (ISO) uses the combination of two terms, “trueness” and “precision” [25]. Trueness was given by the Root Mean Square (RMS), which was used to calculate the mean of the average absolute discrepancy between the initial design file and the STL file obtained after scanning the surgical guide. Precision was given by the Standard Deviation (SD), which allowed to calculate the dimensional discrepancies between the initial design file and the .STL file obtained after scanning the surgical guide [26]. A low RMS value revealed high trueness and a low SD value revealed high precision. Low RMS/SD values revealed high accuracy.

Due to the small sample size, we have used the Kruskall-Wallis non-parametric test to compare trueness and precision between small-extent SG and large-extent SG; the same test was used to compare trueness and precision obtained using the different commercial 3D printer two-by- two. The statistical threshold for statistical significance was $\alpha=0.05$, except for the comparison of printers two-by-two where a Bonferroni

corrected significance level of 0.0033 was used. XLSTAT® software (Addinsoft, Paris, France) was used for these calculations.

RESULTS

The surface matching allowed to obtain a color map of the surfaces according to the measured difference between the initial STL file and the scanned file (Figure 2). Green color showed a surface matching of ±0.1 mm. Areas in blue (negative divergence) indicated a smaller surgical guide, while areas in yellow, orange and red (positive divergence) indicated a larger surgical guide than the corresponding initial STL file.

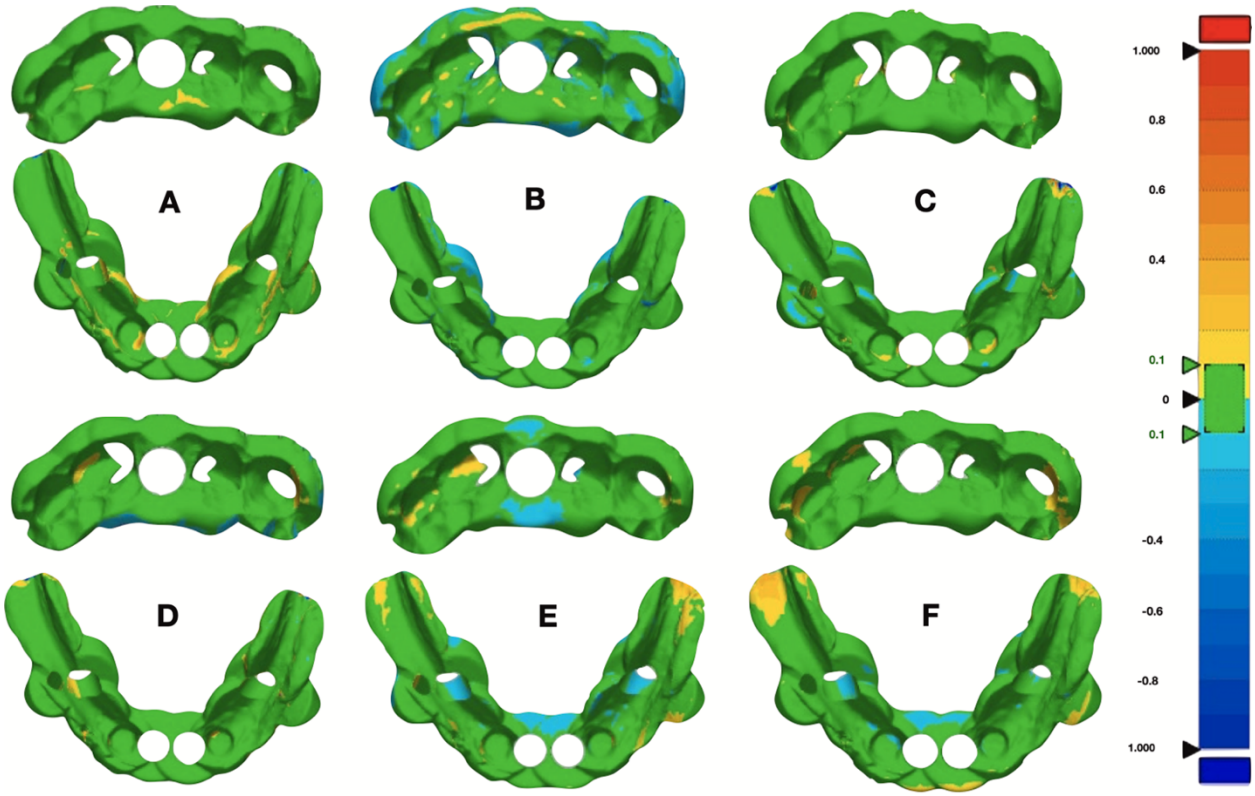

Figure 2. Colorimetric maps after superimposing the scanned guide with initial STL file. A. Stratasys J750; B. Prodways P1000; C. Raise 3D Pro2; D. Form2; E. Rapid Shape D40; F. Cara Print 4.0.

1. Trueness

For the small-extent SG, Rapid Shape D40 obtained the lowest RMS value (64.28 ± 7.95 µm) followed by Form2 (67.75 ± 10.63 µm), Stratasys J750 (70.43 ± 5.41 µm), Cara Print 4.0 (75.53 ± 13.95 µm), Prodways P1000 (97.93 ± 13.62 µm) and Raise 3D Pro2 (104.33 ± 22.24 µm) (Table 1).

The RMS value remained similar for the printers Stratasys J750, Form2, Rapid Shape D40 and Cara Print 4.0 (Figure 3a). Besides, these printers performed no significant differences in two-by-two Kruskall-Wallis non-parametric test with Bonferroni correction (table 2).

Commercial 3D Printers	Trueness/ precision Mean (µm)	Small-extent surgical guide (mean ±sd)	Large-extent surgical guide (mean ±sd)	p-value* (α=0.05)
Stratasys J750	Trueness	70.43 ± 5.41	109.02 ± 18.59	0.004
	Precision	70.02 ± 5.43	110.47 ± 19.36	0.004
Prodways P1000	Trueness	97.93± 13.62	125.6 ± 21.57	0.025
	Precision	97.82 ± 13.04	111.47 ± 25.88	0.423
Raise 3D Pro2	Trueness	104.33 ± 22.24	139.55 ± 22.44	0.037
	Precision	95.12 ± 12.17	139.62 ± 20.05	0.004
Form2	Trueness	67.75 ± 10.63	93.12 ± 13.22	0.010
	Precision	64.3 ± 9.83	98.05 ± 12.16	0.004
Rapid Shape D40	Trueness	64.28 ± 7.95	106.52 ± 23.74	0.006
	Precision	64.02 ± 7.17	101.22 ± 21.04	0.006
Cara Print 4.0	Trueness	75.53 ± 13.95	98.67 ± 25.57	0.055
	Precision	72.65 ± 16.61	94.1 ± 19.05	0.078

Sd=standard deviation; *calculated with Kruskall-Wallis test.
Data obtained from a small-extent surgical guide and a large-extent surgical guide printed six times by each printer.

Table 1. Trueness and precision of commercial printers for the manufacturing of either small-extent surgical guide or large-extent surgical guide.

	Stratasys J750	Prodways P1000	Raise 3D Pro2	Form2	Rapid Shape D40	Cara Print 4.0
Stratasys J750	1	0.018	0.015	0.502	0.304	0.722
Prodways P1000	0.018	1	0.934	**0.002**	**0.001**	0.045
Raise 3D Pro2	0.015	0.934	1	**0.002**	**0.001**	0.037
Form2	0.502	**0.002**	**0.002**	1	0.722	0.304
Rapid Shape D40	0.304	**0.001**	**0.001**	0.722	1	0.166
Cara Print 4.0	0.722	0.045	0.037	0.304	0.166	1

Table 2. P-values from two-by-two comparisons of trueness between the commercial 3D printers to manufacture a small-extent surgical guide (with Bonferroni corrected significance α= 0.0033).

Likewise, the RMS value was similar for the printers Prodways P1000 and Raise 3D Pro2 with no significant differences (Figure 3a). However, there was a significant difference in the trueness of small-extent SG between Raise 3D Pro2 and Form2 (p = 0.002), between Raise 3D Pro2 and Rapid Shape D40 (p = 0.001), between Prodways P1000 and Form2 (p = 0.002), between Prodways P1000 and Rapid Shape D40 (p = 0.001) (Table 2).

On the other hand, for the large-extent SG, Form2 obtained the lowest RMS value (93.12 ± 13.22 µm) followed by Cara Print 4.0 (98.67 ± 25.57 µm), Rapid Shape D40 (106.52 ± 23.74 µm), Stratasys J750 (109.02 ± 18.59 µm), Prodways P1000 (125.60 ± 21.57 µm) and Raise 3D Pro2 (139.55 ± 22.44 µm).

The RMS value remained similar for the printers Form2, Cara Print 4.0, Rapid Shape D40, Stratasys J750 and Prodways P100 (Figure 4a). Besides, these printers performed no significant differences in the two- by-two Kruskall-Wallis non-parametric test with Bonferroni correction. However, there was a significant difference in the trueness of large- extent SG only between Raise 3D Pro2 and Form2 ($p = 0.001$) (Table 3).

The RMS values was not similar for printing small-extent or large- extent SG guide with the same commercial printer (Table 1). Significant statistical differences were observed between small-extent SG and large-extent SG, regardless of the commercial printer except for Cara Print 4.0 ($p = 0.055$) (Figure 5a).

	Stratasys J750	Prodways P1000	Raise 3D Pro2	Form2	Rapid Shape D40	Cara Print 4.0
Stratasys J750	1	0.255	0.053	0.212	0.934	0.502
Prodways P1000	0.255	1	0.427	0.017	0.223	0.071
Raise 3D Pro2	0.053	0.427	1	**0.001**	0.044	0.009
Form2	0.212	0.017	**0.001**	1	0.244	0.565
Rapid Shape D40	0.934	0.223	0.044	0.244	1	0.556
Cara Print 4.0	0.502	0.071	0.009	0.565	0.556	1

Table 3. P-values from two-by-two comparisons of trueness between the commercial 3D printers to manufacture a large-extent surgical guide (with Bonferroni corrected significance $\alpha = 0.0033$).

2. Precision

For the small-extent SG, Rapid Shape D40 obtained the lowest SD value (64.02 ± 7.17µm) followed by Form2 (64.30 ± 9.83µm), Stratasys J750 (70.02 ± 5.43µm), Cara Print 4.0 (72.65 ± 16.61µm), Raise 3D Pro2 (95.12 ± 12.17µm) and Prodways P1000 (97.82 ± 13.04µm) (Table 1).

The SD value remained similar for the printers Stratasys J750, Form2, Rapid Shape D40 and Cara Print 4.0 (Figure 3b). Besides, these printers performed no significant differences in two-by-two Kruskall-Wallis non-parametric test with Bonferroni correction (Table 4). Like- wise, the SD value was similar for the printers Prodways P1000 and Raise 3D Pro2 with no significant differences (Figure 3b). However, there was a significant difference in the precision of small-extent SG between Raise 3D Pro2 and Form2 ($p = 0.002$), between Raise 3D Pro2 and Rapid Shape D40 ($p = 0.002$), between Prodways P1000 and Form2 ($p = 0.001$), between Prodways P1000 and Rapid Shape D40 ($p = 0.001$) (Table 4).

	Stratasys J750	Prodways P1000	Raise 3D Pro2	Form2	Rapid Shape D40	Cara Print 4.0
Stratasys J750	1	0.016	0.026	0.381	0.411	0.891
Prodways P1000	0.016	1	0.848	**0.001**	**0.001**	0.011
Raise 3D Pro2	0.026	0.848	1	**0.002**	**0.002**	0.018
Form2	0.381	**0.001**	**0.002**	1	0.956	0.459
Rapid Shape D40	0.411	**0.001**	**0.002**	0.956	1	0.493
Cara Print 4.0	0.891	0.011	0.018	0.459	0.493	1

Table 4. P-values from two-by-two comparisons of precision between the commercial 3D printers to manufacture a small-extent surgical guide (with Bonferroni corrected significance α= 0.0033).

On the other hand, Cara Print 4.0 obtained the lowest SD value (94.10 ± 19.05µm) followed by Form2 (98.05 ± 12.16 µm), Rapid Shape D40 (101.22 ± 21.04µm), Stratasys J750 (110.47 ± 19.36µm), Prod- ways P1000 (111.47 ± 25.88µm) and Raise 3D Pro2 (139.62 ± 20.05µm) for the large-extent SG (Table 1).

The SD values remained similar for the printers Form2, Cara Print 4.0, Rapid Shape D40, Stratasys J750 and Prodways P100 (Figure 4b). Besides, these printers performed no significant differences in the two- by-two Kruskall-Wallis non-parametric test with Bonferroni correction. However, there was a significant difference in the precision of large- extent SG only between Raise 3D Pro2 and Cara Print 4.0 ($p = 0.002$) (Table 5). The SD values were not similar for printing small-extent or large- extent SG guide with the same commercial printer (Table 1). Significant statistical differences were

observed between small-extent SG and large-extent SG regardless of the commercial printer except for Cara Print 4.0 (p = 0.078) and Prodways P1000 (p = 0.423) (Figure 5b).

	Stratasys J750	Prodways P1000	Raise 3D Pro2	Form2	Rapid Shape D40	Cara Print 4.0
Stratasys J750	1	1.000	0.080	0.298	0.493	0.179
Prodways P1000	1	1	0.080	0.298	0.493	0.179
Raise 3D Pro2	0.080	0.080	1	0.005	0.015	**0.002**
Form2	0.298	0.298	0.005	1	0.722	0.763
Rapid Shape D40	0.493	0.493	0.015	0.722	1	0.511
Cara Print 4.0	0.179	0.179	**0.002**	0.763	0.511	1

Table 5. P-values from two-by-two comparisons of precision between the commercial 3D printers to manufacture a large-extent surgical guide (with Bonferroni corrected significance a= 0.0033).

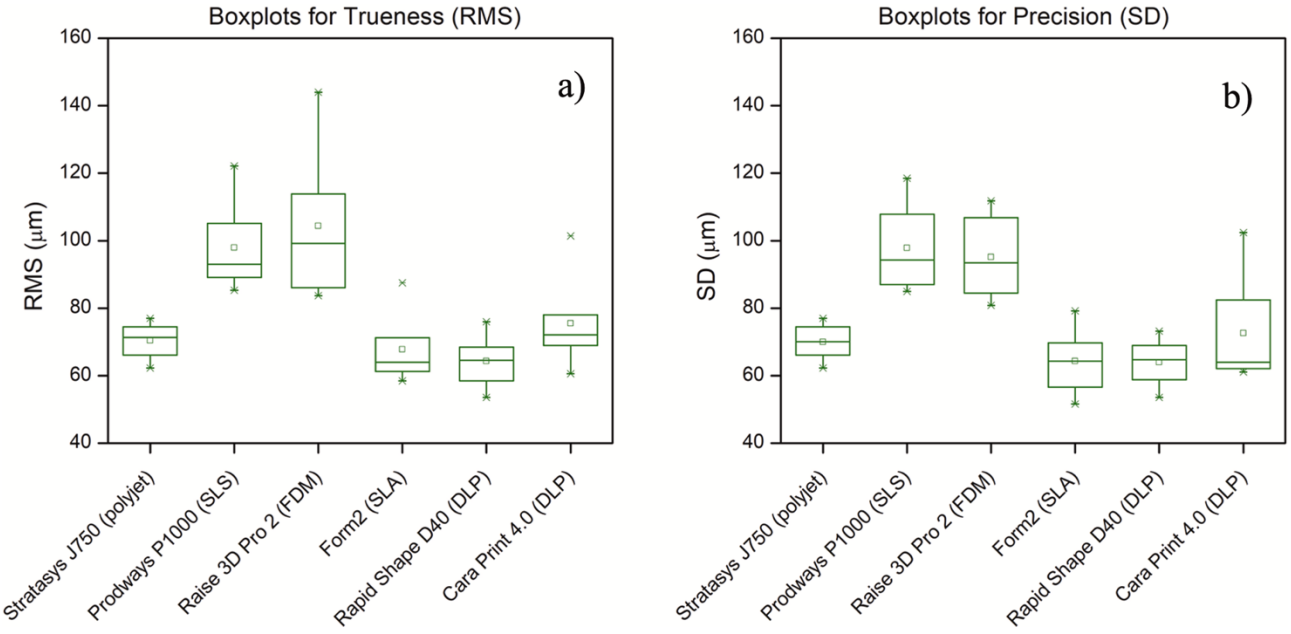

Figure 3. Boxplot of a) the trueness (RMS value) and b) the precision (SD value) obtained among the different 3D-printer devices for small-extent SG

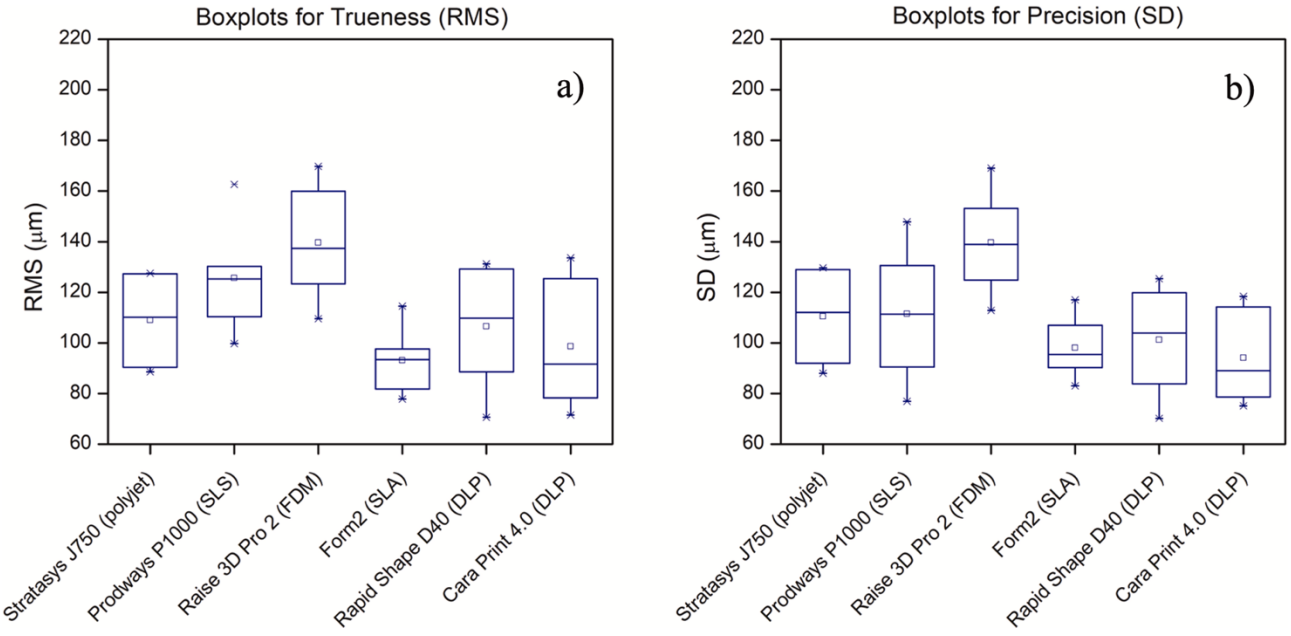

Figure 4. Boxplot of a) the trueness (RMS value) and b) the precision (SD value) obtained among the different 3D-printer devices for large-extent SG.

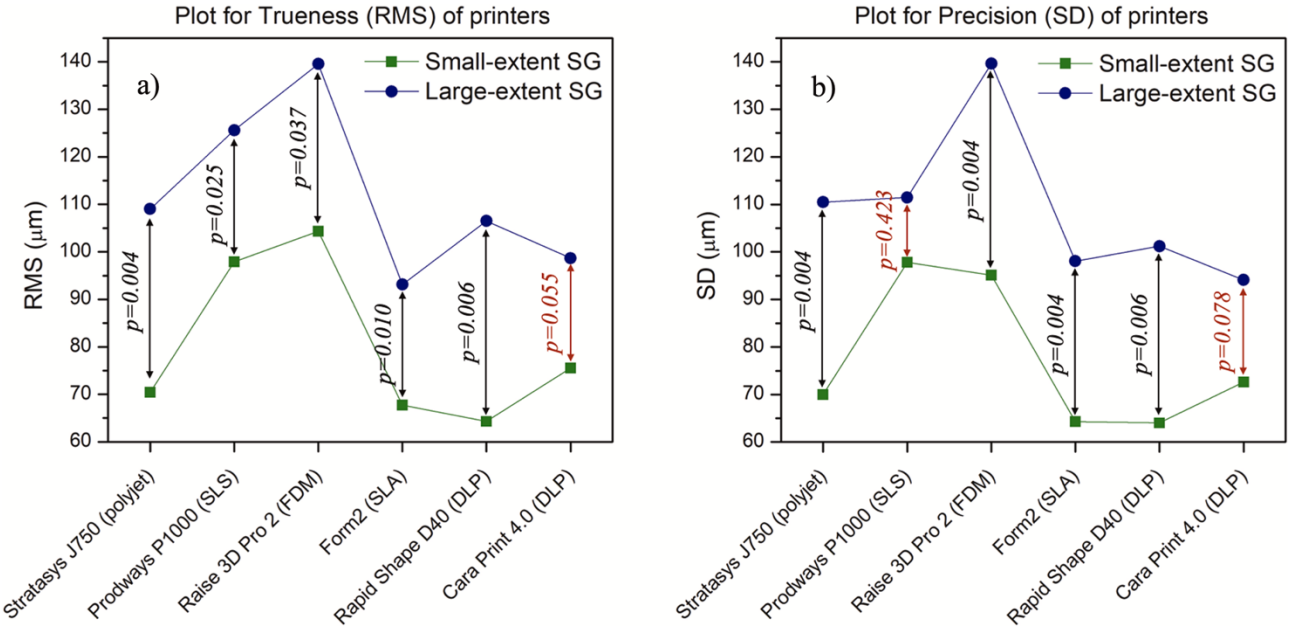

Figure 5. Impact of guide size (small-extent versus large-extent) for each printer to a) Trueness (RMS value) and b) Precision (SD value).

DISCUSSION

Null hypotheses were rejected in the basis of statistical analysis of the results, as additive manufacturing technology and surgical guide size affected accuracy and reproducibility of CAD-CAM surgical guides. Many factors can affect accuracy and reproducibility of 3D printed surgical guides, including data acquisition, data processing and surgical guides manufacturing. These depend on the 3D printer as well as on the dental technician using the device. An accuracy defect leads to a deviation of the implant positioning. It is therefore necessary to identify factors and study them individually, in order to improve accuracy and reproducibility. The present study evaluated the influence of AM technology on trueness and precision, as well as the influence of the guide size.

First, the trueness and the precision of each printer were compared, according to the guides' size. Small-extent SG exhibited overall higher trueness and precision than large-extent SG. Statistical Kruskall-Wallis test showed a significant difference for most printers when comparing small-extent to large-extent guides. Exceptions were DLP (Cara Print 4.0) for trueness and precision and SLS (Prodways P1000) for precision. These results were in accordance with Kholy et al. [27], who had studied influence of surgical guide support on accuracy of implant site location. The authors showed that an implant placed by a surgical guide sup- ported by four teeth exhibited 3D deviation values similar to implants placed with full-arch guides. However, surgical guides supported by only two teeth demonstrated significantly higher deviation

values than implants placed using surgical guides supported by four teeth or more. Moreover, Matsumura et al. [10] showed that an insufficient number of teeth supporting the guide, or an excess of teeth supporting the guide can influence errors of implant positioning during guided surgery. Balance fit and stability were therefore not sufficient to allow an accurate implant placement. Further studies are needed to determine the threshold guide size for which both guide accuracy and correct implant placement position can be optimized.

Trueness and precision were also compared between the different printers, for both small-extent SG and large-extent SG. For small-extent SG DLP (Rapid Shape D40) and SLA (Form2) printing technologies showed the lower RMS and SD value, while FDM (Raise 3D Pro2) and SLS (Prodways P1000) printing technologies showed the higher RMS and SD value. According to the Kruskall-wallis statistical test, there is a significant difference between the two groups. For the large-extent SG, the statistical differences are less pronounced. These results were different from observations by Kim et al. [22], who reported a significant difference in trueness and precision between Polyjet® and DLP on the one hand and SLA and FDM on the other hand. It should be noted, however, that the printers in our study were produced by different manufacturers. Interestingly, Li et al. [17] compared two technologies, Polyjet® and SLA, from the same manufacturers and reported a significant difference between the two technologies. On the opposite, our study found no significant difference between the

Polyjet® and SLA technologies. Our Polyjet printer (Stratasys J750) was different that the model used by Li et al. [17] (Eden260VS Stratasys Ltd, Eden Prairie, MN, USA).

In another field of health application, a study by Salmi et al. [28] compared 3D skull models printed with SLS, 3DP and Polyjet® techniques. They reported that the models printed with the Polyjet® printer had the smallest dimensional error, followed by models printed with 3DP and SLS. In another study, Ibrahim et al. [29] have printed mandibular models using SLS, 3DP and Polyjet®. The dimensional error was lowest for the SLS technique, followed by Polyjet and 3DP. Taehum et al. [30] have printed a simplified surgical guide with 3 technologies i. e. SLA, Polyjet® and Multijet Printing (MJP): they concluded that Polyjet® and SLA technologies had the best accuracy compared to the MJP technique. Although 3DP and MJP techniques were not used in our study, no significant difference was reported between the Polyjet® and SLS systems or Polyjet® and SLA. Moreover, the accuracy of 3D printers can differ depending on the nature of the printed materials. When manufacturing surgical guides involving photosensitive resin, errors could occur during the production and curing of the materials. The polymerization of the resin, the residual processing, the creation and removal of support structures (to avoid unsupported or weakly supported parts) can have an impact on the final result [31–33]. Thus, Piedra-Cascó n et al. [34] have studied impact of 3D-printing parameters, supporting structures, slicing, and post-processing procedures of vat-polymerization additive manufacturing technologies. Authors shown via a narrative study that the accuracy of the

manufactured dental device is significantly influenced by these parameters. For example, they recommended to re-calibrate the printing parameters for each resin available for the printer.

The accuracy of the scanner used in our study to obtain the STL files may have influenced the results. Indeed, dental laboratory scanners showed an accuracy of about 10–15 µm. Compared to dental laboratory scanners, industrial scanners can offer a higher level of accuracy (5–7 µm) [35,36]. In the present study, Helling 3D Scan Spray was used with minimal material thickness on all guides during the scanning procedure with the laboratory laser scanner, which was set to an accuracy of 15 µm to improve the consistency of the scan results [37]. However, as all the samples were processed with the same procedure, it can be assumed that the dental laboratory scanner and the powdering of the SG did not in- fluence the comparisons between the printers.

To study the printing accuracy of the different 3D printers, the RMS value given by the Geomagic software was used. These determinants have also been used in different studies and have shown their value [26, 38,39]. Other methods could have been used as described elsewhere [40] such as the absolute average (ABS AVG) or the (90° − 10°)/ 2 (where 90° is the 90th percentile and 10° is the 10th percentile).

In our study, only surgical guides manufactured with SLA/DLP technologies could find final clinical applications due to the biocompatibility of the resin. Indeed, surgical guides are manufactured using resin designed as class 1 materials and having the CE

marking, which can be sterilized and used intraorally [41]. Many studies [42–44] have investigated the impact of sterilization procedure as a dimensional change in the manufactured guide. These studies agree that sterilization of any type (heat or plasma) does not have a significant impact on the dimensional changes of the guides tested. SLA and DLP technologies are similar and classified in the same category of AM by the ASTM. No significant difference between the SLA and DLP printers was observed for both small-extent SG and large-extent SG. These results are different from those obtained by Mangano et al. [45], who have studied the ac- curacy of six printers. In this study, 9 parallelepipeds were printed with 6 different 3D-printer, using the proprietary material and with the layer thickness indicated by the manufacturer for the fabrication of dentate models. The results have shown a significant difference between the models printed by SLA and DLP. This difference could be explained by the layer thickness (as suggested by the manufacturer). Similar obser- vations were made by Rungrojwittayakul et al. [46] where the different layer thickness might affect the dimensional accuracy of the model. Favero et al. [47] reached the same conclusion. The x-y-z resolution of each layer influence the surface accuracy of the device. Even the design of the base can influence 3D-printer accuracy as observed by Camarella et al. [48]. Indeed, they have shown that for the same SLA printer, the shape of the base (regular base vs horseshoe-shaped base) influenced the printing accuracy. In our study, the models were printed with different resolutions:

equal layer thickness, x-y resolution, and manufacturing environments. All these parameters limit the generalization of these findings.

The intrinsic lesser accuracy of DLP compared to SLA did not impact the accuracy of the printed guides related to their size. However, two differences should be noted: the manufacturing of surgical guide is eight time longer for SLA (SLA≈4 h; DLP≈30 min) and the cost of the ma- chines which ranges from 2 to 3 k€ for the SLA printer, compared to 5 to 100 k€ for the DLP printer.

Finally, further limitations of our study include the in vitro settings and the two surgical guides used. Further in vitro and clinical studies are needed to evaluate and compare the scanning accuracy of different printers in a larger variety of clinical situations.

CONCLUSION

Within the limitations of the present in vitro study, the small-extent surgical guides were more accurate than the large-extent guides, regardless of the 3D-printer technology. Nonetheless, SLA and DLP technologies showed similar results in terms of trueness and precision for both small-extent and large-extent surgical guides. FDM technology was the least accurate. Several parameters have an influence on the accuracy of the parts produced and we have shown that the type of 3D- printer matters in some cases. It’s also important to consider other parameters such as the printing material, the use of supporting structures, the slicing method and the type of

software, the use of a post-processing polymerization and other printing parameters. The adequate combination of these parameters is essential to obtain the best accuracy and reproducibility of the printed parts that are essential to obtain reliable surgical procedures. The minimum is to follow the process described by the manufacturer, but the dental technician has also an important role to optimize these parameters. Further studies are needed on each parameter involved, in order to identify critical processes that determine the best printing accuracy.

BIBLIOGRAPHY

[1] Whitley D, Eidson RS, Rudek I, Bencharit S. In-office fabrication of dental implant surgical guides using desktop stereolithographic printing and implant treatment planning software: a clinical report, J. Prosthet. Dent. **2017** 118:256–263

[2] Hammerle CHF, Stone P, Jung RE,Kapos T,Brodala N.Consensus Statements and Recommended Clinical Procedures Regarding Computer-Assisted Implant Dentistry. *International Journal of Oral & Maxillofacial Implants* **2009** pp. 126–129

[3] Varga E, Antal M, Major L, Kiscsaťari R, Braunitzer G, Piffkó J. Guidance means accuracy: a randomized clinical trial on freehand versus guided dental implantation. *Clin Oral Implants Res* **2020** 31:417–430,

[4] Younes F, Eghbali A, Bruyckere TD, Cleymaet R, Cosyn J. A randomized controlled trial on the efficiency of free-handed, pilot-drill guided and fully guided implant surgery in partially edentulous patients. *Clin Oral Implants Res* **2019** 30:131–138

[5] Kühl S,Zürcher S, Mahid T, Müller-Gerbl M, Filippi A, Cattin P. Accuracy of full guided vs. half-guided implant surgery. *Clin Oral Implants Res* **2013** 24:763–769

[6] Jorba-García A, Gonz´alez-Barnadas A, Camps-Font O, Figueiredo R, Valmaseda-Castell´o E. Accuracy assessment of dynamic computer–aided implant placement: a systematic review and meta-analysis. *Clin Oral Invest* 25 **2021** 25:2479–2494

[7] M Vercruyssen M, Laleman I, Jacobs R, Quirynen M. Computer-supported implant planning and guided surgery: a narrative review. *Clin Oral Implants Res* **2015** 26:69–76

[8] Zhou W, Liu Z, Song L, Kuo C, Shafer DM. Clinical Factors Affecting the Accuracy of Guided Implant Surgery - A Systematic Review and Meta-analysis. *Journal of Evidence Based Dental Practice* **2018** 18:28–40

[9] Geng W, Liu C, Su Y, Li J, Zhou Y. Accuracy of different types of computer-aided design/computer-aided manufacturing surgical guides for dental implant placement *Int J Clin Exp Med* **2015** 8:8442–8449

[10] Matsumura A, Nakano T, Ono S, Kaminaka A, Yatani H, Kabata D. Multivariate analysis of causal factors influencing accuracy of guided implant surgery for partial edentulism: a retrospective clinical study. *Int J Implant Dent* **2021** 7:28

[11] Hinckfuss S, Conrad HJ, Lin L, Lunos S, Seong W-J. Effect of Surgical Guide Design and Surgeon's Experience on the Accuracy of Implant Placement. J. Oral Implantol **2012** 38:311–323

[12] Liang X, Jacobs R, Hassan B, Li L, Pauwels R, Corpas L, Souza PC, Martens W, Shahbazian M, Alonso A, Lambrichts *I*. A comparative evaluation of Cone Beam Computed Tomography (CBCT) and Multi-Slice CT (MSCT). *Eur J Radiol* **2010** 75:265–269

[13] Abduo J, Lau D. Effect of Manufacturing Technique on the Accuracy of Surgical Guides for Static Computer-Aided Implant Surgery. *Int J Oral Maxillofac Implants* **2020** 35:931–938

[14] Rubayo DD, Phasuk K, Vickery JM, Morton D, Lin WS. Influences of build angle on the accuracy, printing time, and material consumption of additively manufactured surgical templates. *J Prosthet Dent* **2020**

[15] Putra RH, Yoda N, Astuti ER, Sasaki K. The accuracy of implant placement with computer-guided surgery in partially edentulous patients and possible influencing factors: a systematic review and meta-analysis. *J Prosthodont Res* **2021**

[16] Azari A, Nikzad S. The evolution of rapid prototyping in dentistry: a review. *Rapid Prototyp J* **2009** 15:216–225

[17] Chen L, Lin WS, Polido WD, Eckert GJ, Morton D. Accuracy, reproducibility, and dimensional stability of additively manufactured surgical templates. *J Prosthet Dent* **2019** 122:309–314

[18] Negi S, Dhiman S, Kumar Sharma R. Basics and applications of rapid prototyping medical models. *Rapid Prototyp J* **2014** 20:256–267,

[19] Revilla-León M, Özcan M. Additive Manufacturing Technologies Used for Processing Polymers: current Status and Potential Application in Prosthetic Dentistry: polymer Additive Manufacturing for Prosthodontics. *J Prosthodont* **2019** 28:146–158

[20] Taormina G, Sciancalepore C, Messori M, Bondioli F. 3D printing processes for photocurable polymeric materials: technologies, materials, and future trends. *J Appl Biomater Funct Mater* **2018** 16:151–160,

[21] Snyder TJ, Andrews M, Weislogel M, Moeck P, Stone-Sundberg J, Birkes D, Hoffert MP, Lindeman A, Morrill J, Fercak O, Friedman S, Gunderson J, Ha A, McCollister J, Chen Y, Geile J, Wollman A, Attari B, Botnen N, Vuppuluri V, Shim J, Kaminsky W, Adams D,Graft J. 3D Systems' Technology Overview and New Applications in Manufacturing, Engineering, Science, and Education. *3D Printing Additive Manuf 2014* 1:169–176,

[22] Kim S-Y, Shin Y-S, Jung H-D, Hwang C-J, Baik H-S, Cha J-Y. Precision and trueness of dental models manufactured with different 3-dimensional printing techniques. *Am J Orthod Dentofacial Orthop* **2018** 153:144–153

[23] Torabi K, Farjood E, Hamedani S. Rapid Prototyping Technologies and their Applications in Prosthodontics, a Review of Literature. *J Dent (Shiraz)* **2015** 16:1–9.

[24] Kristiawan RB, Imaduddin F, Ariawan D, Arifin Ubaidillah Z. A review on the fused deposition modeling (FDM) 3D printing: filament processing, materials, and printing parameters. *Open Eng* **2021** 11:639–649,

[25] International Organisation of Standardization, ISO5725-1, Accuracy (trueness and precision) of Measurement Methods and Results — Part 1: General principles and Definitions. **1994** Accessed July 21, 2021, https://www.iso.org/obp/ui/ #iso:std:iso:5725:-1:ed-1:v1:en.

[26] Revilla-León M, P´erez-Barquero JA, Barmak BA, Agustín-Panadero R, Fern´andez-Estevan L, Att W. Facial scanning accuracy depending on the alignment algorithm and digitized surface area location: an in vitro study *J Dent* **2021** 110:103680

[27] Kholy KE, Lazarin R, Janner SFM, Faerber K, Buser R, Buser D Influence of surgical guide support and implant site location on accuracy of static Computer-Assisted Implant Surgery. *Clin Oral Implants Res* **2019** 30:1067–1075

[28] Salmi M. Additive Manufacturing Processes in Medical Applications, *Materials (Basel)* **2021** 14:191

[29] Ibrahim D, Broilo TL, Heitz C, de Oliveira MG, de Oliveira HW, Nobre SMW, dos Santos Filho JHG, Silva DN. Dimensional error of selective laser sintering, three-dimensional printing and PolyJetTM models in the reproduction of mandibular anatomy. *Journal of Cranio-Maxillofacial Surgery* **2009** 37:167–173

[30] Kim T, Lee S, Kim GB, Hong D, Kwon J, Park J-W, Kim N. Accuracy of a simplified 3D-printed implant surgical guide. *J Prosthet Dent* **2019**

[31] Choi J-Y, Choi J-H, Kim N-K, Kim Y, Lee J-K, Kim M-K, Lee JH, KimM-J. Analysis of errors in medical rapid prototyping models. *Int J Oral Maxillofac Surg* **2002** 31:23–32

[32] Unkovskiy A, Bui PH-B, Schille C, Geis-Gerstorfer J, Huettig F, Spintzyk S. Objects build orientation, positioning, and curing influence dimensional accuracy and flexural properties of stereolithographically printed resin. *Dent Mater* **2018** 34:e324–e333

[33] Quan H, Zhang T, Xu H, Luo S, Nie J, Zhu X. Photo-curing 3D printing technique and its challenges*. Bioact Mater* **2020** 5:110–115

[34] Piedra-Cascón W, Krishnamurthy VR, Att W, Revilla-León M. 3D printing parameters, supporting structures, slicing, and post-processing procedures of

vat- polymerization additive manufacturing technologies: a narrative review. *J Dent* **2021** 109:103630

[35] Mandelli F, Gherlone E, Gastaldi G, Ferrari M. Evaluation of the accuracy of extraoral laboratory scanners with a single-tooth abutment model: a 3D analysis *J Prosthodont Res* **2017** 61:363–370,

[36] Lee J-J, Jeong I-D, Park J-Y, Jeon J-H, Kim J-H, Kim W-C. Accuracy of single-abutment digital cast obtained using intraoral and cast scanners. *J Prosthet Dent* **2017** 117:253–259

[37] Goodacre BJ, Goodacre CJ, Baba NZ, Kattadiyil MT. Comparison of denture base adaptation between CAD-CAM and conventional fabrication techniques. *J Prosthet Dent* **2016** 116:249–256

[38] Papaspyridakos P, Chen Y, Alshawaf B, Kang K, Finkelman M, Chronopoulos V, Weber H-P. Digital workflow: in vitro accuracy of 3D printed casts generated from complete-arch digital implant scans. *J Prosthet Dent* **2020** 124:589–593

[39] M. Doukantzi, P. Mojon, A. Todorovic, N. Chebib, B.E. Pjetursson, S. Maniewicz, I. Sailer, Comparison of the Accuracy of Optical Impression Systems in Three Different Clinical Situations. *Int J Prosthodont* **2021** 34:511–517,

[40] Lerner H, Nagy K, Pranno N, Zarone F, Admakin O, Mangano F. Trueness and precision of 3D-printed versus milled monolithic zirconia crowns: an in vitro study. *J Dent* **2021** 113:103792

[41] Caiti G, Dobbe JGG,. Strijkers GJ, Strackee SD, Streekstra GJ. Positioning error of custom 3D-printed surgical guides for the radius: influence of fitting location and guide design. *Int J Comput Assist Radiol Surg* **2018** 13:507–518,

[42] Marei HF, Alshaia A, Alarifi S, Almasoud N, Abdelhady A. Effect of Steam Heat Sterilization on the Accuracy of 3D Printed Surgical Guides. *Implant Dent* **2019** 28:372–377

[43] Török G, Gombocz P, Bogn´ar E, Nagy P, Dinya E, Kisp´elyi B, Hermann P. Effects of disinfection and sterilization on the dimensional changes and mechanical properties of 3D printed surgical guides for implant therapy - pilot study. *BMC Oral Health* **2020** 20:19

[44] Shaheen E, Alhelwani A, Van De Casteele E, Politis C, Jacobs R. Evaluation of Dimensional Changes of 3D Printed Models After Sterilization: a Pilot Study. *Open Dent J* **2018** 12

[45] Mangano F, Admakin O, Bonacina M, Biaggini F, Farronato D, Lerner H. Accuracy of 6 Desktop 3D Printers in Dentistry: a Comparative In Vitro Study, *Eur J Prosthodont Restor Dent* **2020** 28

[46] Rungrojwittayakul O, Kan JY, Shiozaki K, Swamidass RS,. Goodacre BJ, Goodacre CJ, Lozada JL. Accuracy of 3D Printed Models Created by Two Technologies of Printers with Different Designs of Model Base. J Prosthodont **2020** 29:124–128

[47] Favero CS, English JD, Cozad BE, Wirthlin JO, Short MM, Kasper FK. Effect of print layer height and printer type on the accuracy of 3-dimensional printed orthodontic models. *Am J Orthod Dentofacial Orthop* **2017** 152:557–565

[48] Camardella LT, de Vasconcellos Vilella O, Breuning H. Accuracy of printed dental models made with 2 prototype technologies and different designs of model bases. *Am J Orthod Dentofacial Orthop* **2017** 151:1178–1187

Chapter VI

Predictability of intraoral scanner error for full-arch implant-supported rehabilitation

INTRODUCTION

In the past decade, the applications of digital technologies in dentistry have undergone exponential growth [1]. A reliable impression, acquired with an intraoral scanner (IOS), is the first and most crucial step in all digital workflows [2]. IOS, as defined by the ISO 20896 (International Organization for Standardization), is the combination of a hand-held scanning device suited for use in the oral cavity, and computer hardware and software that outputs a numerical, three-dimensional description of scanned surfaces. An IOS must be practical, user-friendly, cost-effective, fast, powder-free, and accurate [3].

Accuracy is defined as the result of trueness and precision by the ISO 5725 (International Organization for Standardization). Trueness refers to the closeness of agreement between the arithmetic mean of a large number of test results and the true or accepted reference value. Precision refers to the closeness of agreement between repeated test results. Therefore, a precise scanner delivers consistent results after repeated scans, while a true scanner obtains a three-dimensional object rendition that closely matches the scanned object. These two features are not

necessarily correlated; for example, a scanner with high (low) trueness may have low (high) precision.

The overall performance of full-arch scans in edentulous patients for implant-supported prostheses has been a topic of debate among researchers and clinicians. There is no consensus regarding whether IOSs can substitute traditional impressions for the fabrication of implant-supported prostheses in completely edentulous patients [4–10]. Instead of relying on transfer copings, IOSs retrieve the information regarding implant position, angle, and height through implant scan body (SB) [11]. When performing full-arch digital scans, SB geometry, material and position could affect final accuracy. [11,12]

Most of the literature, varying in methods and superimposition techniques,[13] describes accuracy analyses in terms of absolute variability between scan bodies and implant analog interdistances [14,15]. To our knowledge, no published studies have analyzed the relationship between the amount of error and interdistance or angle value (i.e., the predictability of IOS error).

Our research hypothesis was: “Is it possible to find out predictable errors assessing intraoral scanner accuracy in full arch-scan for implant supported rehabilitations?”. Thus, an *in vitro* study was performed, involving different IOSs, by addressing the error predictability in models with varying numbers of dental implants. We evaluated interdistances among scan bodies and their corresponding inclination angles.

MATERIALS AND METHODS

Study protocol

This *in vitro* study was performed to evaluate the error predictabilities of three commercial IOSs. According to the ISO 20896, that assess the accuracy evaluation of IOSs, under constant conditions, the same expert operator scanned six different plaster models made with a variable number of scan bodies. The model-reference data were acquired through a coordinate measuring machine (CMM). The interdistances and inclinations of the scan body's axes were calculated using the retrieved STL files. These data were compared with data obtained from the CMM.

The precision and trueness of each scanner were analyzed via statistical tests of interdistances and axes inclinations. The mathematical relationship between these measurements, as the scan-abutment distances increased, was investigated (Figure 1).

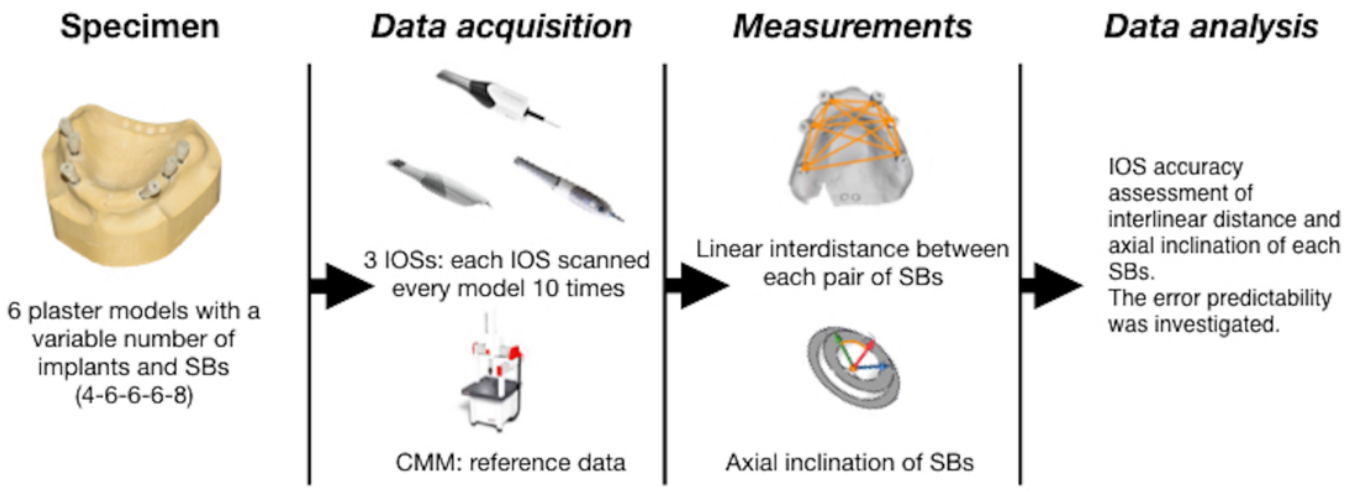

Figure 1. Overview of the study protocol.

Models

Six models, based on the same mold of an edentulous maxilla, were made using plaster class IV (GC Fujirock, Belgium). The operator then created holes in the models, using a core drill (diameter: 4 mm), in the middle of the bone crest. Four to eight implant analogs (Implant Way Mix; diameter: 3.8 mm; IESS Group, Italy) were placed with an unknown orientation and fixed in class IV plaster.

Four models with 6 implant analogs, one model with 4 implant analogs, and one model with 8 implant analogs were fabricated. One IESS Group scan body was screwed on each implant analog. This polyether-ether ketone scan body had a titanium metallic connection, a diameter of 5 mm, and a height of 8 mm.

CMM test

A mechanical CMM measures the geometry of an object by detecting discrete points on the surface of the object using a probe. The Coord3 CMM Benchmark, Perceptron (Coord3, Italy) was used in this study with a power-head PH10M plus, Renishaw 7.5° step 15 axis position A, 105° 48 axis position B ± −180°, sensor Ø1 mm TP20 SF, Renishaw 0.5 µm reprod., and uniaxial ± 1 µm reprod. on changing module. To acquire the analog space position data, one metallic cylinder (i.e., locator) with known dimensions was screwed on each implant analog.

After multiple contacts, the CMM registered the diameter and the plane at the top of the cylinders. With the resulting space position data and cylinder dimensions, the

researchers were able to obtain the origin P_0, which corresponded to the circle inscribed in the polygon at the base of the analog. Thus, P_0 represented the spatial position of the analog on 3 axes (x, y, and z). The CMM was capable of a three-dimensional maximum error assessed as E3-xyz (L) = 2.8 + 5 L/1000 mm (where L is the measured distance in millimeters, according to ISO 10360 standard). Therefore, the CMM data were regarded as true data.

Digital impressions

In this study, three different intraoral scanners were used: CS3600 version 3.1.0 (Carestream Dental, USA), Trios3 (3shape, Denmark), and Cerec Primescan version 5.1.3 (Dentsply Sirona, USA). Each model was scanned ten times by the same expert operator, in accordance with the manufacturer's instructions and under the same conditions (21°C and 80% humidity). The operator waited 10 min between scans. Each scanner performed 60 digital impressions.

Scanning strategy

The operator employed the same scanning strategy with all the IOSs. At the adequate scan high, the most distal scan body was scanned on the upper side, followed by the buccal and the palatal ones. Subsequently, the mucosa between the scan body detected and the following one was scanned without interrupting the scan flow at any moment. Then, the reached scan body was scanned on each side. The operator

scanned all the scan bodies in continuous flow. Scanning defects were fixed once the full-arch scan was acquired.

STL-file processing

To derive P0 from digital impressions, scan files were imported on Exocad (Exocad GmbH, Germany), a dental computer-aided design software. The STL files were opened and scan bodies, registered with the IOSs, were superimposed on standard scan bodies present in the Exocad library. These two scan bodies had been aligned using the "Best-Fit" algorithm. Following the matching, knowing the mathematical quotes of each library scan body, the P_0 of scan body platforms were obtained. P0, representing the spatial coordinates of the analog platform (Figure 2), was extracted both from the stl file and the models through the CMM. Thank to P0 was possible to analyze discrepancies between measurements retrieved through IOSs and the CMM.

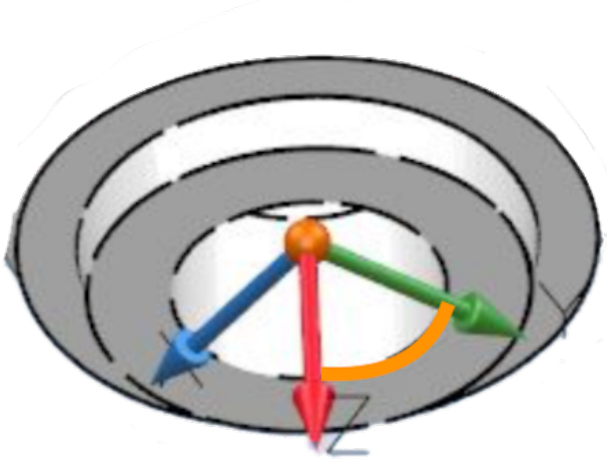

Figure *2.* P_0: the point that represents the spatial coordinates of the SB platform.

Inter-distance measurements

P_0, the origin point of each analog, was used to measure the distance between each pair of analogs. This point was represented by three axial coordinates (x, y, and z); distances were calculated using the formula below. The distance of every possible analog pair was considered, as shown in Figure 3. Distances evaluated on the IOS data were compared with distances obtained from the CMM. Both precision and trueness were determined via statistical analyses.

$$d = \sqrt{(x_m - x_n)^2 + (y_m - y_n)^2 + (z_m - z_n)^2}$$

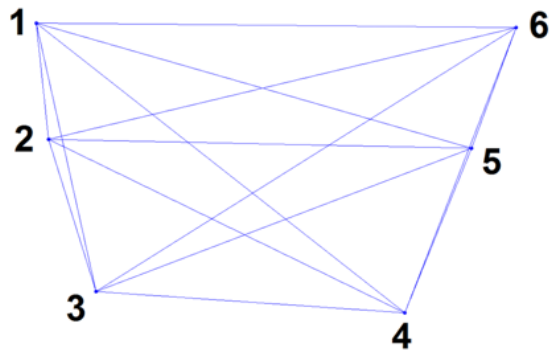

Figure 3. Formula and scheme used to analyze the interdistance measurements.

Axial inclination measurements

Errors in the axial inclinations of the scan bodies were calculated with P_0 as the origin. Each origin measurement was made of three vectors (i, j, and k); angles between each couple of scan body origins were calculated using the formula below (Figure 4). Each vector has three components in the Cartesian planes (xy, yz and yz), physically measuring the angle between two distinct vectors. So, it was possible to find the plane

in common and calculate the angle on this plane and to evaluate the misalignment between the axes of the scan body.

Eventually, the retrieved angles were compared with angles obtained from the CMM. Both precision and trueness were determined via statistical analyses.

$$\theta = \arccos\left(\frac{\vec{u}\cdot\vec{v}}{|\vec{u}|\,|\vec{v}|}\right) = \arccos\left(\frac{i_u\cdot i_v + j_u\cdot j_v + k_u\cdot\ k_v}{\sqrt{(i_u^2+j_u^2+k_u^2)}\cdot\sqrt{(i_v^2+j_v^2+k_v^2)}}\right) =$$

$$= \arccos\left(\frac{i_u\cdot i_v + j_u\cdot j_v + k_u\cdot\ k_v}{1\cdot 1}\right) = \arccos(i_u\cdot i_v + j_u\cdot j_v + k_u\cdot\ k_v)$$

Figure 4. Formula used to analyze the axial inclination.

Statistical analysis

The term “accuracy,” as defined by ISO standard 5725-1, encompasses both trueness and precision. “Trueness” is the measured deviation from the actual value or dimension of the object. “Precision” is a measure of repeatability or how close a set of results are to each other. Evaluating the precision means to analyze the error variability among replicates: the more precise a device is, the less error variability it shows.

Precision has been calculated as the standard deviation of replicates (n=10; i.e. scans) of each interdistance or axial inclination measured by all pairs of scan bodies (n=15 values for models 1, 2, 4 and 6, n=28 values for model 3 and n=6 values for model 5,

for 94 total values). The calculation was performed considering all values together and then stratified by model. Trueness was calculated as the difference between the mean value of 10 scans and the value obtained by CMM, for each combination of pairs of scan bodies, both for interdistance and axial inclination. Also in this case, 94 total values for each IOS were used and then stratified by model.

Bland–Altman analyses were performed to investigate precision and trueness [16]. These analyses were performed for the interdistances and the axial inclinations of the scan bodies. Linear regression analyses were performed using Pearson's r^2 to investigate IOS precision in terms of interdistances and axial inclinations. The distributions of trueness deviations were also reported.

Because of deviations from normality in the variability data, comparisons among IOSs were performed using Friedman's test followed by Dunn's post hoc test. Finally, the overall deviation from zero was tested by using the hypothesis test on a mean, with zero regarded as the null hypothesis.

A mixed model was used to analyze the deviation from reference values (defined as the difference between values of 10 scans and real measure for each combination of pairs of scan bodies), with model and type of IOS as between factors and scans as repeated measure (within factor). If Mauchly's sphericity assumption was met, Mauchly's test was used, whereas if Mauchly's sphericity assumption was not met, Huynh-Feldt test was used.

A p-value < 0.05 was considered statistically significant. All Bland–Altman analyses were performed using Origin Pro 2021 (OriginLab Corp., Northampton, MA, USA), while statistical comparisons were performed using GraphPad Prism 8.0 (GraphPad, San Diego, CA, USA).

RESULTS

Precision evaluation of linear interdistances

As previously affirmed, assessing the precision means to analyze the error variability. Thus, the graphs show *variability* on the *x* axes. The statistical results for IOS linear variability are shown in Figure 5. Primescan showed the best performance (mean: 0.047 mm; standard deviation: 0.020 mm), followed by Trios3 (mean: 0.069 mm; standard deviation: 0.042 mm) and CS3600 (mean: 0.073 mm; standard deviation: 0.042 mm)

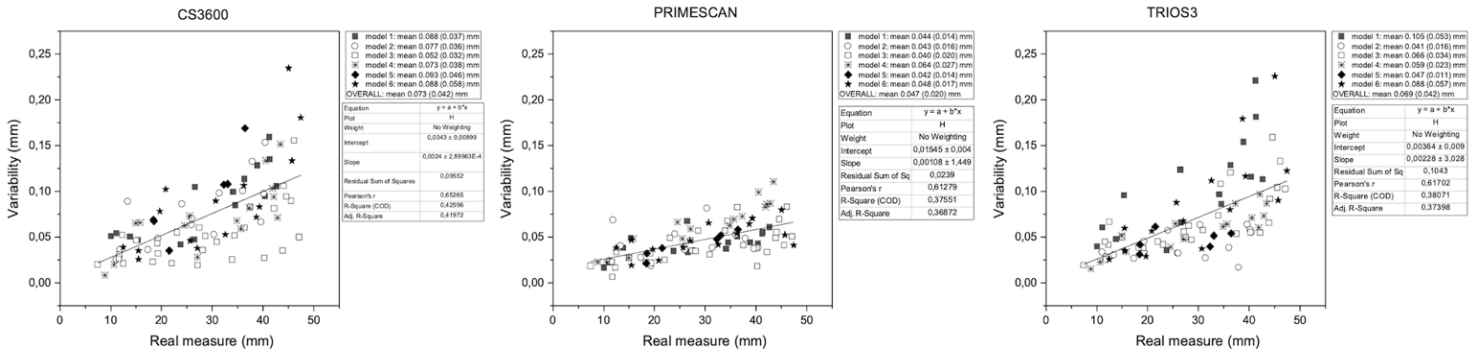

Figure 5. Graphical representation of precision analysis for the interdistance measurements.

For all IOSs, error variability increased with distance. As heteroscedasticity was observed, we performed a linear mixed model with model and type of IOS as between factors and scans as repeated measure (within factor). This approach revealed significant scan, IOS, scan*model, scan*IOS, model*IOS and scan*model*IOS effects ($p<0.001$ for all factors), while model did not show a significant effect ($p=0.857$). Scan and IOS are significant factors affecting the precision of three IOSs, and interestingly, their behaviors appear different from each other.

When the absolute variability was transformed into coefficient of variation as percentage (CV%, defined as $variability_{IOS}$/real $measure_{CMM}$*100), the resulting percentage relative error generally remained constant among measurements (Figure 6).

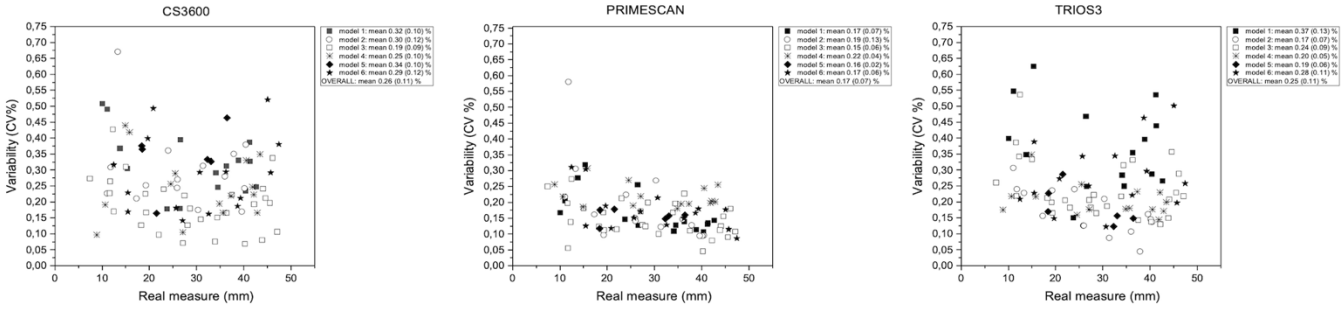

Figure *6*. Absolute error transformed into percentage relative error.

Trueness evaluation of linear interdistances

The results about IOS trueness are presented in Figure 7, showing the Bland-Altman plots. For CS3600 we observed a trueness with a mean of −0.012 mm and standard deviation of 0.049 mm. Both devices, CS3600 and Primescan tended to underestimate the real measure of linear interdistance ($p = 0.018$, $p<0.001$, respectively). Trios3 showed underestimation of the real measure ($p < 0.001$), which increased with increasing distance for Trios3. This device exhibited the worst trueness (mean: −0.079 mm; standard deviation: 0.048 mm).

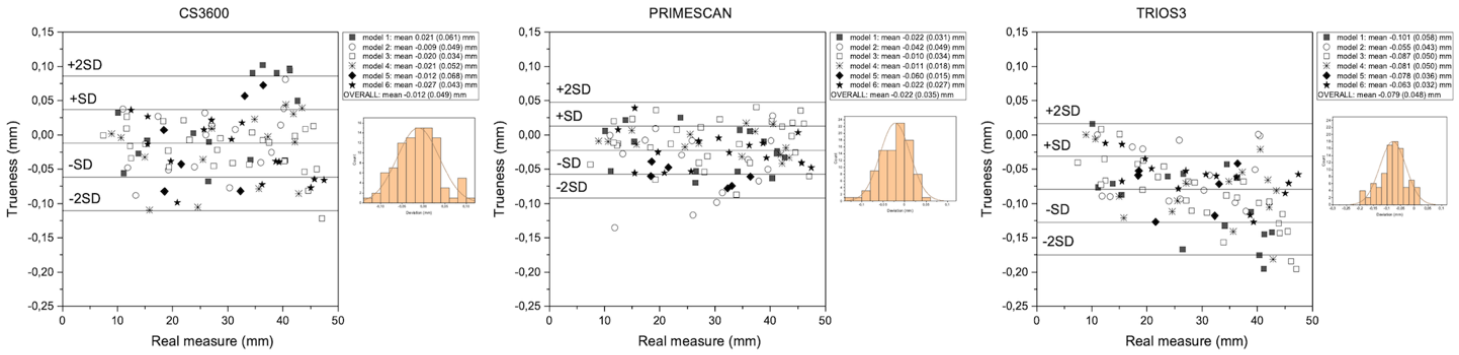

Figure 7. Graphical representation of trueness analysis for the interdistance measurements.

Linear interdistance: comparison among IOSs

Comparisons of variability and trueness are shown in Figure 8. The precisions of Trios3 and CS3600 were similar, while Primescan showed fewer outliers and less variability. Regarding trueness, Trios3 underestimated measurements, compared with the other scanners; CS3600 and Primescan exhibited similar findings (Figure 8).

As suggested by the linear mixed model previously mentioned, scan and IOS are significant factors affecting the accuracy of three IOSs, and interestingly, their behavior's appear different from each other.

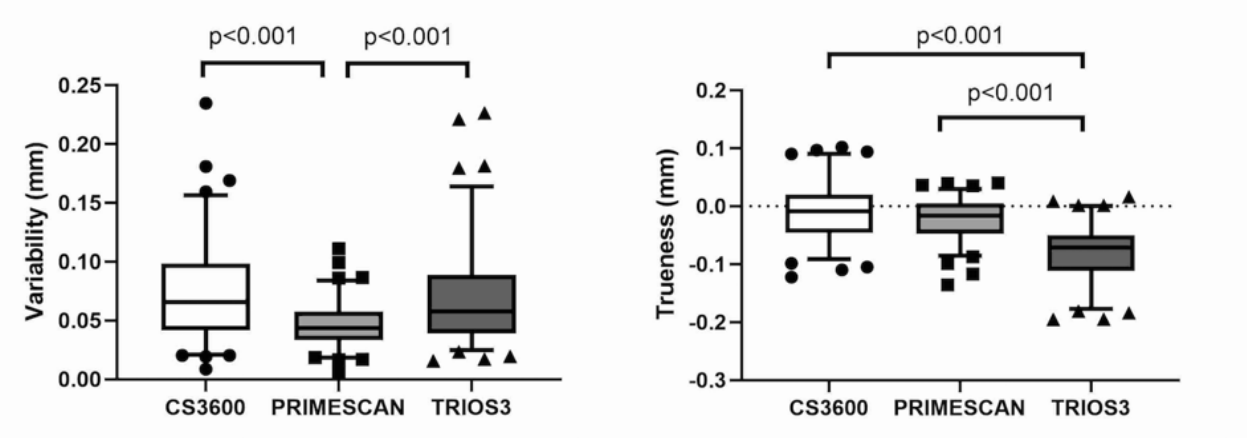

Figure 8. Absolute linear discrepancy comparison among IOSs in terms of precision and trueness. Solid black line represents the median value. Top and bottom of the box represent the 75th and 25th percentiles, respectively. Whiskers represent the maximum and minimum values, while geometric figures represent

Precision evaluation of axial inclination angles

The analysis of precision (variability) in axial inclination angle is depicted in Figure 9. Precision was not influenced by increasing angle. Primescan showed fewer outliers, compared with CS3600 and Trios3 (Figure 9).

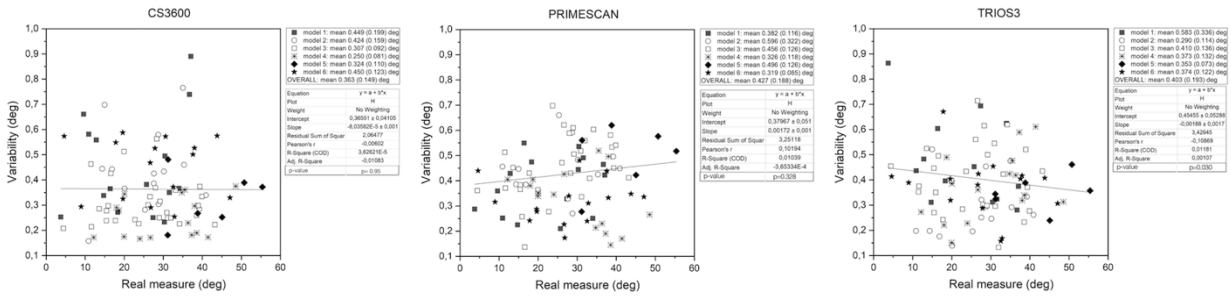

Figure 9. Graphical representation of precision analysis of the axial inclination of SBs

Trueness evaluation of axial inclination angle

The trueness evaluation of axial inclination angle for the three scanners and the Bland-Altman plots are presented in Figure 10.

The analysis on CS3600 showed that some cases were not included in the confidence interval and suggesting deviation from congruency between the scanner and the CMM ($p > 0.001$). Wider angle was related with greater underestimation by CS3600. In contrast, Primescan slightly overestimated the angles ($p = 0.008$). The residuals distribution of Primescan tended to be bimodal, with an irregular tendence to add 0.4° and 0.6°. This could explain the tendency towards overestimation. Trios3 tended to overall slightly overestimate the angles ($p = 0.01$). Left asymmetry was present in

the distribution, indicating that underestimation could affect important values. The residuals did not increase with increasing angle (Figure 10).

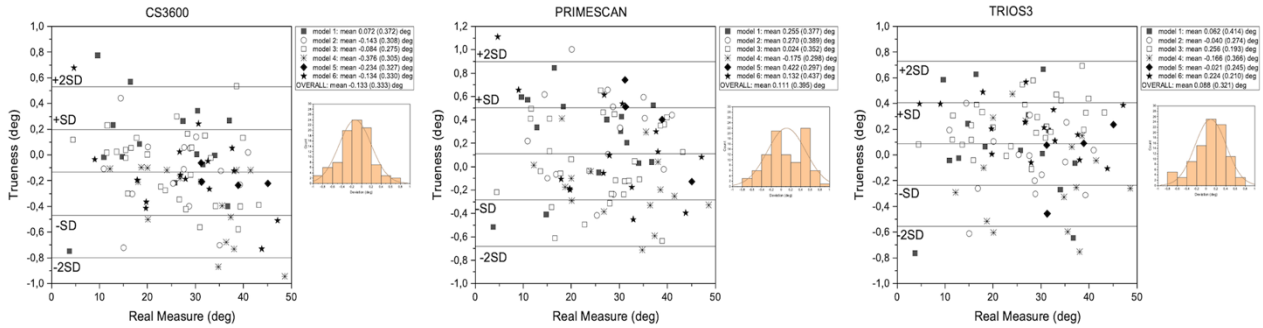

Figure 10. Graphical representation of trueness analysis of the axial inclination of SBs

Axial inclination angle: comparison among IOSs

There were no significant differences in inclination angle variability among IOSs (Figure 11). Regarding trueness, CS3600 tended to underestimate, while the other two scanners overestimated the values (Figure 11).

The analysis of variance of axial inclination data showed a significant effect of scan ($p=0.002$), model ($p<0.001$), IOS ($p<0.001$) and their interactions ($p<0.001$ for scan*model, scan*IOS, model*IOS and scan*model*IOS).

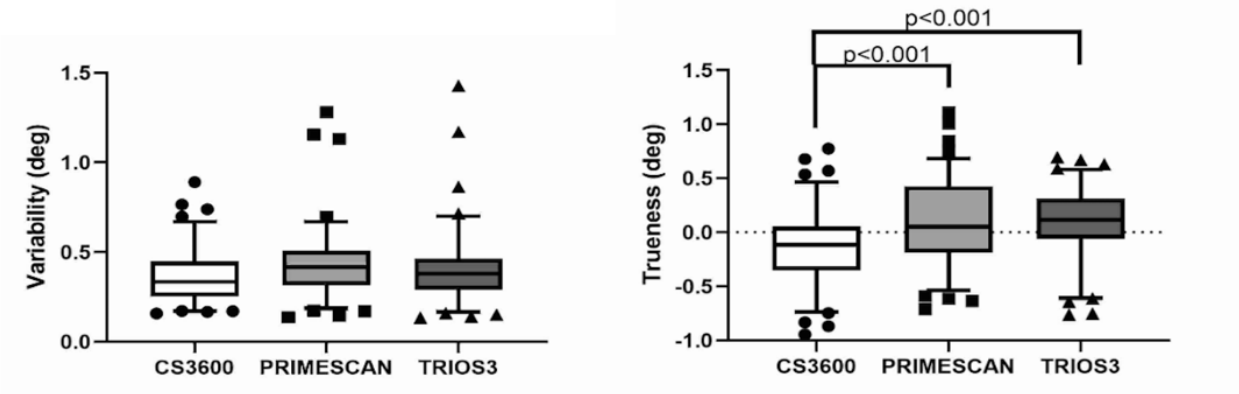

Figure 11. Axial inclination comparison among IOSs in terms of precision and trueness. Solid black line represents the median value. Top and bottom of the box represent the 75th and the 25th percentiles, respectively. Whiskers represent the maximum and minimum values, while geometric figures represent the outliers

DISCUSSION

The main findings of the present study revealed that Primescan, CS3600 and Trios3 showed predictable errors in assessing intraoral scanner accuracy in full arch-scan for implant supported rehabilitations. In particular, they tended to overestimate or underestimate linear measurements and axial inclinations of scan bodies, one added about 0.4-0.6° to the angle inclination values. Furthermore, we observed a heteroscedastic behavior probably related to the software or the device itself.

Accuracy is crucial for the fabrication of implant-supported prostheses because prosthetic misfits lead to clinical failure. Many authors have investigated the accuracies of IOSs for full-arch scans to determine whether they could replace conventional impressions [4,6,17,18]. Several studies have shown conflicting results regarding the accuracies of scanners employed in implant-prosthetic workflows. This

suggests that some IOSs are unsuitable for full-arch digital impressions [17]. The acceptable level of inaccuracy ranges from 50 μm to 150 μm [21,22].

Unfortunately, it is difficult to compare these studies because of differences in measurement methods, IOS versions, scan body shapes and sizes, materials, and sample types [20,23]. Some studies have involved dentate models [4,17,24,25], while others have used edentulous samples [10,26–28]. Furthermore, the methodology for evaluating accuracy differed among studies. Reference measurements obtained using CMMs are preferable, compared with measurements obtained using industrial scanners [20]. Nevertheless, it is important to process the meshes to identify unique scan-abutment points through the original computer-aided design files used to produce the abutments [19]. Many authors have used computer-aided design software with best-fit algorithms to perform mesh-to-mesh alignment [6,15,25,29–31]. From a metrological perspective, the accuracy estimate obtained using this methodology is unacceptable for assessment of IOS performance according to ISO 10360 standards [20]. In addition, operator experience [2], powder use [32], and the scan body [11] and sample materials [33] can influence the results. ISO20896 is the standard that defines test methods and procedures for assessing IOS accuracy. According to this document, the models were fabricated with plaster class IV, more than 30 scans for every IOS (i.e., 60 scans/IOS) were performed and SBs with an adequate dimension (ø5±0.01 mm) were screwed on implant analogs.

In addition, the test models showed a suitable minimum number of reference objects (i.e., 4-6-8 SBs). Despite the efforts to follow ISO20896, the presented method differs from the ones involved in ISO 20896. SBs, that give the possibility to investigate axial inclination, were used instead of the spheres, the statistic goes beyond the ISO20896 one, considering trueness and precision separately, and CMM measurement were regarded as true data.

According to the previous consideration, we prefer not to compare our results with previous findings.

The purpose of this study was to analyze the behaviors of these devices, focusing on error predictability.

Multiple predictable behaviors were found: a tendency to overestimate or underestimate the linear measurements, heteroscedasticity in analyses of linear variability when scanning longer spans, and tendency to add 0.4–0.6° in the axial inclination. These errors may have been caused by the software or the device itself. Regarding interlinear distances, Primescan was the most precise scanner, while CS3600 had the best trueness. Primescan showed fewer outliers and had a tendency towards underestimation. The tendency for underestimating linear measurements was present in all IOSs, although it was greater in Trios3 than in CS3600.

Focusing on interdistances measurements' precision, all the intraoral scanners showed heteroscedasticity, even if the variability error transformed into relative variability (CV%) showed different behavior with the tendency of variability to be

constant for increasing distances. Focusing on Trios 3 and CS3600 results, variability increased in absolute volume with increasing measurement values. However, the percentage error remained constant. Thus, accuracy was dependent on a coefficient linked to the instrument, which is equally important to the distance itself. On the other hand, the Primescan percentage relative error tended to slightly decrease for increasing distances.

A linear mixed model was performed and the variance components of different scanning replicates (i.e. scans), models, IOSs and their interaction terms were analyzed. Regarding the interdistances, the mixed model revealed that IOS and scans significantly affect the trueness of measurements ($p<0.001$). Furthermore, a significant effect was described for scan*model, scan*IOS, model*IOS and scan*model*IOS interaction terms ($p<0.001$ for all factors), showing different behaviors of scans, models, and IOSs on measurement. On the other hand, we did not observe a significant effect of model ($p=0.857$).

The analysis of variance of axial inclination data showed a significant effect of scan ($p=0.002$), model ($p<0.001$), IOS ($p<0.001$) and their interactions (scan*model, scan*IOS, model*IOS and scan*model*IOS: $p<0.001$ for all factors). It can be inferred that scan, model and IOS are significant factors, that affect the accuracy of IOSs. Researchers and IOSs manufacturers should investigate the correlation between variance components because they showed different behaviors and impact on the final result. Further studies are necessary to understand whether by modifying a

variance component might lead to an enhancement of performance in terms of resulting accuracy.

Regarding the axial inclination angle, none of the IOSs showed a heteroscedastic behavior. Primescan performed better than did Trios3 or CS3600, although it tended to add 0.4–0.6° to the measurements. Primescan bimodal distribution of residuals was unique. Moreover, CS3600 underestimated in proportion to the angle, while Trios3 overestimated the values by a constant amount.

Precision decreased with longer distances presumably because of the stitching process.[34] Scanning errors associated with image stitching tend to accumulate when the scanned objects are flat or planar, such as a residual ridge [35]. Trueness was reported to improve when scanning aids were used [36]. Miyoshi et al. suggested that digital impressions for implant treatment should be limited to small prostheses, such as a 3-unit superstructure supported by two implants [26]. Kernen et al. showed that intraoral scanning resulted in clinically unacceptable accuracy for long-span virtual models [37]. However, several authors have reported the superiority of digital impressions, compared with conventional impressions. Pesce et al. reported successful clinical results using intraoral scanners and scanning powder [38]. The present study used scan bodies in polyether-ether ketone that showed the best performance in previous literature [27,33].

Most studies thus far have not considered various factors that can affect intraoral scans, such as the presence of saliva, light conditions, soft and hard tissue reflections,

humidity, intermittent acquisition, and movement of the soft tissue and tongue [23,39,40]. In contrast to these factor, the employed type IV plaster models are optimal material for scanning. Indeed, reflective material can have a dramatic impact in scan accuracy.[33] Mucosal displacement achieved by conventional impressions cannot be replicated by IOSs [41]. Further *in vivo* studies are necessary to explore the applications of IOSs in implant treatment and to determine whether IOSs have clinically acceptable accuracy for the fabrication of implant-supported prostheses.

CONCLUSION

Based on the findings of this *in vitro* study regarding IOSs, the following conclusions were drawn:

- All the IOSs showed a heteroscedastic behavior when variability was evaluated: scanners' precision decreased in proportion to measure length. Thus, considering the percentage relative error, the variability of interdistance measurements tended to be constant for increasing distance. The analysis of trueness showed for all IOSs a tendency to underestimate the interdistance measurements.
- Overall, scans, models, IOSs and their interactions are significant factors affecting the variability of the enrolled scanners. Surprisingly, the number of scan bodies does not significantly impact the precision of interdistance measurement.

- Primescan and Trios3 tended to overestimate the inclination angles, while angles measured by CS3600 are overall underestimated. Primescan showed a bimodal distribution of residuals showing an overestimation of 0.4°–0.6° to angle measurement.

BIBLIOGRAPHY

[1] Naveau A, Bou C, Sharma A. Evolution of Topics in Maxillofacial Prosthetics Publications. *Int J Prosthodont* **2018** 31:565–568

[2] Lim JH, Park JM, Kim M, Heo SJ, Myung JY. Comparison of digital intraoral scanner reproducibility and image trueness considering repetitive experience. *J Prosthet Dent* **2018** 119:225–232

[3] Joda T, Brägger U. Patient-centered outcomes comparing digital and conventional implant impression procedures: a randomized crossover trial. *Clin Oral Implants Res* **2016** 27:e185–e189

[4] Ajioka H, Kihara H, Odaira C, Kobayashi T, Kondo H. Examination of the position accuracy of implant abutments reproduced by intra-oral optical impression. *PLoS One* **2016** 11:1–12

[5] Patzelt SBM, Emmanouilidi A, Stampf S, Strub JR, Att W. Accuracy of full-arch scans using intraoral scanners. *Clin Oral Investig* **2014** 18:1687–1694

[6] Ender A, Mehl A. Accuracy of complete-Arch dental impressions: A new method of measuring trueness and precision. *J Prosthet Dent* **2013** 109:121–

128.

[7] Rhee YK, Huh YH, Cho LR, Park CJ. Comparison of intraoral scanning and conventional impression techniques using 3-Dimensional superimposition. *J Adv Prosthodont* **2015** 7:460–467

[8] Osnes CA, Wu JH, Venezia P, Ferrari M, Keeling AJ. Full arch precision of six intraoral scanners in vitro. *J Prosthodont Res* **2020** 64:6–11.

[9] Amin S, Weber HP, Finkelman M, El Rafie K, Kudara Y, Papaspyridakos P. Digital vs. conventional full-arch implant impressions: a comparative study. *Clin Oral Implants Res* **2017** 28:1360–1367

[10] Tan M, Yee S, Wong K, Tan Y, Tan K. Comparison of Three-Dimensional Accuracy of Digital and Conventional Implant Impressions: Effect of Interimplant Distance in an Edentulous Arch. *Int J Oral Maxillofac Implants* **2019** 34:366–380

[11] Mizumoto RM, Yilmaz B, McGlumphy EA, Seidt J, Johnston WM. Accuracy of different digital scanning techniques and scan bodies for complete-arch implant-supported prostheses. *J Prosthet Dent* **2020** 123:96–104

[12] Revell G, Simon B, Mennito A, Evans ZP, Renne W, Ludlow M, Vág J. Evaluation of complete-arch implant scanning with 5 different intraoral scanners in terms of trueness and operator experience. *J Prosthet Dent* **2021** 1–7

[13] Vág J, Nagy Z, Simon B, Mikolicz Á, Kövér E, Mennito A, Evans Z, Renne

W. A novel method for complex three-dimensional evaluation of intraoral scanner accuracy. *Int J Comput Dent* **2019** 22:239–249.

[14] Mangano F, Gandolfi A, Luongo G, Logozzo S. Intraoral scanners in dentistry: A review of the current literature. *BMC Oral Health* **2017** 17:1–11

[15] Mangano FG, Admakin O, Bonacina M, Lerner H, Rutkunas V, Mangano C. Trueness of 12 intraoral scanners in the full-arch implant impression: A comparative in vitro study. *BMC Oral Health* **2020** 20:1–21

[16] Bland JM, Altman DG. Statistical methods for assessing agreement between two methods of clinical measurement. *Lancet* **1986** 62:307–310

[17] Chew A, Esguerra R, Teoh K, Wong K, Ng S, Tan K. Three-Dimensional Accuracy of Digital Implant Impressions: Effects of Different Scanners and Implant Level. *Int J Oral Maxillofac Implants* **2017** 32:70–80

[18] Ender A, Mehl A. In-vitro evaluation of the accuracy of conventional and digital methods of obtaining full-arch dental impressions. *Quintessence Int* **2015** 46:9–17

[19] Giménez B, Özcan M, Martínez-Rus F, Pradíes G. Accuracy of a digital impression system based on active wavefront sampling technology for implants considering operator experience, implant angulation, and depth. *Clin Implant Dent Relat Res* **2015** 17:e54–e64

[20] Di Fiore A, Meneghello R, Graiff L, Savio G, Vigolo P, Monaco C, Stellini E. Full arch digital scanning systems performances for implant-supported fixed

dental prostheses: a comparative study of 8 intraoral scanners. *J Prosthodont Res* **2019** 63:396–403

[21] Vigolo P, Fonzi F, Majzoub Z, Cordioli G. An evaluation of impression techniques for multiple internal connection implant prostheses. *J Prosthet Dent* **2004** 92:470–476

[22] Jemt T. Failures and complications in 391 consecutively inserted fixed prostheses supported by Brånemark implants in edentulous jaws: a study of treatment from the time of prosthesis placement to the first annual checkup. *Int J Oral Maxillofac Implants* **1991** 6:270–276

[23] Braian M, Wennerberg A. Trueness and precision of 5 intraoral scanners for scanning edentulous and dentate complete-arch mandibular casts: A comparative in vitro study. *J Prosthet Dent* **2019** 122:129-136.e2

[24] Fukazawa S, Odaira C, Kondo H. Investigation of accuracy and reproducibility of abutment position by intraoral scanners. *J Prosthodont Res* **2017** 61:450–459

[25] Kim RJY, Benic GI, Park JM. Trueness of digital intraoral impression in reproducing multiple implant position. *PLoS One* **2019** 14:1–11

[26] Miyoshi K, Tanaka S, Yokoyama S, Sanda M, Baba K. Effects of different types of intraoral scanners and scanning ranges on the precision of digital implant impressions in edentulous maxilla: An in vitro study. *Clin Oral Implants Res* **2020** 31:74–83

[27] Arcuri L, Pozzi A, Lio F, Rompen E, Zechner W, Nardi A. Influence of implant scanbody material, position and operator on the accuracy of digital impression for complete-arch: A randomized in vitro trial. *J Prosthodont Res* **2020** 64:128–136

[28] Papaspyridakos P, Wei Chen Y, Alshawaf B, Kang K, Finkelman M, Chronopoulos V, Weber HP. Digital workflow: In vitro accuracy of 3D printed casts generated from complete-arch digital implant scans. *J Prosthet Dent* **2020** 124:589–593

[29] Imburgia M, Logozzo S, Hauschild U, Veronesi G, Mangano C, Mangano FG. Accuracy of four intraoral scanners in oral implantology: A comparative in vitro study. *BMC Oral Health* **2017** 17:1–13

[30] Vandeweghe S, Vervack V, Dierens M, De Bruyn H. Accuracy of digital impressions of multiple dental implants: an in vitro study. *Clin Oral Implants Res* **2017** 28:648–653

[31] Mangano FG, Veronesi G, Hauschild U, Mijiritsk E, Mangano C. Trueness and precision of four intraoral scanners in oral implantology: A comparative in vitro study. *PLoS One* **2016** 11:1–18

[32] Prudente MS, Davi LR, Nabbout KO, Prado CJ, Pereira LM, Zancopé K, Neves FD. Influence of scanner, powder application, and adjustments on CAD-CAM crown misfit. *J Prosthet Dent* **2018** 119:377–383

[33] Dutton E, Ludlow M, Mennito A, Kelly A, Evans Z, Culp A, Kessler R, Renne

W. The effect different substrates have on the trueness and precision of eight different intraoral scanners. *J Esthet Restor Dent* **2020** 32:204–218

[34] Nagy Z, Simon B, Mennito A, Evans Z, Renne W, Vág J. Comparing the trueness of seven intraoral scanners and a physical impression on dentate human maxilla by a novel method. *BMC Oral Health* **2020** 20:1–10

[35] Flügge T, Van der Meer WJ, Gonzalez BG, Vach K, Wismeijer D, Wang P. The accuracy of different dental impression techniques for implant-supported dental prostheses: A systematic review and meta-analysis. *Clin Oral Implants Res* **2018** 29:374–392

[36] Oh HS, Bongju K, Myung-Joo K, Ho Beom K, Yeon-Wha B. Effect of scanning-aid agents on the scanning accuracy in specially designed metallic models: a laboratory study. Materials **2021** 14:2340

[37] Kernen F, Schlager S, Alvarez S, Mehrhof J, Vach K, Kohal R, Nelson K Accuracy of intraoral scans : An in vivo study of different scanning devices. *J Prosthet Dent* **2021** 1–7

[38] Pesce P, Pera F, Setti P, Menini M. Precision and Accuracy of a Digital Impression Scanner in Full-Arch Implant Rehabilitation. *Int J Prosthodont* **2018** 31:171–175

[39] Renne W, Ludlow M, Fryml J, Schurch Z, Mennito A, Kessler R, Lauer A. Evaluation of the accuracy of 7 digital scanners: An in vitro analysis based on 3-dimensional comparisons. *J Prosthet Dent* **2017** 118:36–42

[40] Treesh JC, Liacouras PC, Taft RM, Brooks DI, Raiciulescu S, Ellert DO, Grant GT, Ye L. Complete-arch accuracy of intraoral scanners. *J Prosthet Dent* **2018** 120:382–388

[41] Lo Russo L, Caradonna G, Troiano G, Salamini A, Guida L, Ciavarella D. Three-dimensional differences between intraoral scans and conventional impressions of edentulous jaws: A clinical study. *J Prosthet Dent* **2020** 123:264–268

Chapter VII

PCL/β-TCP customized biomaterial development as bone grafting material

INTRODUCTION

Biomimicry, the tendency to learn and imitate the strategies found in nature to solve engineering, architectural or medical challenges is driving improvements in many fields, especially in the replacement of lost tissues, representing a prominent solution to one of the most challenging problems that oral clinicians must interface with: the surgical treatment of bone defects and bone tissue engineering (BTE) [1-3]. Bone formation is finely regulated by a process defined as bone turnover in which new bone deposition acts in contrast to bone resorption [4]. When a critical size defect occurs due to a high-energy trauma, a tumor or congenital deformation, it is not possible for the body to self-heal and the consequent healing may result in deformation or dysfunction of the specific site. In such cases, when bone homeostasis is altered, for example by bacteria infiltration that may initiate the injurious process that can lead to periodontitis which, in the worst cases, can bring to loss of periodontal ligament and alveolar bone [5]. Periodontitis is nowadays one of the major challenges in

dentistry as it is related to the reconstruction of a non-containing cavity caused by generalized alveolar bone resorption.

Whereby, bone replacement is mandatory as a consequence of different damages as oral or maxillofacial diseases and still many challenges have to be faced to limit the related complications [5-11]. Nowadays, the “gold standard” to be used as bone grafting material is represented by autografts or allografts. In the first one the tissue is directly harvested from the donor himself, with a high number of disadvantages (i.e. comorbidity of the donor site, risk of infections, long healing, variable resorption time, etc.) that characterize this surgical approach and that are progressively leading to autografts replacement with synthetic biomaterials and scaffolds [5,12]. Also, in the use of allografts there are limitations due to the risk of presence of antigens or pathogens not removed during the tissue treatment process and thus a high risk of rejection or disease transmission [13]. On the other hand, synthetic scaffolds present many innovative aspects as the possibility to design specific internal architectures which strictly resemble the structure of trabecular or cortical bone, the possibility to modulate interconnections and porosity, beside the shape or dimension of the scaffold and its surface characteristics. The development of bioactive three-dimensional constructs produced through several methods and making use of a wide range of biomaterials is taking over thank to the easiness in the design, the precision of the printing and the possibility to customize the scaffold to the patient’s defect via CAD software (i.e. computed tomography, magnetic resonance imaging, laser

digitizing or cone beam computed tomography) capable to generate a highly accurate virtual three-dimensional model of the anatomical region, thus perfectly filling the empty space, providing a substrate for new bone deposition and remodeling [14,15]. It is widely known that the ideal scaffold for BTE should resemble as much as possible the native tissue in terms of structure and mechanical properties to maximize cell colonization, extracellular matrix (ECM) deposition and consequently the resorption of the graft with its substitution by newly formed tissue, thus leading to a complete healing [16]. Seen what before, it seems even more central the role played by a well-defined micro or submicron patterned surface, surface wettability, exogenous growth factors, and highly biocompatible biomaterials for their possible use in regenerative medicine [16-19]. Moreover, recent studies have underlined how scaffold's mechanobiology, as mechanical resistance to traction and compression can determine the activation of specific intracellular signaling, thus affecting cellular behavior (i.e. adhesion, migration, proliferation, and differentiation) [20].

In this context, it is fundamental to underline the role of 3D printing focusing, more specifically, on the role a fuse deposition modelling (FDM) approach. This 3D printing method based on layer-by-layer material addition allows to obtain extremely customized prototypes suitable for every need also achieving results that could not be reached by fabrication methods commonly present in the modern literature [12,21]. FDM is one of the most common techniques used for the production of scaffolds to be used in BTE due to its relative low cost, lower energy consumption and

the possibility to obtain extremely customized prototypes using a wide range of polymers [22,23]. Indeed, the possibility to combine different biomaterials, both natural or synthetic, to create a composite biomaterial suitable for every need, is playing a pivotal role in the increasing use of this techniques in personalized medicine [9,24]. Among the huge variety of biomaterials which can find application in BTE (e.g. polyglycolic acid, polylactic acid, alginate, chitosan, etc.) polycaprolactone (PCL) is constantly gaining relevance in treatments of bone injury [25,26]. Its biocompatibility, high resorbability and low immunogenicity make this material one of the most interesting candidates for 3D printed scaffold for BTE [27]. Moreover, the degradation rate of PCL is quite long (about 12 months), thus allowing the complete regeneration and remodeling of bone tissue, keeping the correct structural stability and without interfering with the environment, as it does not acidify the surrounding environment. Despite of its great versatility, PCL presents several limitations. It shows a lower tensile strength and elastic modulus compared to other biomaterials used in tissue engineering and high hydrophobicity which negatively affects the early phase of protein adsorption from the blood and the first layer deposition [28,29]. Consequently these characteristics leads to an impaired cellular adhesion and slackening scaffold degradation [27]. To ameliorate PCL features with a specific regard to applications in bone regeneration, it is useful to combine it with other biomaterials which might share the crystal structure and the chemical characteristics of the inorganic components of bone tissue, such as hydroxyapatite (HA) and tricalcium

phosphate-based materials (TCP, α-TCP, β-TCP, etc.)[30,31]. Specifically, for more than three decades, β-TCP has played a central role in reconstructive surgeries making it one of the most widely used materials in BTE, due to its more emphasized osteoconductive and osteoinductive properties at the expenses of poor bioresorbability [31-33].

Nevertheless, even if β-TCP is an adequate material for clinical use, in vitro and in vivo studies are still lacking and there are no precise information on the specific concentrations or granule dimensions to be used for tissue engineering [15]. Interestingly, its presence may alter scaffold surface topography, creating a specific roughness that can influence cell behavior and that could potentially be used to enhance the bioactivity of the material or the integration of the graft [34]. Indeed, nano- and micro-scaled substrates can pave the way to specific cellular cues, as also the ECM encompasses all the micro and nano-scale levels, modulating cellular behavior [34]. Also, the composition of adsorbed proteins and their folding depend on the microtopography of the biomaterial as well as the specific protein layer at the tissue-biomaterial interface that can lead tissue healing [35,36].

In this light, the aim of this work is the definition of the best concentration of β-TCP powder to be used for the customization of PCL/β-TCP scaffolds for bone regeneration. We also investigated how PCL 3D-printed scaffolds can modulate osteoblastic behavior in terms of proliferation and differentiation, with the final

objective to maximize scaffolds regenerative potential for applications in bone reconstruction.

MATERIALS AND METHODS

Poly-Ɛ-caprolactone (PCL - Mw= 100000 g/mol, Evonik Industries, Essen, Germany) and β-tricalcium phosphate (β-TCP - Mw= 310.18 g/mol, Sigma-Aldrich, St. Louis, MO, USA) medical grade powders were selected and used to develop the PCL/β-TCP biomaterials as candidate for the customization of scaffolds for bone tissue regeneration.

1. PCL/β-TCP filaments development

Suitable filaments for three-dimensional printing were produced starting from medical grade powder of Poly-Ɛ-caprolactone and β-tricalcium phosphate. Initially, β-TCP powders were selected in a range between 38nm and 56nm through a vibrating sieving process (Fritsch, Idar-Oberstein, Germany).

PCL and β-TCP were subsequently mixed obtaining three different concentrations w/w (Table 1) in order to assess the maximum amount of β-TCP able to be incorporated into such filament and to not interfere with the 3D-printing process, thus enhancing the regenerative potential of the final scaffolds.

Sample name	wt.% PCL	wt. % β-TCP
100/0	100	0
60/40	60	40
30/70	30	70

Table 1. Relative powders concentration developed for filament extrusion.

Powders mixtures were weighed and introduced in a dedicated extrusion system (Felfil Evo, Milan, Italy) to obtain printing filaments suitable for FDM printing, as showed in Figure 1.

Figure 1. Extrusion system composed by a filament extruder, a cooling fan array and a spooler.

Briefly, inside the hopper, through a steel screw, the powder mixture is transferred in a heating chamber which allowed the filament extrusion through a 2,85 mm nozzle. The obtained filament was then cooled with a fan system and transferred to the printer.

2. 3D-printing process

PCL/β-TCP filaments were used as “print cartridges” for a FDM 3D printer to create customized scaffolds. The printing process is composed by three steps: modelling, printing and finishing/post-processing. Briefly, cylindrical scaffolds with defined dimensions of 5mm in diameter and 2mm in height were designed through the 3D CAD software Sharpr 3D. Afterwards, the model of the scaffold was exported in a StereoLitography file format (.stl). The stl file was then imported on the slicing software Ultimaker Cura which mathematically sliced the model in a series of thin layers and generates a G-CODE to prepare and train the 3D printer for the material deposition phase. The final file in a .upf format was subsequently uploaded on a 3D printer Ultimaker S3 and PCL/β-TCP samples were finally extruded by the printer through a 400 µm nozzle. Semi-solid PCL/β-TCP scaffold was deposited onto the plate surface where it quickly solidified due to the difference of temperature between the glass plate and the biomaterial, thus allowing the deposition of the next layer.

3. Physical and mechanical characterization of the surfaces

Thermal analysis –Differential Scanning Calorimetry (DSC)

The thermal behavior of the composites was investigated by using a differential scanning calorimeter (DSC, Q2000, TA instruments, New Castle, DE, USA). Pure indium was used as standard for calibrating the temperature and the enthalpy (Tm = 156.4 °C; ΔHm = 28.15 J/g). Analyses were carried out in nitrogen atmosphere (30 mL/min)

by heating about 8 mg of sample to 110 °C and maintained at this temperature for 5 min under nitrogen to erase the previous thermal history. Then the sample was cooled from 110 °C to 0 °C (cooling run) and heated again from 0 °C to 110 °C (second heating run). The crystallinity degree of PCL and its composites was calculated by using the following formula:

$\chi c = (\Delta H_m)/(〖\Delta H〗_0^{PCL} (1-\alpha))\times 100$

where ΔHm is the measured enthalpy of melting and ΔH0PCL is the enthalpy of melting per gram of 100% crystalline PCL (139.5 J/g) and α is the weight fraction of HA filler in PCL.

Mechanical test

An Instron 5966 dynamometer (Norwood, MA, USA) in tensile configuration was used for obtaining mechanical parameters. Specimen dimension was 3.5 x 50 x 1 mm3. The elongation zone was defined by positioning the clamps at 3 cm. The tests were performed at room temperature. The method applied was 5 mm/min until breaking. For each type of composites, ten independent measurements were performed.

Surface wettability

The wettability of the samples was investigated using contact angle measurements through a self-made apparatus consisting of a micropipette to deposit the drop and an image acquisition system (EOS 80D, Canon). The measurements were carried out at a temperature of 27°C and atmospheric pressure in a dehumidified room. Deionized water drops were bubbled freely from a micropipette to the center of the

sample with a volume of 10 µl/drop. Images of the contact angle were acquired after 0seconds and after 20 seconds from the deposition of the drop and the contact angles were subsequently measured with the ImageJ Software.

Surface roughness

Surface roughness evaluation was performed through a contact profilometer (Tencor Instruments, Mountain View, CA 94043, United States), considering Ra parameter. Briefly, a diamond stylus moves vertically in contact with the sample and then laterally across it to measure specific contact forces and distances. The height position of the diamond stylus generates an analogic signal which is converted into digital signal, analysed, and sent to a display for the final analysis.

4. In vitro biological testing

Cell cultures and samples preparation

In vitro cellular assays were performed using murine pre-osteoblastic cells (MC3T3-E1) obtained from the American Type Culture Collection (ATCC, Manassas, VA, USA, distributed from LGC Standards srl, Milan, Italy). Cells were cultured in complete a-MEM (a-MEM, Thermo Fisher Scientific, Waltham, Massachusetts, USA) supplemented with 10% Foetal Bovine Serum (FBS; Thermo Fisher Scientific), 1% Penicillin and Streptomycin (PenStrep, Thermo Fisher Scientific) and 1% L-Glutamine (Thermo Fisher Scientific) and kept in humidified atmosphere at 37°C with 5%ppCO_2.

Before proceeding to the in vitro testing phase 3D printed PCL/β-TCP scaffolds were sterilized. Briefly, scaffolds were quickly immersed in EtOH 70% and soaked in a solution of sterile deionized water with 5% PenStrep and 5% Amphotericin B (Mediatech Inc, Corning, Manassas, USA) for 5 minutes. Subsequently, the solution was replaced with deionized water and 1% PenStrep for ten minutes and then the discs were soaked in sterile deionized water and air-dried in sterile conditions.

Indirect and direct contact cytotoxicity assays

To exclude the release of any cytotoxic agents from the 3D printed scaffolds, an indirect contact cytotoxicity test was performed in accordance with ISO 10993-5 guidelines for the cytotoxicity analysis of porous materials. To this purpose, discs of the synthetized biomaterials were submerged with complete medium (in a ratio of 1mg/ml) in sterile environment and stored at 37°C and 5% CO2 in humidified atmosphere for 1, 3, 7 and 10 days. At experimental time points, conditioned medium was collected from the scaffolds and added to pristine medium at percentages of 50%, 70% and 100% of the total final volume. Culturing medium was then added to previously seeded osteoblastic cells that were then cultured for further 24 hours. At the term of the incubation time a CellTiter-Glo (Promega, Madison, WI, USA) chemiluminescent proliferation assay, was performed to assess cell viability through the quantitation of the ATP present in the samples. Briefly, culture medium was discarded, samples were rinsed in PBS and a 50:50 solution of CellTiter-GLO Lysis Buffer and complete culture medium was added. Each sample was incubated for 2

min on an orbital shaker, the solution was then collected and luminescence was stabilized for 10 min in the dark. Samples were centrifuged for 30 sec to eliminate any bubble and luminescence was measured with a luminometer with double injectors (GLOMAX 20/20, Promega).

Cell morphology

To observe cell morphology and the interaction with the underlying biomaterial substrate, Scanning Electron Microscopy (SEM) was performed after 24h of culture. Briefly, cells were fixed with 2.5% glutaraldehyde solution (Sigma-Aldrich) in 0,1M Na-Cacodylate buffer for 30 min at RT, thus washed in Na-Cacodylate buffer for 5 min at RT and subsequently dehydrated in an ascendant series of alcohol (Sigma-Aldrich) at RT, for 10min each dilution (EtOH 35%, 50%, 70%, 75%, 90%, 95%, 99%). Specimens were then coated with a nanometric gold layer through a SCD 040 coating device (Balzer Union, Wallruf, Germany) and micrographs of cells distribution and morphology were taken in a dual beam Zeiss Auriga Compact system equipped with a GEMINI Field-Emission SEM column operated at 5keV.

Gene expression analysis

To analyze differences in terms of osteoblastic maturation, total RNA was extracted from cell cultures at 3, 7 and 14 days after seeding and using RNeasy columns (Qiagen, Hilden, Germany) according to manufacturer's indications. The purity of extracted RNA was measured through a NanoPhotometerTM P class (Implen GmbH, München,

Germania) and RNA was retrotranscribed to cDNA with a High-Capacity cDNA Reverse Transcription Kit (Thermo Fisher Scientific). TaqMan quantitative RT-PCR was performed on samples through a Real Time PCR machine (StepOne Plus, Thermo Fisher Scientific) analyzing the expression of Osteocalcin (OCN), Osteopontin (OPN) and Bone Sialoprotein (BSP). The housekeeping gene mouse glyceraldehyde-3-phosphate dehydrogenase (GAPDH) was used as reference gene for the normalization.

5. Statistical analysis

Data were analyzed using Prism7 (GraphPad, La Jolla, CA, USA). All the values were reported as the mean ± standard deviation of at least three repeated measurements. Differences between groups were evaluated with two-way ANOVA statistical tests. Then the Tukey post-test was applied for multiple comparisons. Differences were considered statistically significant when $p<0.05$.

RESULTS

1. PCL/β-TCP filament development

The identification of extrusion parameters had a fundamental role in the filament development. Different attempts were done to set the best combination of extrusion parameters in terms of melting temperature (Tm), screw speed rotation (RPM) and extruder diameter able to create a filament suitable for the purpose. A heating

chamber temperature of 95°C and a screw speed rotation of 2 RPM allowed the fabrication of 100% PCL and PCL/β-TCP filaments with 60% and 30% of PCL. The filament had a diameter of 2,85mm and its external aspect was observed with a stereomicroscope (Nikon) as shown in Figure 2.

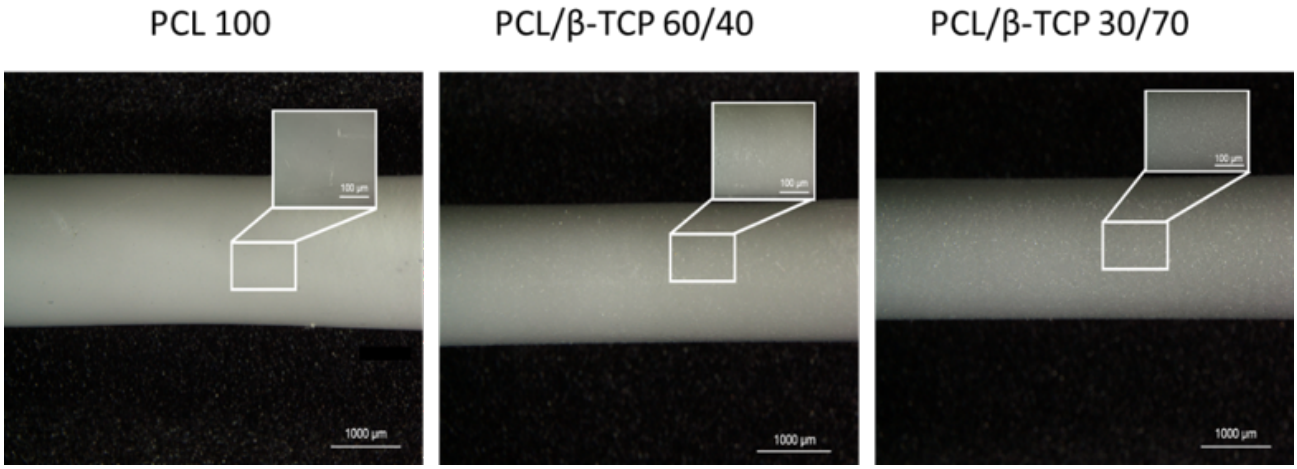

Figure 2. a) 100% PCL filament, b) 60% PCL – 40% β-TCP filament and c) 30% PCL – 70% β-TCP filament.

The increase of β-TCP concentration leads to a gain of roughness on the surface of the filaments which seem proportional to the amount of the inorganic powder. This specific microtopography can be also detected on the final scaffold surface.

2. 3D-printing process

Different printing setups were tested until the most appropriate conditions were established : a printing temperature of 120°C, printing speed of 5 mm/s, flow of 110% and an infill density equal to 100%.

The selected settings allowed the printing of three-dimensional disks presenting 5mm in diameter and 2mm in height, as reported in Figure 3.

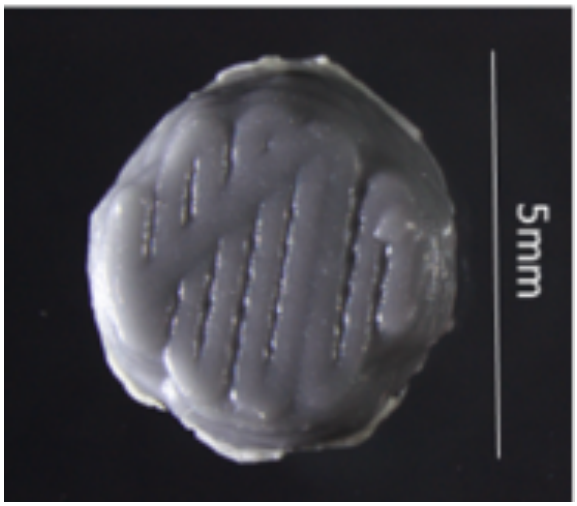

Figure 3. PCL 3D printed scaffolds.

3. Physical characterization of the surfaces

Surface wettability

To evaluate biomaterial wettability and the interaction between scaffold and cells measurements of water-in-air contact angle was performed. Typically, a water contact angle <90° is linked to hydrophilic characteristics. Figure 4 shows the results of the water contact angle measurement performed on the 3D-printed scaffolds at two different time points (0s and 20s). All contact angles slightly decreased by approximately 4° after 20 seconds. A marked decrease in contact angle amplitude was found in the scaffolds loaded with the inorganic powder, with a statistically significant difference only between PCL and 60/40 at both the time points ($p=0.0027$ and $p=0.0045$).

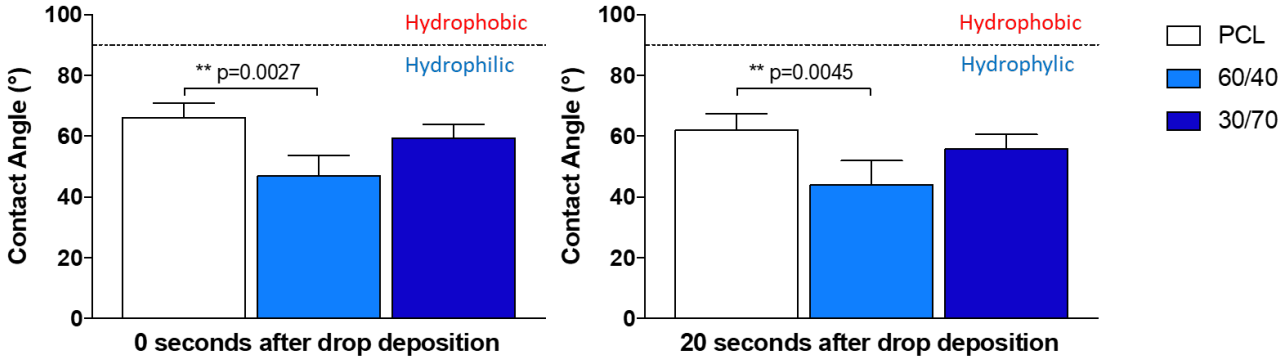

Figure 4. Wettability evaluation through contact angle measurements. a) at 0 seconds after drop deposition and b) after 20 seconds from drop deposition.

Topographical characterization

Scaffold surface topography was observed through SEM, while the surface roughness was quantitatively evaluated through a profilometric analysis.

SEM images highlighted that surface roughness (Figure 5 lower panel) increased by increasing the β-TCP concentration. PCL scaffold showed a smoother surface if compared to 3D printed structures loaded with defined concentration of ceramic powder which, conversely, evidenced a microtopography marked by the presence of micro peaks and micro pits. The profilometric results (Figure 5 upper panel) confirmed the expectations inferred from SEM images. PCL surface roughness, with a Ra=0.160 µm was sensibly lower with respect to the surface roughness of scaffolds loaded with β-TCP powder (i.e. Ra=2.495 µm for PCL/ β-TCP 60/40 and Ra=3.477 µm for PCL/ β-TCP 30/70).

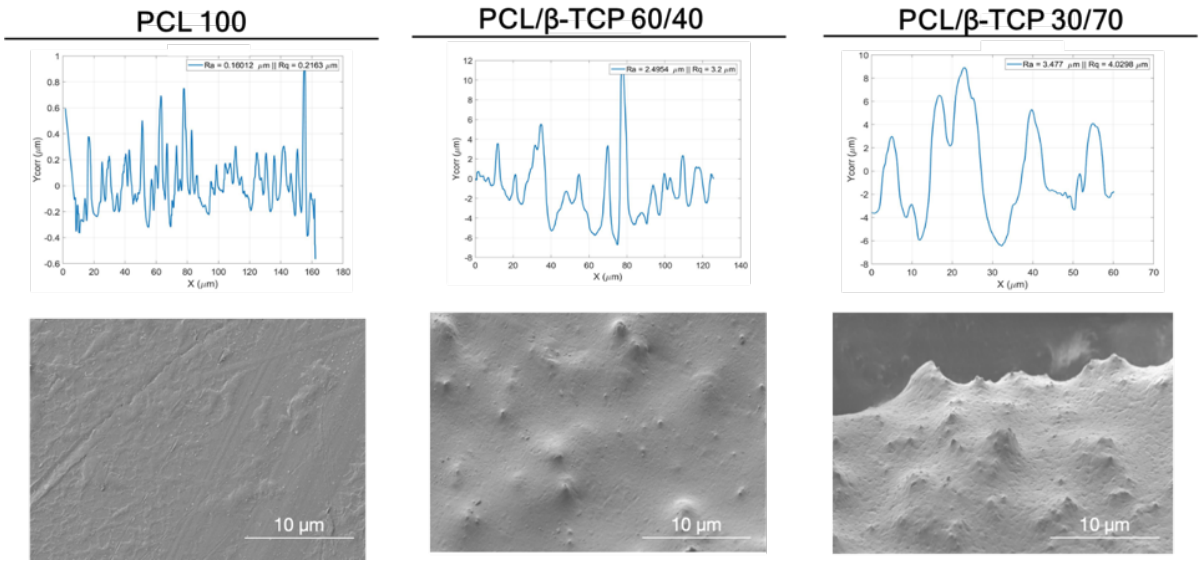

Figure 5. The upper panel shows PCL, 60/40 and 30/70 surface roughness quantification performed by a profilometric analysis, while the lower panel shows the correspondent SEM microphotograph of scaffolds surface.

4. Thermal analysis –Differential Scanning Calorimetry (DSC)

The cooling and second heating DSC curves are shown in Figure 6. The values of estimated thermal parameters are reported in Table 2. During the cooling from the melt (Figure 6a), PCL underwent crystallization with a temperature peak of 27.1 °C. The temperature of the crystallization peak of both composites is slightly higher than that of the neat PCL. Moreover, the enthalpy of crystallization (ΔH_c) obtained with a cooling rate of 10 °C/min has the highest value for neat PCL (46.6 J/g), becoming 20.4 and 25.4 J/g for the composites). This occurs because of the PCL molecular chain becoming adsorbed on the β-TCP surface and forming a nucleate, which contributes to heterogeneous nucleation, thus increasing the crystallization ability. The lower dispersion of β-TCP in the PCL/β-TCP 30/70 composite hampers the nucleation

process in some extent, resulting in a crystallization temperature decrease with respect to PCL/β-TCP 60/40 composite.

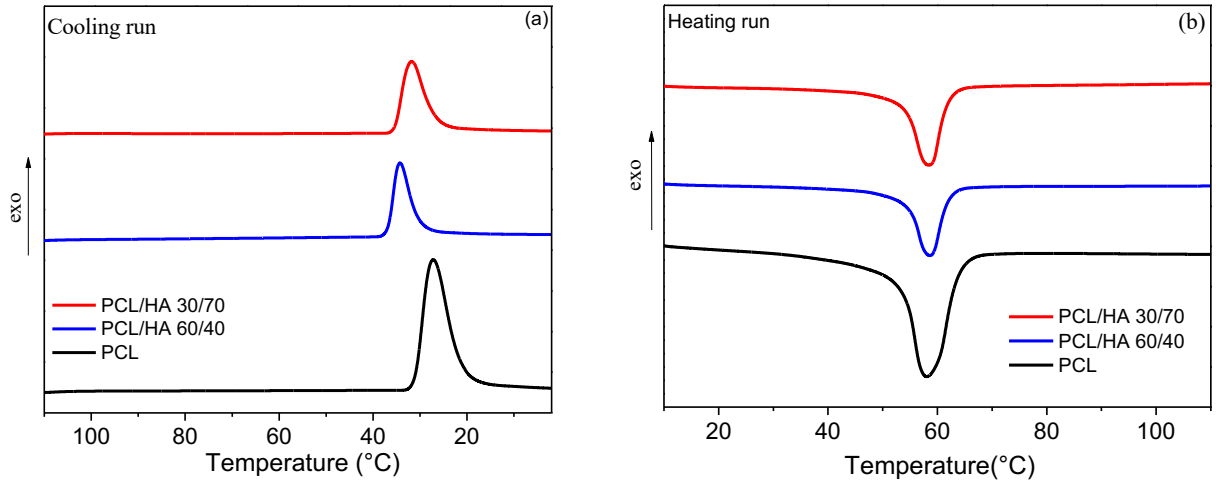

Figure 6. (a) DSC melt crystallization and (b) melting curves of PCL and PCL/β-TCP composites. HA diventaβ-TCP

	T_c (°C)	T_m (°C)	ΔH_c (J/g)	ΔH_m (J/g)	χ_c (%)
PCL100	27.1	57.6	50.3	46.8	34
60/40	34.3	58.6	20.4	20.1	25
30/70	31.8	58.5	25.4	24.4	58

Table 2. Thermal parameters by DSC

During the second heating run (Figure 4b) the endothermic melting peaks are visible. The neat PCL melting temperature is 57.6 °C; this value is about 1° lower than those of the PCL/β-TCP composites. By increasing the β-TCP amount, the crystallinity degree (χ_c), determined using Equation (1), first decreases and then increases.

5. Mechanical properties

Figure 7 reports the average stress strain curves of PCL and PCL/β-TCP composites. Mechanical parameters are shown in table 3. Neat PCL presents a classical plastic behavior characterized by yielding, cold crystallization and fracture. A brittle behaviour is found for 30/70 composite. The Young's Modulus of the composites is higher than that of pristine PCL scaffold and increases significantly with β-TCP content, shifting from 577 MPa for neat PCL to 2320 MPa for 30/70, i.e. more than four times higher than that of unfilled PCL. This indicates that intrinsic strength of β-TCP is beneficial to enhance Elastic modulus of the composites scaffolds. Moreover, the strength and elongation at yield are lower than those of neat PCL in the 60/40 composite, whereas they are not more detectable in 30/70 composite, which means that β-TCP acts as a plasticizer increasing the PCL chain mobility. However, the greater the amount of β-TCP, the lower the elongation and strength at break. This behaviour, also reported in literature could be due to the presence of β-TCP aggregates and inner defects acting as stress concentration points where cracks begin to develop.

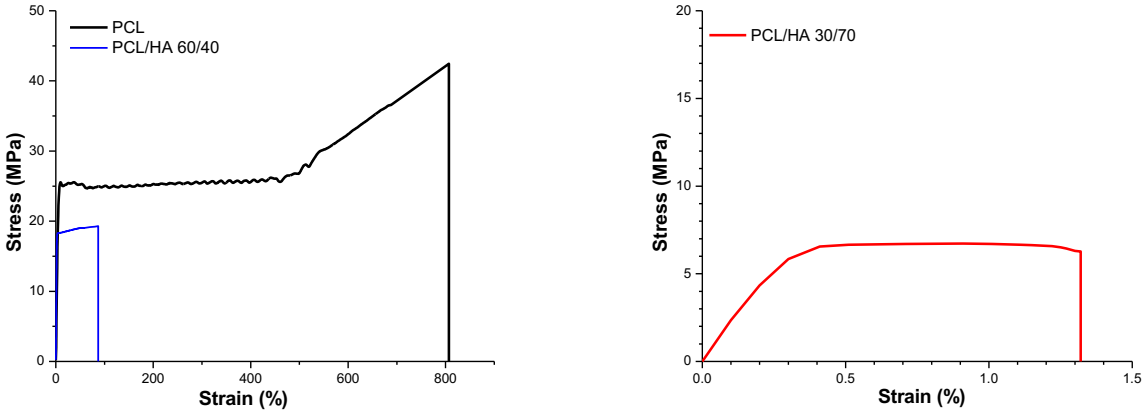

Figure 7. Stress-strain curves for PCL and composites. HA diventa β-TCP

Sample	*E* (MPa)	ε_y (%)	σ_y (MPa)	ε_b (%)	σ_b (MPa)
PCL100	577 ± 56	9.7 ± 1.6	25.8 ± 1.7	807 ± 77	42.4 ± 4
PCL/β-TCP 60/40	1330 ± 106	4.2 ± 0.8	18.3 ± 0.9	87 ± 28	19.3 ± 1.1
PCL/β-TCP 30/70	2320 ± 653	-	-	6 ± 2	1.0 ± 0.20

Table 3. Mechanical parameters of PCL and PCL/β-TCP scaffolds

6. Indirect and direct contact cytotoxicity assays

The behavior of cell seeded on 3D printed scaffolds was investigated through indirect and direct cytotoxic assays. According to ISO 10933-5 guidelines, describing the methods to assess *in-vitro* cytotoxicity of medical devices, a porous structure is biocompatible if cell viability is greater than 70%. In this study, the release of putative toxic chemical agents in the cultural medium after 1,3,7 and 10 days was evaluated by CellTiter GLO® assays.

The results showed in Figure 8 evidenced that cell viability was not affected by the conditionated media by scaffolds presenting different amount of β-TCP at any vehicle concentration (50, 70 and 100%).

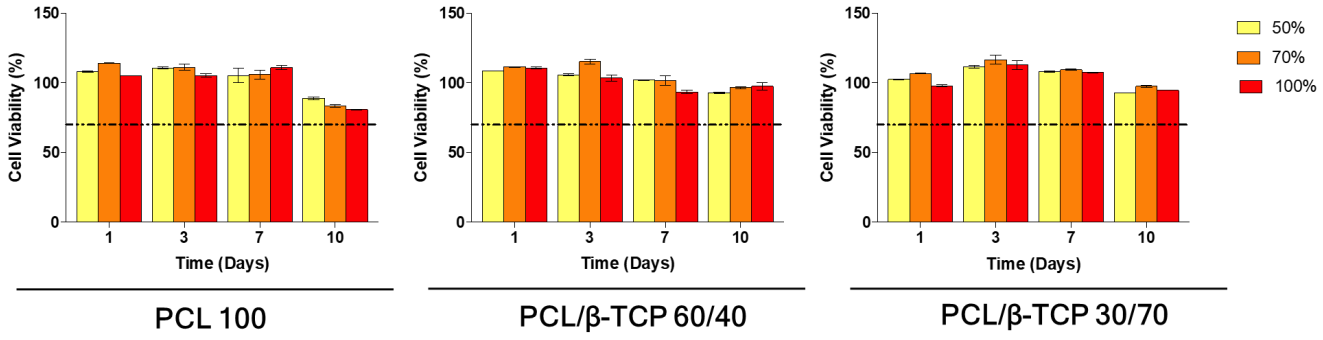

Figure 8. Indirect contact cytotoxicity assays of MC3T3-E1 according to ISO 10933-5 guidelines on different 3D printed structures

All conditions showed a viability above 70%, the minimum value to assess a not cytotoxic behavior. Also, the results agreed with each other, proving that 3D printed scaffolds with different amounts of β-TCP presumably were not involved on release of any cytotoxic agent in culturing medium.

The positive outcome obtained by indirect cytotoxicity assays was also confirmed by direct contact cytotoxicity assay, the proliferation analyses (Figure 9).

In this case murine osteoblasts were seeded directly onto the scaffolds and the proliferation rate at 1, 3, 7 and 10 days was measured in terms of quantification of ATP molecules in the sample.

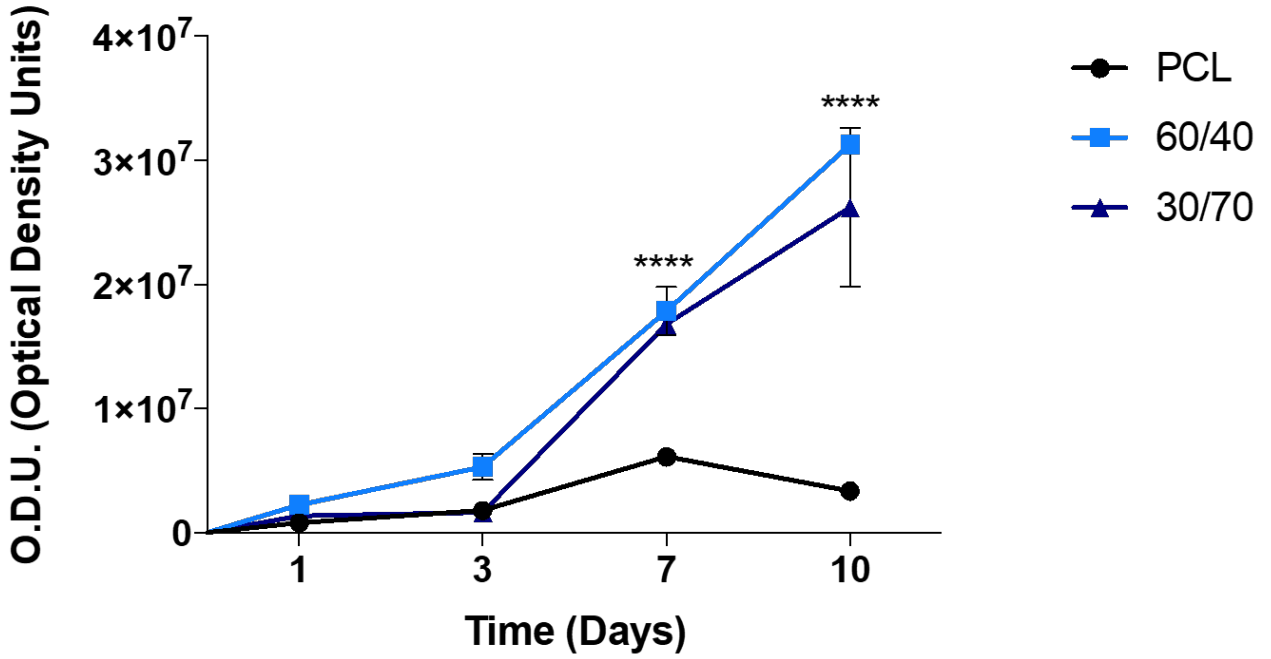

Figure 9. Proliferation curve of MC3T3-E1 cells seeded on 3D printed scaffolds with the selected concentration of β-TCP. ****p<0.0001 day 7 PCL vs 30/70 and day 10 PCL vs 30/70.

The proliferation curve shows that the behavior of osteoblasts seeded on PCL/β-TCP scaffolds seemed to be positively affected by the presence of ceramic powder. On the other hand, cells grown on control PCL scaffolds rapidly reached a plateau and then started to decrease.

Moreover, the proliferation activity tented to be more pronounced on scaffolds with an intermediate concentration of β-TCP (i.e. PCL/β-TCP 60/40) if compared to scaffolds with the maximum amount of β-TCP (i.e. PCL/β-TCP30/70).

7. Gene expression analysis

Osteoblastic differentiation was analyzed through RT-PCR evaluating cellular gene expression of mRNA encoding for Osteoprotegerin, Osteopontin and Bone Sialoprotein, typical marker of late osteoblastic differentiation (Figure 10). Relative mRNA expression levels were determined by using the expression level of GAPDH as endogenous standard.

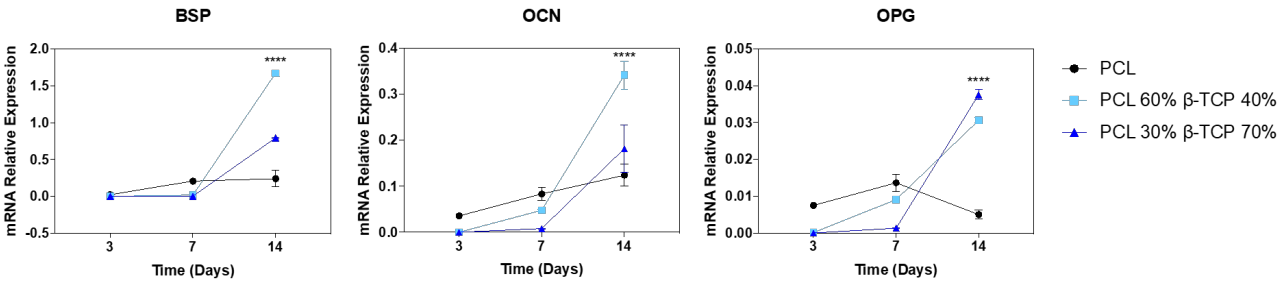

Figure 10. RT-PCR results obtained for Bone Sialoprotein (BSP), Osteocalcin (OCN) and Osteoprotegerin (OPG) in MC3T3-E1 cell line cultured on scaffolds with different concentration of β-TCP for 3, 7 and 14 days. BSP: ****p<0,0001 60/40 and 30/70 vs. PCL and 60/40 vs. 30/70; OCN: ****p<0,0001 60/40 vs. PCL and 60/40 vs. 30/70; OPG: ****p<0,0001 60/40 and 30/70 vs. PCL and 60/40 vs. 30/70

In general, RT-PCR results showed that scaffolds loaded with β-TCP powder presumably induced a more pronounced pro-differentiative effect if compared to PCL scaffolds despite of longer time expression at day 7.

The mRNA expression profiles of OPG and BSP were higher on PCL/β-TCP 60/40 scaffold at day 14 if compared to PCL/β-TCP 30/70 one, whereas a different behavior was detected for OCN which presented a more pronounced gene expression on PCL/β-TCP 30/70 scaffold instead of on PCL/β-TCP 60/40 scaffold.

8. Cell morphology analysis

MC3T3-E1 osteoblastic cells were seeded on neat PCL and PCL/β-TCP scaffolds and their morphology and adhesion was observed after 24h of culturing through Scanning Electron Microscopy (Figure 11).

After 24h, cells cultured on PCL scaffold showed a rounded shape morphology lifted from the scaffold surface, probably due to its limited roughness. Furthermore, cellular debris were detected on PCL scaffold surface, as signals of a microenvironment not properly suitable for cell colonization.

On the other hand, cells seeded on scaffolds loaded with 40% and 70% of β-TCP showed a well-defined elongated polygonal shape with cytoplasmatic projections which anchored osteoblasts on the scaffold surface. The adhesion seemed to be positively influenced by the superficial microtopography given by the presence of calcium salt integrated during the melting phase of filament extrusion.

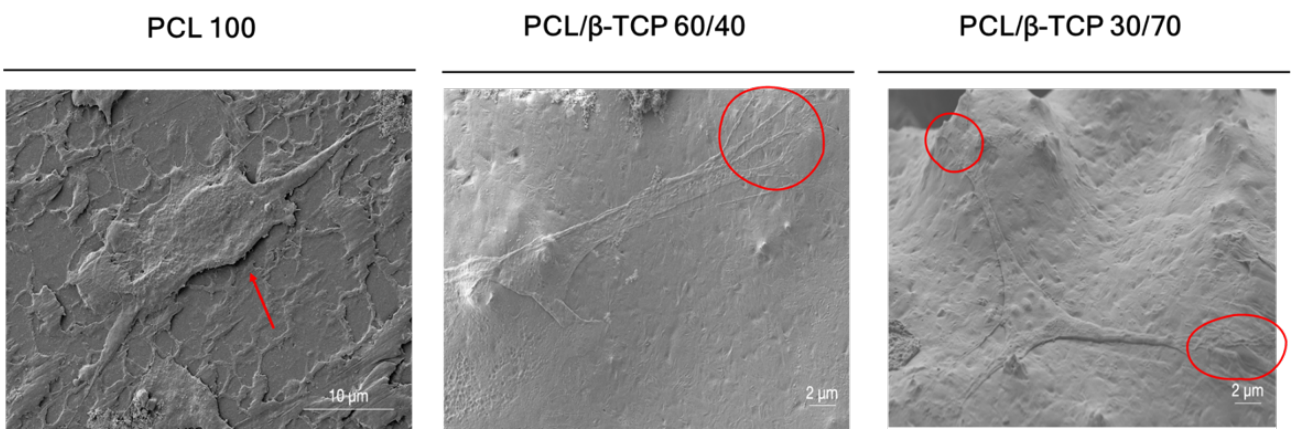

Figure 11. SEM images of osteoblasts seeded for 24h onto PCL, 60/40 and 30/70 3D-printed scaffolds.

DISCUSSION

Nowadays, bone defects due to tumor resection, surgeries, and skeletal deformations can be treated through innovative approaches which mainly involve implantable devices. [39]

The most common biomaterials are obtained from autologous bone or bovine demineralized bone, with many limitations (i.e., difficulties in the evaluation of the resorption time, harvesting sites, diseases), which requires the production of new bioactive scaffolds as bone substitutes.

Innovative combinations of mesenchymal stem cells or progenitor cells and 3D printed structures should provide a microenvironment similar to the native one. In addition they should not eliciting a high inflammatory response and have structural rigidity to withstand external stresses as the native tissue. Finally, these structures should promoting vascularization and inorganic material deposition as well as tissue-resident mesenchymal stem cells recruitment [40,41]. In this regard, the use of 3D

printing-based technologies represents a step forward if compared to commonly used approaches in regenerative medicine applied to bone-related medical treatments, overcoming the clinical limits linked to a higher risk of infections due to bone replacement surgeries, pain persistence and considerably increased costs [8,30]. Specifically, FDM process do not require the use of toxic solvents, allows the control of most mechanical parameters (e.g, printing speed, temperature), thus ensuring a high degree of scaffold customization [42,43]. The aim of the present study is the development of customized 3D printed scaffolds composed of PCL and increasing concentration of β-TCP with subsequent evaluation of mechanical features and biological response of MC3T3-E1 osteoblastic cells. It is well known that the ideal scaffold, from a mechanical point of view, should withstand external forces as closely as possible to native bone tissue [52]. To confirm the mechanical characteristics of the printed scaffolds, tensile tests were carried out. The preparation of scaffolds having a high percentage of TCP, made possible by FDM technology, results in a significant increase in Young's modulus, which reaches 2320 MPa for PCL/β-TCP 30/70 (while only 577 MPa is the E value of pristine PCL). Although this value is still lower compared to that of cortical bone (about 17000 MPa), it exceeds the Young's Modulus of the cancellous bone, which is present in some extent in the maxilla and in the jaw [44]. For this reason, these composites can be considered promising candidates as dental scaffold.

Cell proliferation rate of osteoblasts seeded onto the scaffolds was detected through the quantification of ATP concentration, proportional to cell metabolic activity and consequently to cell number. According to our results, all the scaffolds present no significant differences at day 1 while a sharp increase of ATP concentration is observed for all the samples at day 3 and day 7, signal of great metabolic activity which underlines an increase of cell number due to cell proliferation. Moreover, after 10 days, metabolic activity of MC3T3-E1 osteoblasts on 100% PCL scaffolds drastically decrease compared to cells growth on scaffolds loaded with 40% and 70% β-TCP. These findings are further confirmed by other studies, according to which calcium phosphates incorporation accelerates osteoblasts proliferation, especially in the final stages of the analysis of proliferative activity [45]. A solid explanation of this behavior could be related to the variation of surface microtopography. In fact, it has been widely demonstrated that the rougher surface produced by the presence of β-TCP enables better cell adhesion also providing a larger surface area for cell attachment and proliferation [46-48]. Proliferation results are moreover confirmed by SEM images of PCL, 60/40 and 30/70 scaffolds. β-TCP powder-loaded scaffolds show a surface roughness proportional to the amount of inorganic powder incorporated during the filament extrusion phase. On these, after 24h, murine calvaria MC3T3-E1 cells appear firmly attached on scaffold surface to the point of highlighting the microtopography of the underlying scaffold. In addition, it is possible to appreciate the presence of

membrane extension probably able to bind the micro-peaks given by the presence of β-TCP clusters, further reinforcing the binding with the 3D printed structure. Furthermore, osteoblasts display a well-defined polygonal morphology, sign that PCL/β-TCP surfaces are able to provide a suitable microenvironment for cell attachment and proliferation [18]. On the contrary, MC3T3-E1 osteoblasts cultured on PCL scaffolds show a rounded shape also lift up from the scaffold surface, underlining that the presence of neat PCL is not able to provide the same optimal microenvironment of PCL/β-TCP scaffolds. All the presented evidences are confirmed by recent studies which have highlighted the role of surface topography on cellular behavior, especially in the regulation of the transmission of mechanical signals from the extracellular matrix to the cells, altering their adhesion-shape [15,49,50]. The presence of different surfaces topographies led to different surface characteristics such as hydrophilicity. According to Marrella *et al.,* nanostructured surfaces possess increased surface energy compared to flat surfaces such that the hydrophilicity of the material is improved, resulting in increased protein adsorption, thus promoting cell adhesion [50]. Scaffold wettability was evaluated through quantification of water-in-air contact angle, and the values obtained from the measurement are significantly lower than 90°, indicating that hydrophilic properties seem to be proportional to the amount of β-TCP powder [9]. More in detail, values at 0s and 20s after the release of the drop, range between 66° and 62° for 100% PCL scaffolds. Besides, according to Huang *et al.* findings, water-in-air contact angles tend to decrease proportionally to

the increase of β-TCP granules [9]. In fact, on PCL scaffolds loaded with β-TCP values of 44° and 55° are recorded, remarking a statistical significance between neat PCL and β-TCP-loaded scaffolds. Our data clearly indicate that 3D printed structures with 40% of β-TCP show a more hydrophilic behavior compared to the other scaffolds analyzed in this work which, furthermore, are considerably more hydrophilic than others with lower concentration of the ceramic material [51]. In addition, an increase in the concentration of β-TCP leads to a decrease in contact angle; a similar behavior was observed after treating scaffolds with NaOH, with the aim of chemically increase scaffold hydrophilicity [52,53]. This evidence allows to confirm that the hydrophilicity characteristics are not influenced by the FDM printing technology, depending on only by the properties of the composite biomaterial [32]. Moreover, it is widely known that contact angle width can be deeply influenced by arithmetic surface roughness (R_a). The profilometric analysis conducted to investigate surface microtopography highlights a linear increase of R_a by increase β-TCP concentration, with a consequent reduction of contact angle amplitude. The pronounced roughness detected on our β-TCP-loaded scaffolds further confirms itself as a key factor in protein adsorption regulation, capable to influence cell fate, and improves osteoblastic behavior, especially in terms of adhesion, proliferation, differentiation [54]. The results, also in accordance with the literature, highlights the osteoconductive role of calcium phosphate-based material for both proliferation and differentiation processes [41,55].- Remarkably,

our RT-PCR results highlight that in MC3T3-E1 cell cultured on PCL/β-TCP scaffolds the level of transcripts for osteoprotegerin, osteocalcin and bone sialoprotein are higher at day 14 if compared to PCL scaffolds, despite of a delayed response at day 7. A solid explanation for this behavior is linked to the 'conflict' between proliferation and differentiation. In fact, it is widely known that differentiation process starts when proliferation rate starts to decrease, typically around the second week [56]. This observation is consistent with our proliferation curves, which show that cells seeded on PCL scaffolds rapidly reach a plateau after 7 days. MC3T3-E1 osteoblasts on PCL/β-TCP scaffolds exhibit an increasing linear proliferation still after 7 and 10 days, during which ECM maturation starts and develops. In fact, according to Owen *et al.,* it has been possible to identify two transition phases: the former occurs at the end of proliferative activity, and the latter with the beginning of mineralization, involving genes acting as bone formation regulators and resorption (e.g. OCN) [57,58].

It can be then concluded that cells growth on 100% PCL scaffolds tent to show earlier but lower levels of expression of osteoblastic markers, probably due to the faster proliferation if compared to scaffold loaded with the ceramic powder which, in reverse, highlight later but more abundant level of transcripts, underlining the improved pro-differentiative properties given by high β-TCP concentrations.

CONCLUSION

This work demonstrates the possibility to fabricate a solvent-free FDM 3D printed PCL/β-TCP scaffolds loaded with β-TCP at concentrations up to the 70%, overcoming the limit of 60% currently present in the scientific literature. Moreover, the addition of the inorganic powder improves both surface and biological characteristics, highlighting the central role of surface microtopography on positively affecting cell behavior. Obtained surfaces provide an optimal microenvironment for osteoblasts adhesion, proliferation, and differentiation. This study also confirms the active part of 3D printing technologies on fabrication of highly customized structure able to repair or replace damaged tissues and their fundamental role on bone tissue engineering. In conclusion, the PCL/β-TCP scaffolds manufactured by FDM could lay the foundation for the development of future extremely personalized structures with ideal features for bone and periodontal regeneration.

BIBLIOGRAPHY

[1] MacKinnon RB, Oomen J, Pedersen Zari M. Promises and Presuppositions of Biomimicry. *Biomimetics* **2020**

[2] Anderson M, Dubey N, Bogie K, Cao C, Li J, Lerchbacker J, Mendonça G, Kauffmann F, Bottino MC, Kaigler D. Three-dimensional printing of clinical scale and personalized calcium phosphate scaffolds for alveolar bone reconstruction. *Dent Mater* **2022** *38*:529-539

[3] Langer R, Vacanti J. Advances in tissue engineering. *J Pediatr Surg* **2016** *51*:8-12

[4] Szulc P. Bone turnover: Biology and assessment tools. *Best Practice & Research Clinical Endocrinology & Metabolism* **2018** *32*:725-738

[5] Pilipchuk SP, Plonka AB, Monje A, Taut AD, Lanis A, Kang B, Giannobile W.V. Tissue engineering for bone regeneration and osseointegration in the oral cavity. *Dent Mater* **2015** *31*:317-338

[6] Amini Z, Lari R. A systematic review of decellularized allograft and xenograft–derived scaffolds in bone tissue regeneration. *Tissue and Cell* **2021** *69*:101494

[7] Bracey DN, Seyler TM, Jinnah AH, Smith TL, Ornelles DA, Deora R, Parks GD, Van Dyke ME, Whitlock PW. A porcine xenograft-derived bone scaffold is a biocompatible bone graft substitute: An assessment of cytocompatibility and the alpha-Gal epitope. *Xenotransplantation* **2019** *26*:e12534

[8] Schmidt AH. Autologous bone graft: Is it still the gold standard? *Injury* **2021** *52:*S18-s22

[9] Huang B, Caetano G, Vyas C, Blaker JJ, Diver C, Bártolo P. Polymer-Ceramic Composite Scaffolds: The Effect of Hydroxyapatite and β-tri-Calcium Phosphate. *Materials (Basel)* **2018** *11*

[10] Lee K, Weir M.D, Lippens E, Mehta M, Wang P, Duda G.N, Kim WS, Mooney DJ, Xu HH. Bone regeneration via novel macroporous CPC scaffolds in critical-sized cranial defects in rats. *Dent Mater* **2014** *30*:e199-207

[11] Ou M, Huang X. Influence of bone formation by composite scaffolds with different proportions of hydroxyapatite and collagen. *Dent Mater* **2021** *37*:e231-e244

[12] Ruediger T, Berg A, Guellmar A, Rode C, Schnabelrauch M, Urbanek A, Wagner K, Wyrwa R, Kinne RW, Sigusch BW. Cytocompatibility of polymer-based periodontal bone substitutes in gingival fibroblast and MC3T3 osteoblast cell cultures. *Dent Mater* **2012** *28*:e239-249,

[13] Delloye C, Cornu O, Druez V, Barbier O. Bone allografts: What they can offer and what they cannot. *J Bone Joint Surg Br* **2007** *89*:574-579

[14] Jockusch J, Özcan M. Additive manufacturing of dental polymers: An overview on processes, materials and applications. *Dent Mater J* **2020** *39*:345-354

[15] Gao P, Zhang H, Liu Y, Fan B, Li X, Xiao X, Lan P, Li M, Geng L, Liu D et al. Beta-tricalcium phosphate granules improve osteogenesis in vitro and establish innovative osteo-regenerators for bone tissue engineering in vivo. *Scientific Reports* **2016** *6*:23367

[16] Turnbull G, Clarke J, Picard F, Riches P, Jia L, Han F, Li B, Shu W. 3D bioactive composite scaffolds for bone tissue engineering. *Bioactive materials* **2018** *3*:278-314

[17] Jahangir S, Hosseini S, Mostafaei F, Sayahpour FA, Baghaban Eslaminejad M. 3D-porous β-tricalcium phosphate-alginate-gelatin scaffold with DMOG delivery promotes angiogenesis and bone formation in rat calvarial defects. *J Mater Sci Mater Med* **2018** *30*:1

[18] Ghezzi B, Lagonegro P, Fukata N, Parisi L, Calestani D, Galli C, Salviati G, Macaluso G.M, Rossi F. Sub-Micropillar Spacing Modulates the Spatial Arrangement of Mouse MC3T3-E1 Osteoblastic Cells. *Nanomaterials (Basel, Switzerland)* **2019** *9*:1701

[19] Chan BP, Leong KW. Scaffolding in tissue engineering: general approaches and tissue-specific considerations. *Eur Spine J* **2008** *17 Suppl 4*:467-479

[20] Bershadsky, A.D.; Balaban, N.Q.; Geiger, B. Adhesion-dependent cell mechanosensitivity. *Annu Rev Cell Dev Biol* **2003** *19*:677-695

[21] Ahn SH, Lee J, Park SA, Kim WD. Three-dimensional bio-printing equipment technologies for tissue engineering and regenerative medicine. *Tissue Eng Regen Med* **2016** *13*:663-676

[22] Wickramasinghe S, Do T, Tran P. FDM-Based 3D Printing of Polymer and Associated Composite: A Review on Mechanical Properties, Defects and Treatments. *Polymers (Basel)* **2020** *12*

[23] Foresti R, Ghezzi B, Vettori M, Bergonzi L, Attolino S, Rossi S, Tarabella G, Vurro D, von Zeppelin D, Iannotta S et al. 3D Printed Masks for Powders and Viruses Safety Protection Using Food Grade Polymers: Empirical Tests. *Polymers (Basel)* **2021** *13*

[24] Mazzanti V, Malagutti L, Mollica F. FDM 3D Printing of Polymers Containing Natural Fillers: A Review of their Mechanical Properties. *Polymers* **2019** *11*

[25] Bharadwaz A, Jayasuriya AC. Recent trends in the application of widely used natural and synthetic polymer nanocomposites in bone tissue regeneration. *Mater Sci Eng C Mater Biol Appl* **2020** *110*:110698,

[26] Wang Y, Wang J, Gao R, Liu X, Feng Z, Zhang C, Huang P, Dong A, Kong D, Wang W. Biomimetic glycopeptide hydrogel coated PCL/nHA scaffold for enhanced cranial bone regeneration via macrophage M2 polarization-induced osteo-immunomodulation. *Biomaterials* **2022** *285*:121538

[27] Siddiqui N, Asawa S, Birru B, Baadhe R, Rao S. PCL-Based Composite Scaffold Matrices for Tissue Engineering Applications. *Molecular Biotechnology* **2018** *60*:506-532

[28] Ghezzi B, Lagonegro P, Attolini G, Rotonda PM, Cornelissen C, Ponraj JS, Parisi L, Passeri G, Rossi F, Macaluso GM. Hydrogen plasma treatment confers enhanced bioactivity to silicon carbide-based nanowires promoting osteoblast adhesion. *Materials Science and Engineering: C* **2021** *121*:111772

[29] Parisi L, Ghezzi B, Bianchi MG, Toffoli A, Rossi F, Bussolati O, Macaluso GM. Titanium dental implants hydrophilicity promotes preferential serum fibronectin over albumin competitive adsorption modulating early cell response. *Materials Science and Engineering: C* **2020** *117*:111307

[30] Helaehil JV, Lourenço CB, Huang B, Helaehil LV, de Camargo IX, Chiarotto GB, Santamaria-Jr M, Bártolo P, Caetano GF. In Vivo Investigation of Polymer-Ceramic PCL/HA and PCL/β-TCP 3D Composite Scaffolds and Electrical Stimulation for Bone Regeneration. *Polymers* **2022** *14*

[31] Yuan B, Wang Z, Zhao Y, Tang Y, Zhou S, Sun Y, Chen X. In Vitro and In Vivo Study of a Novel Nanoscale Demineralized Bone Matrix Coated PCL/β-TCP Scaffold for Bone Regeneration. *Macromol Biosci* **2021** *21*:e2000336

[32] Bohner M, Santoni BLG, Döbelin N. β-tricalcium phosphate for bone substitution: Synthesis and properties. *Acta Biomaterialia* **2020** *113*:23-41

[33] Fahimipour F, Rasoulianboroujeni M, Dashtimoghadam E, Khoshroo K, Tahriri M, Bastami F, Lobner D, Tayebi L. 3D printed TCP-based scaffold incorporating VEGF-loaded PLGA microspheres for craniofacial tissue engineering. *Dent Mater* **2017** *33*:1205-1216

[34] Bruinink A, Bitar M, Pleskova M, Wick P, Krug HF, Maniura-Weber K. Addition of nanoscaled bioinspired surface features: A revolution for bone related implants and scaffolds? *J Biomed Mater Res A* **2014** *102*:275-294

[35] Webster TJ, Ergun C, Doremus RH, Siegel RW, Bizios R. Specific proteins mediate enhanced osteoblast adhesion on nanophase ceramics. *J Biomed Mater Res* **2000** *51*:475-483.

[36] Webster TJ, Schadler LS, Siegel RW, Bizios R. Mechanisms of enhanced osteoblast adhesion on nanophase alumina involve vitronectin. *Tissue Eng* **2001** *7*:291-301

[37] Dziadek M, Pawlik J, Menaszek E, Stodolak-Zych E, Cholewa-Kowalska K. Effect of the preparation methods on architecture, crystallinity, hydrolytic degradation, bioactivity, and biocompatibility of PCL/bioglass composite scaffolds. *Journal of Biomedical Materials Research Part B: Applied Biomaterials* **2015** *103*:1580-1593

[38] Di Maro M, Duraccio D, Malucelli G, Faga M.G. High density polyethylene composites containing alumina-toughened zirconia particles: Mechanical and tribological behavior. *Composites Part B: Engineering* **2021** *217*:108892

[39] Ishaug SL, Crane GM, Miller MJ, Yasko AW, Yaszemski MJ, Mikos AG. Bone formation by three-dimensional stromal osteoblast culture in biodegradable polymer scaffolds. *J Biomed Mater Res* **1997** *36*:17-28

[40] Kim HD, Amirthalingam S, Kim SL, Lee SS, Rangasamy J, Hwang NS. Biomimetic Materials and Fabrication Approaches for Bone Tissue Engineering. *Adv Healthc Mater* **2017** *6*

[41] Polini A, Pisignano D, Parodi M, Quarto R, Scaglione S. Osteoinduction of Human Mesenchymal Stem Cells by Bioactive Composite Scaffolds without Supplemental Osteogenic Growth Factors. *PLOS ONE* **2011**, *6*:e26211

[42] Dias D, Vale AC, Cunha EPF, Paiva MC, Reis RL, Vaquette C, Alves NM. 3D-printed cryomilled poly(ε-caprolactone)/graphene composite scaffolds for bone tissue regeneration. *J Biomed Mater Res B Appl Biomater* **2021** *109*:961-972

[43] Roseti L, Parisi V, Petretta M, Cavallo C, Desando G, Bartolotti I, Grigolo B. Scaffolds for Bone Tissue Engineering: State of the art and new perspectives. *Materials Science and Engineering: C* **2017** *78*:1246-1262

[44] Hart NH, Nimphius S, Rantalainen T, Ireland A, Siafarikas A, Newton RU. Mechanical basis of bone strength: influence of bone material, bone structure and muscle action. *J Musculoskelet Neuronal Interact* **2017** *17*:114-139

[45] Kang Z, Zhang X, Chen Y, Akram MY, Nie J, Zhu X. Preparation of polymer/calcium phosphate porous composite as bone tissue scaffolds. *Materials science & engineering. C, Materials for biological applications* **2017** *70*:1125-1131.

[46] Bruyas A, Lou F, Stahl AM, Gardner M, Maloney W, Goodman S, Yang YP. Systematic characterization of 3D-printed PCL/β-TCP scaffolds for biomedical devices and bone tissue engineering: influence of composition and porosity. *J Mater Res* **2018** *33*:1948-1959

[47] Park SH, Park SA, Kang YG, Shin JW, Park YS, Gu SR, Wu YR, Wei J. PCL/β-TCP Composite Scaffolds Exhibit Positive Osteogenic Differentiation with Mechanical Stimulation. *Tissue Eng Regen Med* **2017** *14*:349-358

[48] Han X, Gao Y, Ding Y, Wang W, Liu L, Zhao A, Yang P. In vitro performance of 3D printed PCL−β-TCP degradable spinal fusion cage. *Journal of Biomaterials Applications* **2020** *35*:1304-1314

[49] Pellegrini G, Francetti L, Barbaro B, Del Fabbro M. Novel surfaces and osseointegration in implant dentistry. *J Investig Clin Dent* **2018** *9*:e12349

[50] Marrella A, Lee TY, Lee DH, Karuthedom S, Syla D, Chawla A, Khademhosseini A, Jang HL. Engineering vascularized and innervated bone biomaterials for improved skeletal tissue regeneration. *Materials Today* **2018** *21*:362-376

[51] Liao HT, Lee MY, Tsai WW, Wang HC, Lu WC. Osteogenesis of adipose-derived stem cells on polycaprolactone-β-tricalcium phosphate scaffold fabricated via selective laser sintering and surface coating with collagen type I. *J Tissue Eng Regen Med* **2016** *10*:E337-e353.

[52] Yeo A, Wong WJ, Khoo HH, Teoh SH. Surface modification of PCL-TCP scaffolds improve interfacial mechanical interlock and enhance early bone formation: an in vitro and in vivo characterization. *J Biomed Mater Res A* **2010** *92*:311-321

[53] Nyberg E, Rindone A, Dorafshar A, Grayson WL. Comparison of 3D-Printed Poly-ε-Caprolactone Scaffolds Functionalized with Tricalcium Phosphate, Hydroxyapatite, Bio-Oss, or Decellularized Bone Matrix. *Tissue Eng Part A* **2017** *23*:503-514

[54] Idaszek J, Bruinink A, Święszkowski W. Ternary composite scaffolds with tailorable degradation rate and highly improved colonization by human bone marrow stromal cells. *J Biomed Mater Res A* **2015** *103*:2394-2404

[55] Rai B, Lin JL, Lim ZX, Guldberg RE, Hutmacher DW, Cool SM. Differences between in vitro viability and differentiation and in vivo bone-forming efficacy of human mesenchymal stem cells cultured on PCL-TCP scaffolds. *Biomaterials* **2010** *31*:7960-7970

[56] Erisken C, Kalyon DM, Wang H. Functionally graded electrospun polycaprolactone and β-tricalcium phosphate nanocomposites for tissue engineering applications. *Biomaterials* **2008** *29*:4065-4073,

[57] Komori T. Functions of Osteocalcin in Bone, Pancreas, Testis, and Muscle. *International Journal of Molecular Sciences* **2020** *21*

[58] Owen TA, Aronow M, Shalhoub V, Barone LM, Wilming L, Tassinari MS, Kennedy M.B, Pockwinse S, Lian JB, Stein GS. Progressive development of the rat osteoblast phenotype in vitro: reciprocal relationships in expression of genes associated with osteoblast proliferation and differentiation during formation of the bone extracellular matrix. *J Cell Physiol* **1990** *143*:420-430